NITROGEN IMPLANTED SILICON, GERMANIUM AND SILICON CARBIDE

AN INVESTIGATION INTO THE ELECTRICAL AND RADIATION DAMAGE PROPERTIES OF NITROGEN IMPLANTED SILICON, GERMANIUM AND SILICON CARBIDE

by

JAMES BLAIR MITCHELL, B.A.Sc.

A Thesis

Submitted to the Faculty of Graduate Studies

in Partial Fulfilment of the Requirements

for the Degree

Doctor of Philosophy

McMaster University

September 1973

DOCTOR OF PHILOSOPHY (1973)
(Electrical Engineering)

MCMASTER UNIVERSITY
Hamilton, Ontario

TITLE: An Investigation into the Electrical and Radiation Damage Properties of Nitrogen Implanted Silicon, Germanium and Silicon Carbide

AUTHOR: James Blair Mitchell, B.A.Sc.
(University of British Columbia)

SUPERVISOR: Dr. J. Shewchun

NUMBER OF PAGES: xvi, 191

Abstract

The radiation damage and electrical properties of nitrogen implanted silicon, germanium and silicon carbide have been investigated. The object of this investigation has been to relate the damage annealing properties of the implanted semiconductor to the observed electrical behaviour, in an attempt to understand the role of nitrogen in these materials.

The study has shown that donor behaviour can be obtained in nitrogen implanted silicon. Capacitance-voltage and Hall effect measurements performed on the implanted layer have indicated that less than 1% of the implanted nitrogen has become electrically active, following anneals in the 700-900°C range. The ionization energy of nitrogen in silicon has been found by low temperature Hall measurements to be 0.017 ± 0.002 eV. This result has been shown to be independent of the annealing time and the implantation temperature. For doses above $\sim 6 \times 10^{14}$ N/cm^2, donor results are no longer observed and the damage results have shown that the silicon crystal has not recrystallized well. The results of the above measurements, together with the characteristics of nitrogen implanted diodes and the results of a damage study of nitrogen implanted silicon are presented, and the role of nitrogen in silicon is discussed.

The results of electrical and lattice location measurements on nitrogen implanted germanium have shown that nitrogen does not become a donor in germanium. The lattice location measurements have used the $^{14}N(d,\alpha)^{12}C$ nuclear reaction, and have shown that the implanted nitrogen atoms are on interstitial lattice positions. The results of damage

measurements obtained by backscattering techniques, together with the electrical and lattice location results are presented.

This study has shown that nitrogen implanted silicon carbide exhibits donor behaviour following a high temperature anneal. This result was deduced from the properties of nitrogen implanted silicon carbide diodes and from lattice location measurements performed with the $^{15}N(p,\alpha)^{12}C$ nuclear reaction. These lattice location measurements have shown that approximately 50% of the implanted nitrogen atoms are on substitutional lattice sites, following an anneal at 1450°C. This is in excellent agreement with the value of 50% previously reported by other authors as deduced from electrical measurements. Although some problems with the annealing of heavily doped silicon carbide remain to be solved, this study has shown that ion implantation promises to be a useful technique for doping this material.

ACKNOWLEDGMENTS

I wish to express my appreciation to my supervisor, Dr.J. Shewchun, for his guidance and support during this investigation.

It has been a pleasure to work with Dr. H.D. Barber, Dr. J.A. Davies, and Dr. D.A. Thompson, whose comments and suggestions have been invaluable.

I would like to thank Dr. A.B. Campbell, Dr. P.P. Pronko, Mr. L.A. Goodridge, Mr. J. Stark, Mr. V. Tovizi and Mr. R.E. Yager, for their helpful contributions to this work.

I would also like to thank the technical staff at Westinghouse Canada Ltd. for preparation of the diffused contact Hall samples and the staff at the Chalk River Nuclear Laboratories for performing the low energy implantations.

TABLE OF CONTENTS

LIST OF FIGURES

LIST OF TABLES

I

INTRODUCTION

1.1 General

In the past few years, the techniques of ion implantation have become increasingly popular as a method for introducing dopant impurities into semiconductors. Commercial implantation facilities are now available and are being used by semiconductor manufacturers to implant boron and phosphorus into silicon to form semiconductor devices. Some of the advantages of this technique over the standard diffusion process are reproducibility of doping concentration, lower process temperatures, and unique profiles. Using ion implantation, the profile and concentration of the dopant ions may be controlled independently by the accelerating voltage and integrated beam current respectively, whereas in thermal diffusion, both the surface concentration and dopant profile are related to the process temperature. Recently, these advantages have been used to produce devices whose characteristics are not attainable using conventional diffusion techniques.

One potential advantage of the ion implantation process that has not as yet been fully exploited, is its use to dope semiconductors at lower temperatures than required by other technologies. For example, silicon carbide has long been considered an ideal material from which to form high temperature semiconductor devices, but the formation of these devices has been hampered by the high diffusion temperatures required ($\sim$2200°C). Ion implantation can be used to introduce impurities into

silicon carbide at room temperature. Another advantage of ion implantation is that dopant species not readily available by conventional techniques may be produced. For example, nitrogen has long been considered an unusual dopant in the elemental semiconductors as it fails to exhibit donor properties under normal diffusion techniques. However, nitrogen in the atomic form may be introduced by means of ion implantation.

The ion implantation process is not without some serious disadvantages however. The most important of these is the radiation damage of the implanted layer caused by the incident ions. Although most radiation damage can be annealed (following implantation) at temperatures lower than those required by diffusion, any remaining defects may act as scattering centers and reduce the free carrier mobility. In the fabrication of devices by ion implantation, it is important therefore, to have a knowledge of the radiation damage and annealing properties of the substrate as a function of dose, dose rate, implantation temperature and anneal temperature.

This thesis describes an investigation of the radiation damage and electrical behaviour of nitrogen introduced into silicon, germanium and silicon carbide by the techniques of ion implantation. Helium ion backscattering has been used as an analytical tool to investigate the damage annealing of the semiconductor substrate following implantation under various conditions and following various annealing treatments. Preliminary results of a lattice location study for the nitrogen-germanium system are presented. An attempt is made to correlate this information to the corresponding electrical behaviour.

The objective of the present work was to study the electrical transport properties and device applications of nitrogen in silicon and silicon carbide. Although it is generally recognized that ion implanted nitrogen acts as a donor in silicon, the nitrogen-silicon system has not been well characterized. Many of the published results for nitrogen in silicon obtained by different laboratories do not agree. The nitrogen-germanium system has been studied for comparison with the silicon system. Although nitrogen is a natural dopant in silicon carbide, it has only recently been successfully implanted and is not well understood. Each of these systems is discussed briefly below.

1.2 The Nitrogen-Silicon System

Although nitrogen in silicon has been investigated by several authors[1,2,3,4], none have used information about the damage and annealing properties as a guide for the corresponding electrical activity. It has been shown[5] that if the surface of the silicon substrate is totally damaged (ie made amorphous) by the implantation of a regular dopant ion such as boron or phosphorus, a higher percentage of the implanted ions become electrically active following anneals in the 500 - 650°C range than if the layer were only partially damaged. For doses of interest in device fabrication, (typically 10^{14} - 10^{15} ions/cm^2), light ions do not cause total damage in the implanted region. There are a number of ways to achieve total amorphization, including pre- or -post bombardment with an ion such as silicon, or implanting at cryogenic temperatures in order to inhibit any annealing occuring during the implantation.

It is possible that the same phenomena would apply to nitrogen implanted silicon, should the nitrogen behave as a regular donor. Consequently, the present study began with a detailed look at the damage properties of nitrogen in silicon as a function of nitrogen dose, dose rate, and implantation temperature in the temperature range 40 - 300°K. The results were then used to select implantation conditions causing saturation damage for corresponding electrical measurements.

The study of the silicon system comprises a large portion of the time spent on this investigation. As a result, two chapters have been devoted to silicon. Chapter IV discussed the damage and annealing properties of nitrogen implanted silicon, while Chapter V reports the results of the electrical measurements.

1.3 The Nitrogen-Germanium System

Although germanium and silicon both have diamond type lattices, there are many basic differences in the two materials. For example, it is well known that silicon can be readily oxidized whereas germanium can not. Many impurities (for example, oxygen) present in silicon are not present to the same level in germanium. Because of this, a study of the nitrogen-germanium system was undertaken for comparison with nitrogen in silicon. Once again, backscattering studies were performed to determine how nitrogen behaved in germanium as a function of the implantation parameters and subsequent annealing conditions. The results of these damage and electrical measurements are reported here. The nitrogen-germanium system has not been studied in detail, due to the fact that

germanium no longer has the importance in semiconductor device technology that silicon does, and the intention was to see if the germanium and silicon systems were similar.

1.4 The Nitrogen-Silicon Carbide System

Recently[6], ion implantation has been used to dope "p" type silicon carbide and form p-n junctions. Nearly all the SiC device work to date has been done by the same laboratory using crystals grown under well controlled conditions. The present study compares the electrical and radiation damage properties of crystals obtained from the Norton Company, the Carborundum Company and the Westinghouse Astronuclear Laboratory. As with the silicon work, the damage properties of the nitrogen implantation were investigated at different doses, at various dose rates and at various substrate temperatures in order to establish suitable implantation conditions for subsequent electrical measurements. This study has been hampered by a lack of well characterized crystals. Not only are the crystals difficult to obtain but crystals from different sources are usually totally different.

1.5 The Scope of this Thesis

This thesis presents the results of the experiments outlined above. The theoretical concepts behind the experiments are presented in Chapter II. A description of the accelerator facilities for implantation and damage analysis is given in Chapter III. Each material is then discussed in turn. Chapters IV and V are devoted to silicon, while Chapter VI discusses the

results of nitrogen implanted germanium. The results of the silicon carbide study are presented in Chapter VII. In the final Chapter, comparisons are drawn (where possible) between the properties of nitrogen in all three materials.

II

THE ION BOMBARDMENT AND NITROGEN IMPLANTATION OF SEMICONDUCTORS

2.1 Introduction

This chapter presents the theoretical framework on which the experiments described in this thesis are based. Since the results presented in the following chapters will be compared with this theory, the general form of the theoretical expressions has been explained and then discussed specifically for the ions and substrates used in this investigation.

The factors that determine the energy loss processes and hence the ultimate depth distribution of the implanted ions will be discussed first. Not only is the depth distribution of the implanted species related to these energy loss processes, but so is the amount and nature of the lattice disorder caused by the incident ion. Since this is important to the present study, the theoretical distributions of the damage and implanted ions will be discussed in relation to these processes. The use of the channeling behaviour of high energy, low atomic number (Z) particles to study the amount and depth distribution of the damage is explained. This technique can also be applied to lattice location studies, and, as some preliminary lattice location results have been obtained for the nitrogen-germanium and nitrogen-silicon carbide systems, a brief discussion of the procedure nas been included. The nature of the annealing and epitaxial regrowth of

the damaged layer is then considered, followed by a discussion of the expected behaviour of nitrogen in silicon, germanium and silicon carbide based on the chemical properties of nitrogen and these semiconductor materials.

2.2 The Energy Loss Processes

2.2.1 Introduction

When a beam of energetic ions impinges on the surface of a target, the ions will gradually give up their incident energy by means of collisions with the target nuclei and electrons, and eventually come to rest. In the theoretical description of this process, it is assumed that all the incident ions are monoenergetic and that the number of collisions an ion has and the energy given up per collision are random variables, and hence the process may be described in a statistical manner. An actual implantation approximates these conditions quite well, as magnetic mass separation ensures the beam is reasonably monoenergetic and contains only one species, and the large number of incident ions ($> 10^{13}$ ions/cm^2) makes a statistical approach valid. The total distance that an ion travels before stopping is denoted as the range (R) while the projection of this distance onto the direction of incidence is known as the projected range (R_p). These concepts are illustrated in figure 2.1. It is the projected range that is of interest in semiconductor device work, as most implantations are performed within a few degrees of the normal to the crystal surface. Hence the projected range is very close to the experimentally

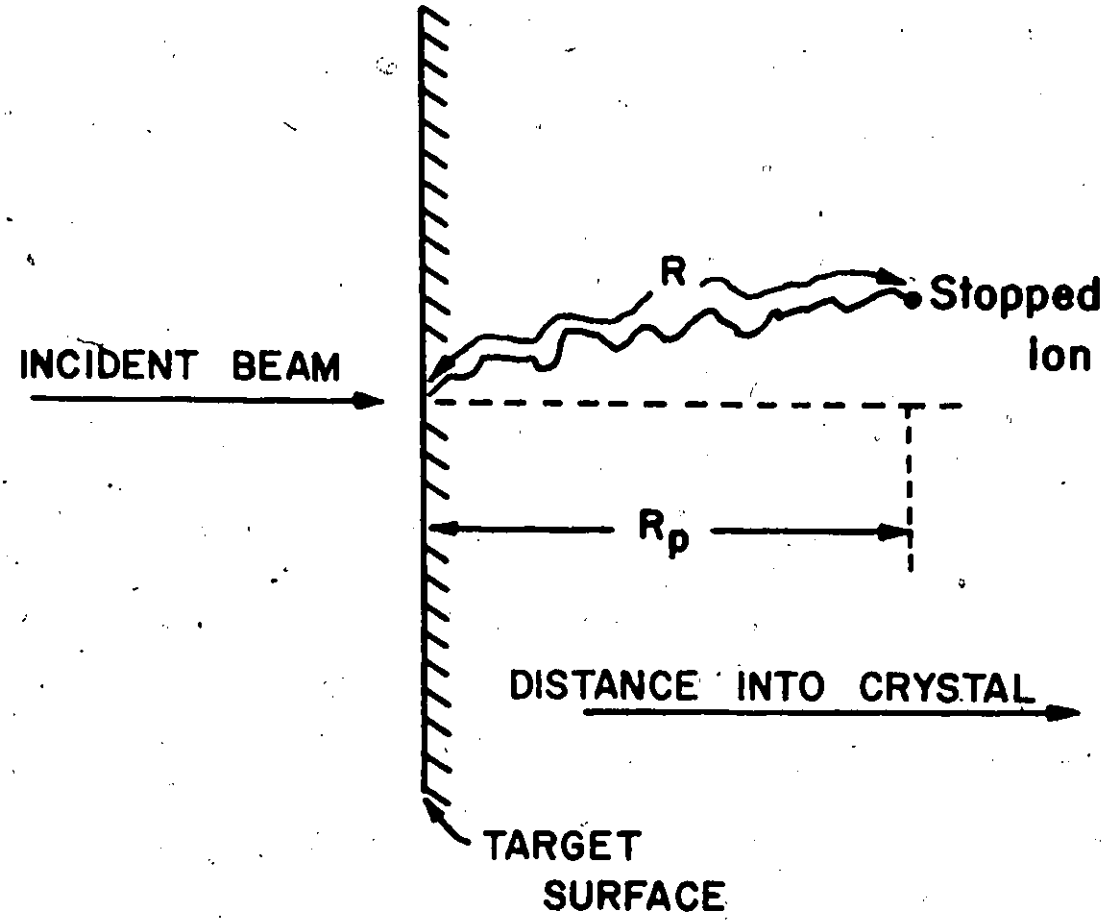

Figure 2.1: The definition of total range (R) and projected range (R_p).

measured ion range.

The total depth to which the ion travels depends critically on the nature of the target. If the target is amorphous, the range will depend on the energy, mass, and atomic number of the ion (E_0, M_1, Z_1), and the mass and atomic number of the target (M_2, Z_2), and the density of the target. For single crystal targets, the range of the ion will depend on the factors mentioned above, and also on the temperature, the dose rate, the total dose, the surface condition of the crystal, and the orientation of the crystal with respect to the incident beam. If a major crystal axis is aligned with the incident beam, the ions can be steered (or channeled) by the rows of atoms, down the open directions between atomic planes. These particles have a much smaller rate of energy loss with distance and hence a much greater range than they would in an amorphous target. This channeling phenomenon will be discussed in more detail in a later section. For the present, it will be assumed that the target is amorphous. This is not an unreasonable assumption for ion implantation into semiconductors, since the crystal is not usually accurately aligned with the beam, and in fact is often deliberately misaligned by a few degrees to prevent channeling. Although there is no true random direction for most single crystal targets, implanting at an angle to the normal direction presents a large density of randomly distributed lattice atoms to the cross section of the beam. The results of such "nonchanneled" ion implantations indicate that the range distributions are reproducible. Of course, once the implantation has begun, the initial radiation damage will tend to make the surface more "amorphous".

There are two forms of energy loss that determine the range-energy relations for ions introduced into solid amorphous targets. These are the interaction of the ion with bound or free electrons in the solid (electronic stopping) and the screened Coulomb interaction of the ion with the target atoms (nuclear stopping). The theoretical concepts behind these energy loss mechanisms and how they are applied to the determination of the final range distribution were first stated by Bohr[7]. Nielsen[8] derived an empirical range-energy relationship where the total stopping was a constant: The most comprehensive theory has been developed by Lindhard, Scharff, and Schiott[9] and by Lindhard and Scharff.[10]. This theory, known as the LSS theory, assumes each of the above forms of energy loss are independent and that the average rate of energy loss of an ion as a function of distance may be expressed as the sum of the electronic and nuclear stopping, viz.-

$$\frac{-dE}{dx} = N \{S_e(E) + S_n(E)\} \qquad (2.1)$$

where E = the energy of the incident ion at the point x along its path

N = the average number of target atoms per unit volume (the target density)

$S_e(E)$ = the electronic stopping power (i.e. the energy lost to electronic interactions when an ion of energy E traverses a thickness Δx of a target of unit density)

$S_n(E)$ = the nuclear stopping power (i.e. the energy lost to target atoms when an ion of energy E traverses a thickness Δx of a target of unit density)

The average total range of an ion in an amorphous target is given by the integral of the above expression:

$$R = \int_0^R dE/(dE/dx)$$

$$= \frac{1}{N} \int_{E_0}^{0} \frac{1}{S_e(E) + S_n(E)} \, dE \qquad (2.2)$$

where E_0 is the incident energy. More will be said about the range following a discussion of the factors influencing the nuclear and electronic stopping powers.

2.2.2 The Nuclear Stopping Power

The nuclear stopping power (S_n) can be thought of as the energy lost due to interactions with the target atoms as an ion of energy E traverses a thickness Δx of the target. LSS have derived a universal expression for S_n by assuming that the interactions between atoms of the target can be neglected, i.e. that each target atom acts independently of the others. The nuclear stopping power is obtained by considering the energy transferred to a given particle within the thickness Δx as the ion moves past it at a distance p', and then summing the energy transfer due to all the particles that lie in that differential thickness Δx. If the energy lost is ΔE, then

$$\Delta E = - N\Delta x \int_0^\infty T_n \, 2\pi p dp \qquad (2.3)$$

where T_n = the amount of energy transferred to each target atom

p = the impact parameter (i.e. the distance that the ion would pass the target atom were it not deflected)

$2\pi pdp$ = the differential cross section $d\sigma$

N = the atomic density

Dividing by Δx and taking the limit yields

$$-\left(\frac{dE}{dx}\right)_n = N \int_0^\infty T_n \, 2\pi p dp \qquad (2.4)$$

Comparing equation (2.4) with (2.1) leads to-

$$S_n = \int_0^\infty T_n \, 2\pi p dp \qquad (2.5)$$

$$= \int T d\sigma \qquad (2.6)$$

The calculation of the nuclear stopping power depends on the calculation of the energy transferred (T_n) during a collision. To calculate T_n, the assumption is made that the collisions are elastic (i.e. energy and momentum are conserved), and the interaction forces can then be obtained from the charges on the two particles. The potential between the particles has been approximated in a number of ways. The early theory of Bohr[7] used an exponential Coulomb potential of the form

$$V(r) = \frac{Z_1 Z_2 q^2}{r} \exp\left(\frac{-r}{a_B}\right) \qquad (2.7)$$

where a_B = Bohr atomic screening radius

$$= a_o(Z_1^{2/3} + Z_2^{2/3})^{-1/2}$$

and a_o = Bohr radius

$$= 5.29 \times 10^{-9} \text{ cm}$$

The exponential factor has the effect of cutting off the interaction sharply at a distance equal to a_B. Range-energy measurements indicated that this decrease of potential was too rapid. Nielsen[8] modified the Bohr potential by substituting an inverse separation screening for the exponential:

$$V(r) = \frac{Z_1 Z_2 q^2}{r} \left(\frac{a_B}{r}\right) \tag{2.8}$$

For the numerical calculations of LSS, the potential used has the form

$$V(r) = \frac{Z_1 Z_2 q^2}{4\pi\epsilon_o r} f(r/z) \tag{2.9}$$

where $f(r/a)$ = the screening function

a = the screening parameter

LSS use the Thomas-Fermi screening function, where the screening parameter a is given by

$$a = 0.885\, a_o(Z_1^{2/3} + Z_2^{2/3})^{-1/2} \tag{2.10}$$

and a_o = Bohr radius

The screening parameter, a, is important in the discussion of the channeling of MeV particles and in the determination of lattice damage

as seen later. By using normalized dimensionless range and energy parameters, ρ and ε, LSS have derived a universal relationship for the nuclear stopping. These parameters have the form

$$\rho = R\pi a^2 N[M_1 M_2/(M_1+M_2)^2] \qquad (2.11)$$

$$\varepsilon = E(a/q^2)[M_2/Z_1 Z_2(M_1+M_2)] \qquad (2.12)$$

The universal curve for $(d\varepsilon/d\rho)_n$ obtained by LSS is shown in figure 2.2 and will be discussed further following a discussion of the electronic stopping power.

2.2.3 The Electronic Stopping Power

There are two models presently used to calculate the electronic stopping power: that due to Firsov[11] and that of LSS. The LSS model for the electronic stopping power is based on the theoretical stopping properties of a free electron gas. This model calculates the energy lost by the nucleus of the incident particle due to collisions with the electrons of the target. As long as the velocity of the ion is less than the velocity of an electron having an energy equal to the Fermi energy of the free electron gas, then the stopping power is proportional to the velocity, and as the velocity is proportional to the square root of the energy, then

$$S_e \propto v \propto E^{1/2} \qquad (2.13)$$

$$\text{or } S_e = kE^{1/2} \qquad (2.14)$$

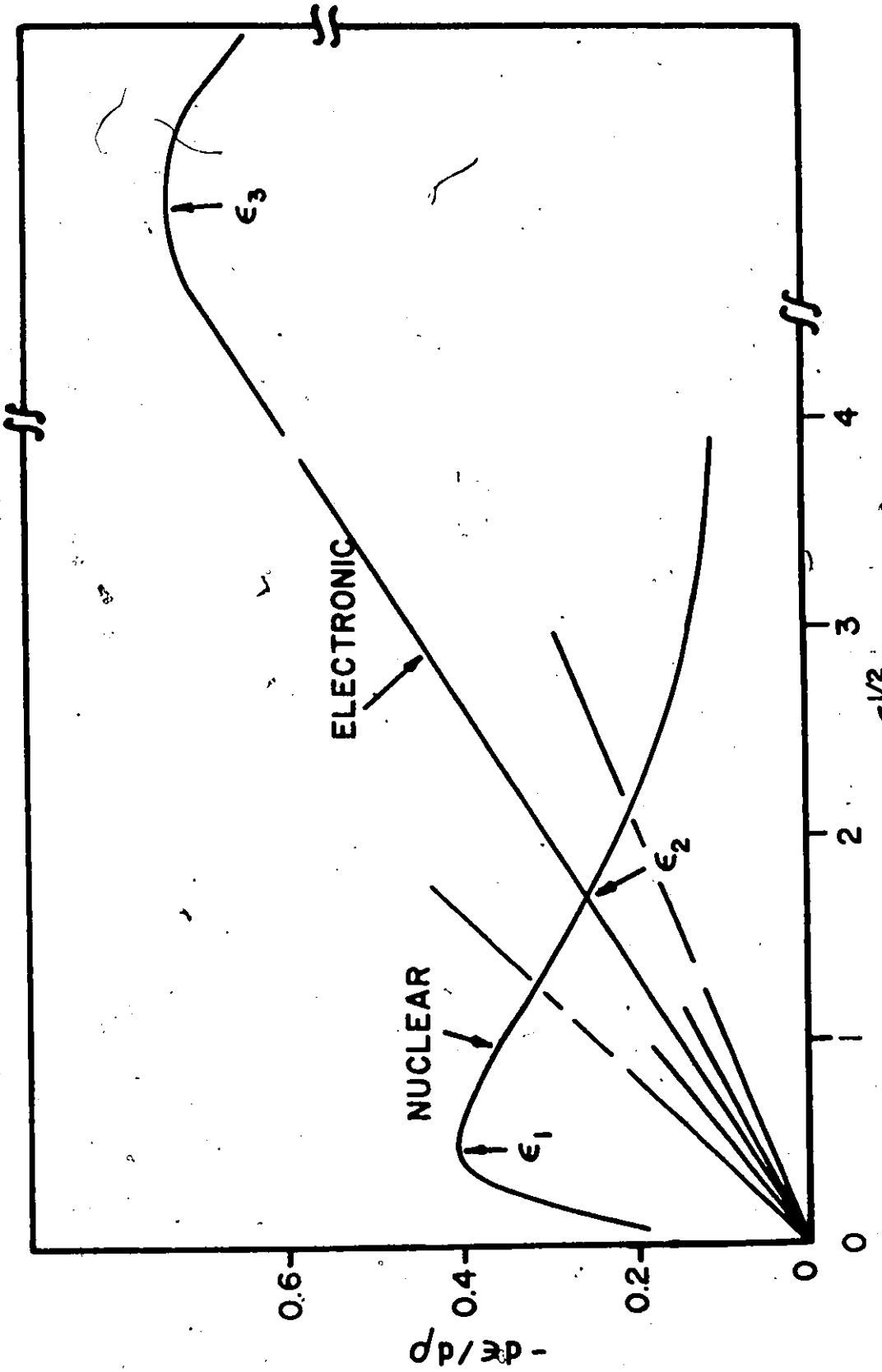

Figure 2.2 The theoretical nuclear and electronic stopping power curves in terms of the normalized variables ρ and ε. For electronic stopping a family of curves is obtained.

Lindhard has chosen the constant k to be consistent with the Thomas-Fermi picture of the ion,

$$k = \frac{\varepsilon_e \; 0.0793 \; Z_1^{1/2} Z_2^{1/2} (M_1 + M_2)^{3/2}}{(Z_1^{2/3} + Z_2^{2/3})^{3/4} \; M_1^{3/2} M_2^{1/2}} \qquad (2.15)$$

$$\text{where } \varepsilon_e = Z_1^{1/6} \qquad (2.16)$$

Thus there is no universal curve for the electronic stopping power as there is for the nuclear stopping power, but rather a set of curves each characterized by a particular value of k, as shown in figure 2.2.

Figure 2.2 shows that nuclear stopping is the more important process at low energies. It reaches a maximum at ε_1, and then falls off while the electronic stopping increases linearly with velocity ($\varepsilon^{1/2}$) over a wide range and becomes the dominant stopping process for energies greater than ε_2. The LSS parameters ε, ρ, and k in figure 2.2 have been calculated for the ion and substrate combinations used in this investigation, and are tabulated in Table 2.1.

In the Firsov model of electronic stopping, the value of S_e is obtained by a computation of the energy transferred due to electronic interactions as the two particles approach each other and then separate. As the two-atoms approach each other, a quasi-molecule is formed and the energy exchanges associated with the forming of this quasi-molecule are responsible for the energy loss to the moving atom. The total energy lost by the moving atom as it moves past the target atom has been calculated by Firsov as

TABLE 2.1

THE LSS PARAMETERS FOR NITROGEN

IN SILICON, GERMANIUM AND CARBON*

	$\varepsilon/E(keV^{-1})$	$\rho/R(micron^{-1})$	$k(keV^{1/2}/micron)$
Si	0.072	32.3	23.81
Ge	0.033	12.0	27.55
C	0.135	173.6	109.30

* The values of ε and ρ for SiC can be interpolated from the values associated with Si and C.

$$T = \frac{(4.3 \times 10^{-8})(Z_1 + Z_2)^{5/2}}{[1 + 3.1 \times 10^{7}(Z_1 + Z_2)^{1/3}p]^5} v \qquad (2.17)$$

where T = energy lost in eV

v = velocity of the incident projectile in cm/s

p = the impact parameter

Firsov assumed that all the electrons in both atoms would participate in these energy exchanges. Recently, it has been shown[12] that electron shielding effects of the most tightly bound electrons should be considered.

2.3 The Total and Projected Ranges

When S_n and S_e are known, they can be substituted into the basic energy loss equation (equation (2.2)) and the total range (R) calculated. The total range is not usually of interest in the ion implantation of semiconductors. The parameter of importance is the projected range (R_p) and the deviations in the projected range due to the fact that all particles do not have the same sequence of collisions. The calculation of the projected range from the range has been discussed in detail by Schiott[13] and by LSS. For implantations where $M_1 < M_2$, which includes the present investigation, an analytical expression is required to determine the projected range. Projected ranges for many common ions implanted into semiconductors have been calculated numerically and tabulated by Johnson and Gibbons.[14] The mean ($\bar{R}_p$) and the standard deviation ($\Delta\bar{R}_p$) of the projected range have also been calculated. These are the parameters required to construct the ion distribution profile resulting from the implantation

into an amorphous target. This profile is assumed to have a Gaussian distribution. This has been found experimentally to be an accurate assumption except for depths considerably outside the standard deviation.

In ion implantation into semiconductors for device fabrication, it is often convenient to have an estimate of the average dopant concentration expressed as ions/cm^3 rather than ions/cm^2. If the distribution is Gaussian, the ion concentration will be normally distributed about R_p, having a peak value of

$$N_{peak} = \frac{(0.4)\, N_{implant}}{\Delta R_p} \qquad (2.18)$$

The distribution will drop by one decade at $x \approx R_p \pm 2(\Delta R_p)$ and by two decades at $x \approx R_p \pm 3(\Delta R_p)$. The theoretical ion distributions for 80 and 40 keV nitrogen into silicon, germanium and silicon carbide are shown in figures 2.3, 2.4 and 2.5 respectively. The peak concentration has been selected to correspond to a dose of 1.4×10^{14} ions/cm^2, which is a typical dose used in the present study.

2.4 The Lattice Disorder Created by Ion Implantation

The previous section has shown that as incident ions lose energy in penetrating a solid, they transfer energy both to electrons, exciting them to higher states, and to the atoms of the solid, resulting in atomic motion or displacement. As only the nuclear collisions normally result in damage, it is necessary to determine the partition of energy between electronic and nuclear processes. The energy partition of the displaced atoms must also be considered. The theoretical distribution of energy

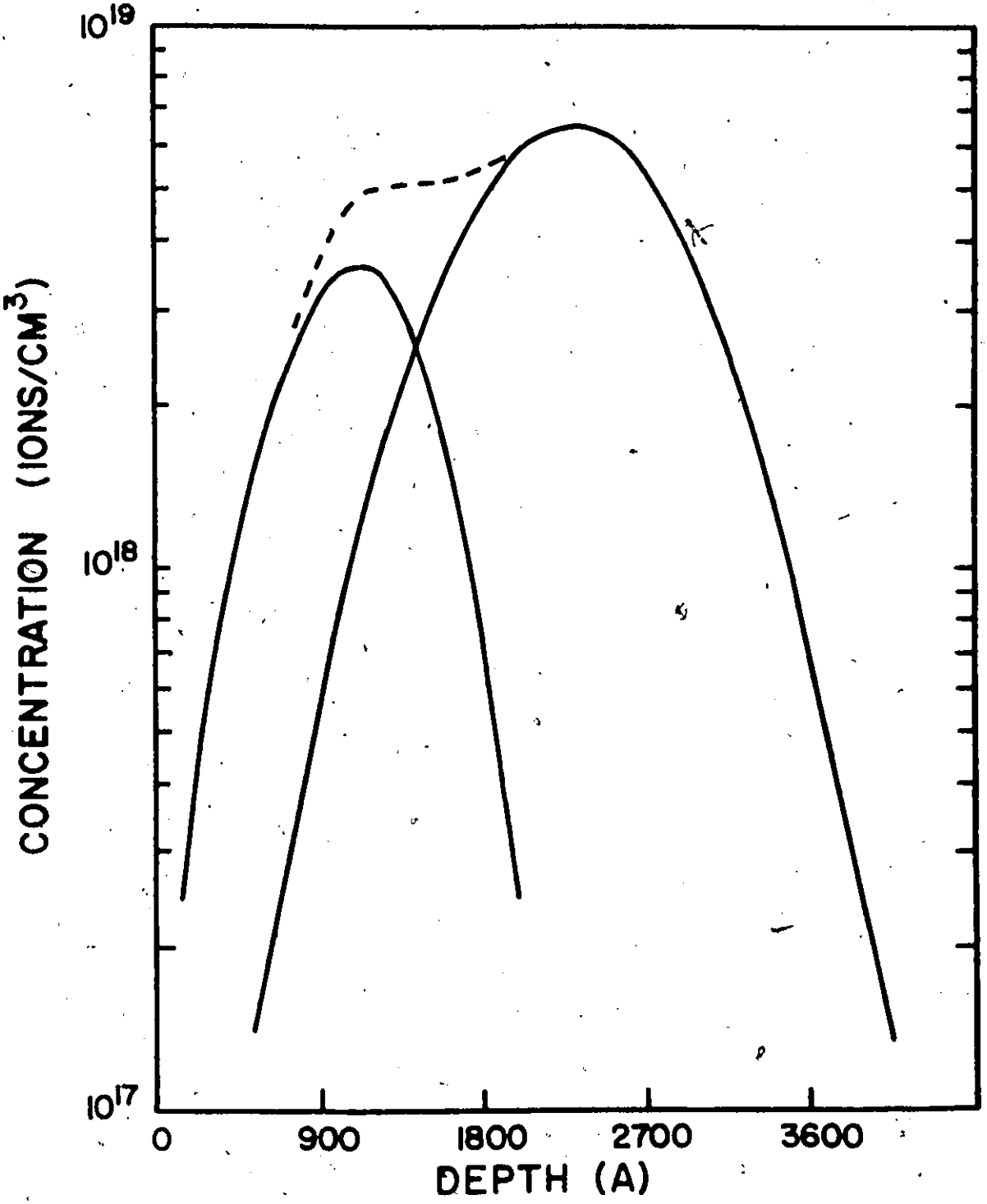

Figure 2.3 The theoretical distribution of 80 and 40 keV nitrogen in silicon. The dose ratio is 3:1. The dotted line is the resultant distribution.

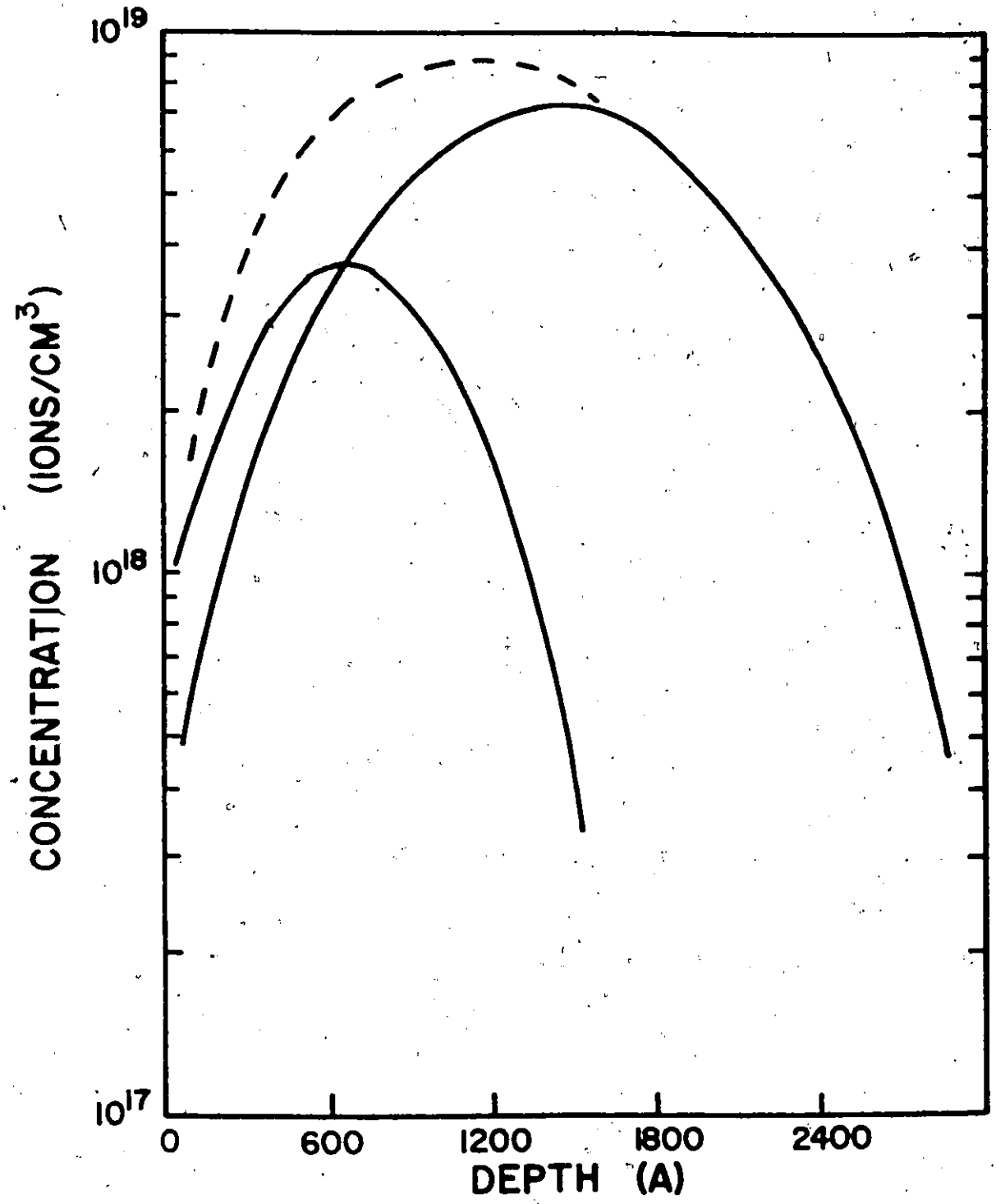

Figure 2.4 The theoretical distribution of 80 and 40 keV nitrogen in germanium. The dose ratio is 3:1. The dotted line is the resultant distribution.

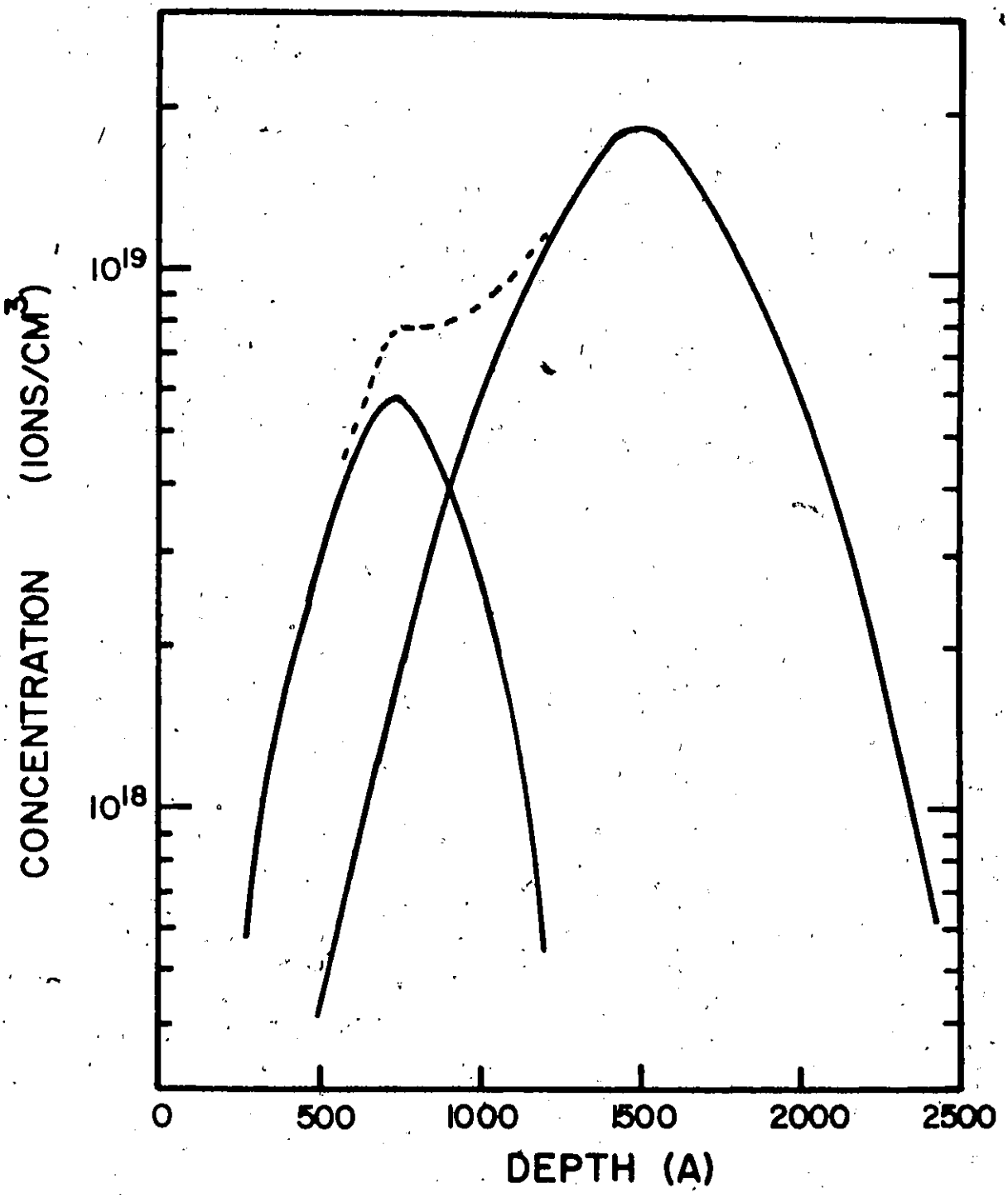

Figure 2.5 The theoretical distribution of 80 and 40 keV nitrogen in silicon carbide. The dose ratio is 3:1. The dotted line is the resultant distribution.

between electronic and nuclear processes for both the primary (incident) particles and the secondary (knocked-on) particles has been derived by Lindhard et al.[15] The two energy components total the incident energy, viz. -

$$E = \eta + \nu \qquad (2.19)$$

where E = the incident energy of the ion

η = the total energy given to electrons

ν = the total energy ending up in atomic motion

Although the exact calculation for this energy partition is complex, a qualitative understanding can be obtained by referring to figure 2.2. Except for low Z ions or high implantation energies, the nuclear stopping process dominates the electronic, and we would expect most of the ion energy to be available for displacement processes. For the low Z high energy particles used in channeling measurements, we would expect the dominant stopping mechanism to be electronic stopping. For 80 keV nitrogen incident on silicon, the partition of energy deposited in electronic excitation versus atomic displacements as a function of depth has been numerically calculated by Winterbon.[16] As shown in figure 2.6, near the surface (i.e. at high energy) the electronic stopping dominates, while at lower energies (greater depth), the nuclear stopping dominates. As only the nuclear stopping creates damage, we would expect most of the disorder to occur after ~1200 Å.

From a knowledge of the amount of energy available for nuclear collisions, it should be possible to estimate the number of displaced atoms

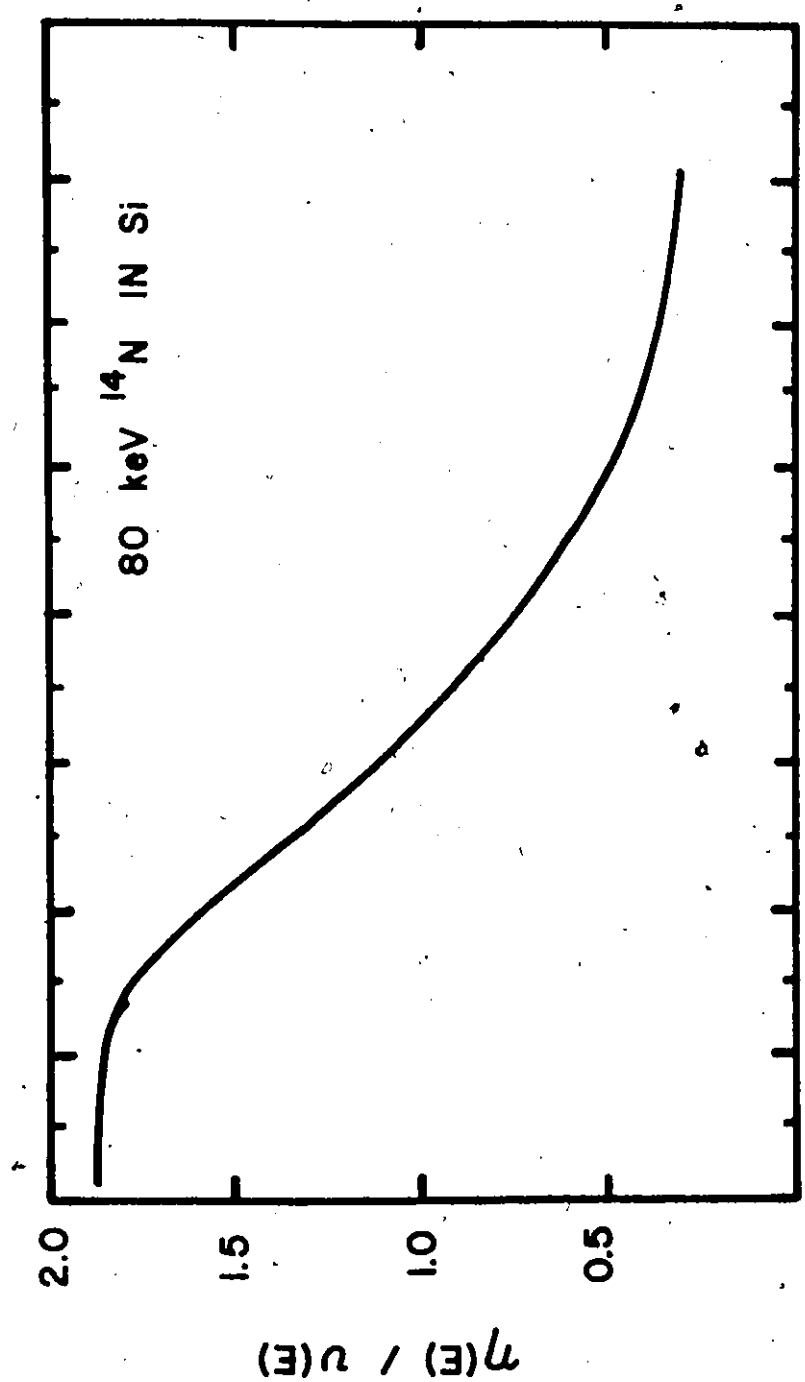

Figure 2.6 The ratio $\eta(E)/\nu(E)$ of energy deposition in electronic excitation versus atomic displacements.

caused by each incident ion. Such a calculation assumes a well defined threshold energy - i.e. the minimum energy needed to displace an atom from its lattice site. This is not a very accurate assumption, since it implies that the displacement events are well separated, completely independent two body scattering collisions, which need not be the case for high dose implants. An estimate of the number of displaced atoms can be based on a relationship derived by Kinchin and Pease,[17]

$$N(E) = \frac{\nu(E)}{2 E_d} \qquad (2.20)$$

where $\nu(E)$ = the amount of the incident energy resulting in atomic displacement

E_d = effective displacment threshold energy

Not only is the total number of displaced atoms of importance, but so is their distribution in space (depth). Sigmund and Sanders[18] have calculated the spatial distribution of defects and of implanted ions by using a power law approximation to the Thomas-Fermi potential and neglecting the electronic stopping component. They actually calculate the spatial distribution of energy available to displace atoms. In general, they find that the incident ion comes to rest at a position that is deeper than the center of the disorder cascade. For light ions, large angle scattering of the primary beam can occur and so both the defect and range distributions are comparable in shape. This will be shown to be the case for nitrogen in silicon, as discussed in chapter IV. Brice[19] has developed a method of calculating the energy deposited per unit depth by determining the rate at which energy is transferred from the incident ion to the host atoms. However, his calculation does not take into account the spread in deposited

energy due to the finite range distribution of the recoiling host atoms. Winterbon[16] has calculated the depth dependence of the damage by considering the cascade effect of secondary particles. Both these theoretical curves for nitrogen in silicon will be presented in chapter IV.

A description of the amount of ion-induced damage expressed in terms of the experimental parameters dose and dose-rate, is quite complex. A convenient but oversimplified description can be obtained by assuming that each incident ion creates a damage cascade which can be described by a cylinder whose length and diameter is equal to the width of the damage distribution at half maximum. As this width is approximately equal to one-half the projected range, the latter is often used. Each incoming ion will not feel the effects of the other ions until the dose reaches a value where the cross-sectional areas of the cylinders overlap. Saturation damage will be achieved when a sufficient number of ions have arrived to displace all the lattice atoms contained in a slab of material whose thickness is equal to the length of the cylinder. This calculation does not allow for any annealing which may occur, and therefore this estimate of the dose needed to cause saturation damage is usually lower than that found experimentally. These ideas can be illustrated by an example. For 80 keV nitrogen into germanium, $R_p/2 = 713\,\text{Å}$[14] and $\nu(E)$, the amount of energy into atomic processes is $0.353\,E_o$[20] If the displacement energy for germanium is assumed to be 14 eV,[21] then the number of displaced atoms per incident ion is.

$$N = \frac{\nu(E)}{2 E_d} \qquad (2.21)$$

$$= \frac{(0.353)(80{,}000)}{(2)(14)} = 1010 \text{ displaced atoms per incident ion}$$

The cross sectional area of the damage cascade cylinder is $\pi(713)^2/4 = 4 \times 10^5$ Å^2. For these cylinders to overlap, a dose of $1\ cm^2/4 \times 10^5$ Å$^2 = 2.5 \times 10^{10}$ ions/cm^2 is required. For saturation damage, all the atoms within a volume of germanium 713 Å x 1 cm^2 must be displaced. Such a volume contains 3×10^{17} germanium atoms. If each incident ion displaces 1010 atoms, then a dose of $3 \times 10^{17}/1010 = 3 \times 10^{14}$ ions/cm^2 is required to cause saturation damage. This simple estimate will be seen to be surprisingly accurate.

The importance of dose rate on the damage can be estimated by a simplified procedure also. The time between the arrival of incident ions in the cross sectional area of the damage cascade can be calculated from the known limits of the experimental dose rate. The defects responsible for dose rate effects have an annealing time, and if another particle arrives in this area before this time has elapsed, a dose rate effect may be observed. Using 80 keV nitrogen in silicon as an example, the cross sectional area of the damage cylinder is $\pi(1135)^2/4 = 1.01 \times 10^6$ Å^2. The dose rate limits for the present experiments were 5 - 500 nA/cm^2, or, equivalently, $3.12 \times 10^{-6} - 3.12 \times 10^{-4}$ ions/sec-Å^2. For the low dose rate, ions will arrive within the 1135 Å diameter region every 3.1 seconds while for the high dose rate, they will arrive 3.1×10^{-2} seconds apart. Picraux and Vook[22] have shown that the negative vacancy can anneal in 10 minutes at 70°K in silicon, and thus dose rate effects may be observed using the above experimental dose rates.

2.5 The Channeling Effect

The above theory for the range and damage distribution of ions has applied to amorphous targets. Single crystal targets that have a low order crystallographic direction aligned with the incident beam show much deeper range distributions and much less damage than when not aligned with the beam. This is due to the incident ions being steered by successive gentle collisons with the strings of atoms that comprise the walls of the crystal channel. The existence of the channeling effect has been demonstrated by experiment[23-27], computer studies[28] and theoretical analysis.[29,30]

Lindhard[31] has presented a theoretical calculation of the largest angle that the incident particle can make with the channel axis before the steering action of the rows of atoms is lost. This angle is referred to as the critical angle ψ_c, and is shown schematically in figure 2.7. He divides the incident projectile energy into two components, that parallel to the axis of the channel and that perpendicular to it. As long as the perpendicular component is less than the repulsive potential of the atomic string, the particle remains channeled. Lindhard shows that the critical angle depends on the velocity of the incident particle, viz. -

$$\text{for } E \geq \frac{Z_1 Z_2 q d}{2\pi\epsilon_0 a^2} \qquad \psi_c = \left(\frac{Z_1 Z_2 q}{d 2\pi\epsilon_0 E}\right)^{1/2} \tag{2.22}$$

$$\text{and for } E \ll \frac{Z_1 Z_2 q d}{2\pi\epsilon_0 a^2} \qquad \psi_c = \left(\frac{2 Z_1 Z_2 q^2}{Ed}\right)^{1/2} \tag{2.23}$$

where d is the lattice spacing as shown in figure 2.7.

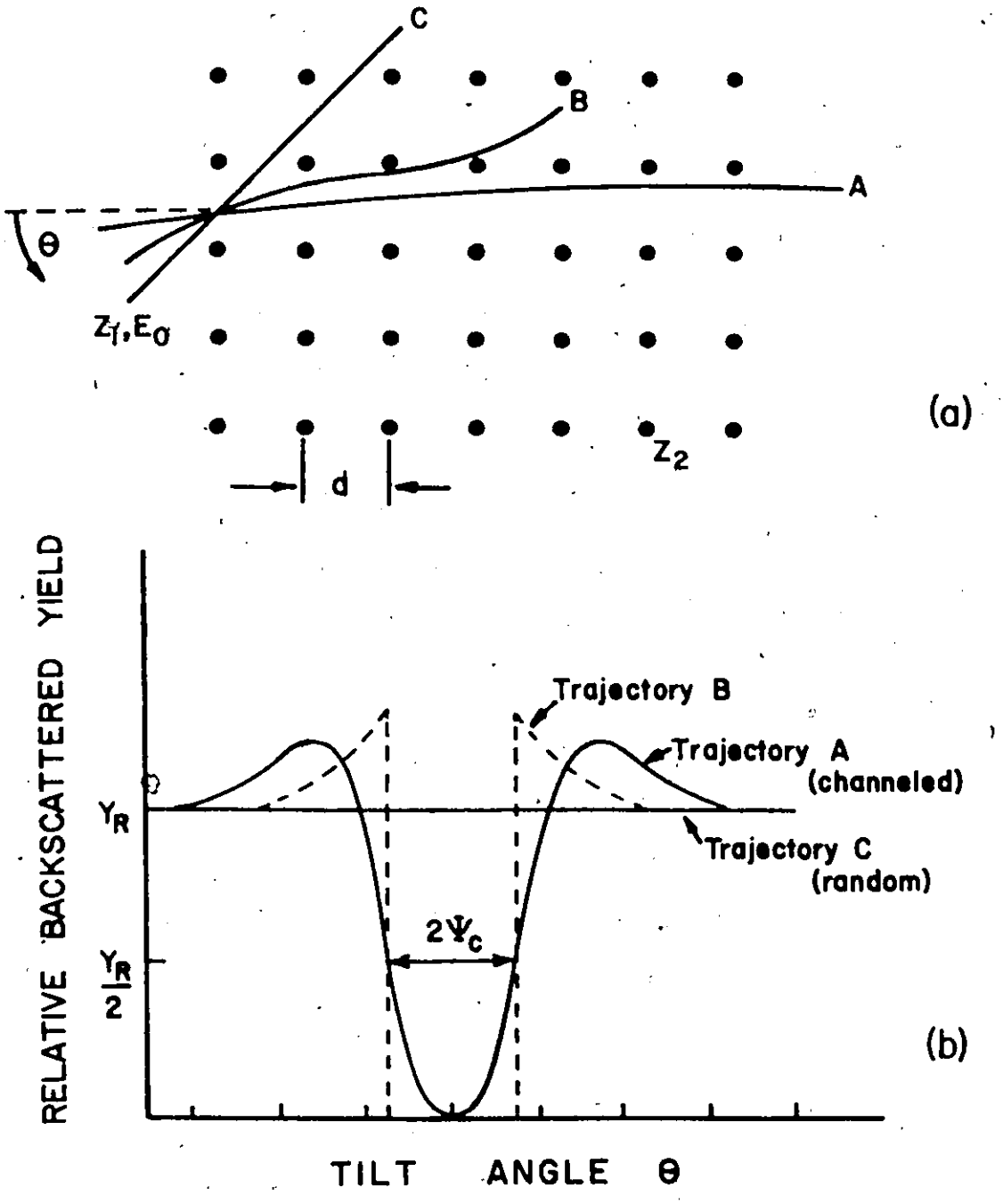

Figure 2.7 Schematic representation of ion trajectories for channeling. The crystal lattice is depicted as a string of atoms. (a) Trajectories for various angles of incidence θ relative to the lattice row. Band C represent trajectories for angles greater than the critical angle. (b) the backscattered yield for the trajectories.

For energies between 30 keV and a few hundred keV, ψ_c is between 3° and 5° for most ions. For 50 keV nitrogen incident in the <111> direction of silicon, ψ_c is 3.4°.

The measured value for the maximum range (R_{max}) of a channeled particle has been shown to depend only on the choice of crystal, the crystal direction, the projectile and the energy. The number of particles that reach R_{max} depends on such factors as the beam divergence, surface contamination and the target temperature. Although the electrical effects of channeled phosphorus[32] and gallium[33] implants have been studied, the fact that reproducible profiles cannot be achieved for heavy ion implants hinders the use of this technique for device fabrication. There is a significant difference in the annealing characteristics of channeled and random implantations, presumably due to the large difference in the amount of lattice disorder between the two methods. The sensitivity of the technique to surface effects would not allow channeled implants to be performed through surface passivating layers, another disadvantage of channeled implants.

Although the range distribution of heavy ions aligned with a channeling direction is not reproducible or well characterized at the present time, this is not the case for high velocity, low Z particles. The channeling effect of MeV particles has its greatest use as far as semiconductor device work is concerned, as an analytical tool to provide a quantitative measure of the amount of disorder present in an ion-implanted sample and to provide information about the location of foreign atoms in a crystalline lattice. Both of these uses utilize the fact that a well channeled particle does not

come closer than the Thomas-Fermi screening distance a (approximately 0.1 - 0.2 Å for silicon) to the lattice atom. Thus close encounter collisions are possible if there is poor crystal structure (i.e. a damaged crystal) or the atom is more than 0.2 Å from the atomic row (i.e. not on a regular lattice site). Each of these uses for channeling has been employed in this study and will be discussed below.

2.5.1 Observation of Crystal Damage using Channeling

Consider a well collimated, monoenergetic beam of low Z particles, for example He^+, striking a solid target that has a crystal axis accurately aligned with the beam. Some of the particles will be channeled, while others will strike the crystal surface atoms and be scattered. If the scattering is assumed elastic, energy and momentum are conserved, and the observed energy of a particle scattered from the surface can be expressed as

$$E_{obs} = k^2 E_o \qquad (2.24)$$

$$\text{where } k = \frac{M_1 \cos\theta}{M_1 + M_2} + \left[\left(\frac{M_1 \cos\theta}{M_1 + M_2}\right)^2 + \frac{M_2 - M_1}{M_1 + M_2}\right]^{1/2}$$

and E_o = the incident energy

θ = the angle through which the particle is scattered

Hence for a He^+ beam and a silicon target, E_1 is 0.59 E_o while for a germanium target E_1 is 0.81 E_o. For silicon carbide, the silicon surface atoms give rise to backscattered particles with 0.59 E_o while the carbon surface atoms yield particles with 0.28 E_o. Those particles

that are channeled will lose energy primarily by electronic stopping as they penetrate into the crystal, and, when backscattered, will also lose energy along the outgoing trajectory. In general, the observed energy of a particle backscattered from a depth s is

$$E_{obs} = [E_o - \int_o^{x\cos\theta_1} S^*(E)dl_1] k_s - \int_{x/\cos\theta_2}^{o} S(E)dl_2 \qquad (2.25)$$

where $$k_s = \{\frac{M_1 \cos\theta_s + (M_2^2 - M_1^2 \sin^2\theta_s)^{1/2}}{M_1 + M_2}^2\} \qquad (2.26)$$

The geometry of the above expression is given by figure 2.8, where it is seen that the integrals in equation (2.25) are the energy loss along the incoming and outgoing trajectories l_1 and l_2. $S^*(E)$ and $S(E)$ are the stopping powers along the incident and outgoing trajectories respectively.

If the crystal is now tilted so that it no longer is accurately aligned with the incident beam, the incoming particles are no longer channeled and the backscattered yield increases. The amount of decrease in the yield when the crystal is aligned from that obtained in a non-aligned direction is a measure of the crystal quality. The minimum ratio of the yield in the aligned direction to that in the random direction is known as χ_{min}. (For silicon $\frac{1}{40} = 0.025$)

For an ion implanted crystal, the region below the surface is damaged and the yield of backscattered particles from this region is greater than for an undamaged crystal, as illustrated in figure 2.9. The increased yield in the damage peak of the aligned spectrum can be corrected for the dechanneled background and used to obtain a quantitative measure of the disorder. This dechanneling correction accounts for these particles

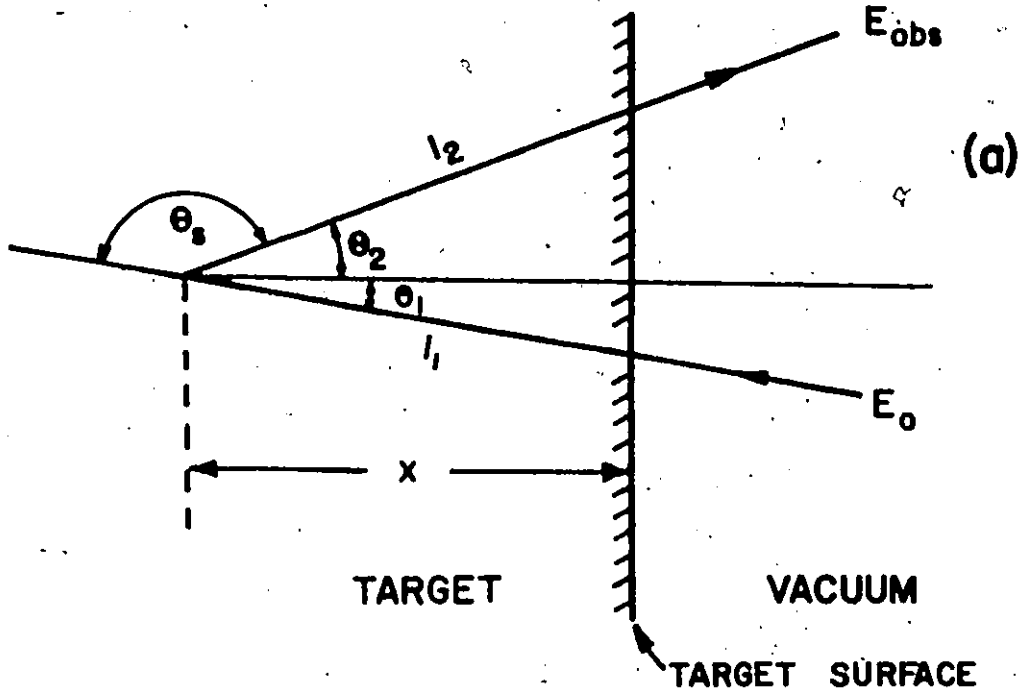

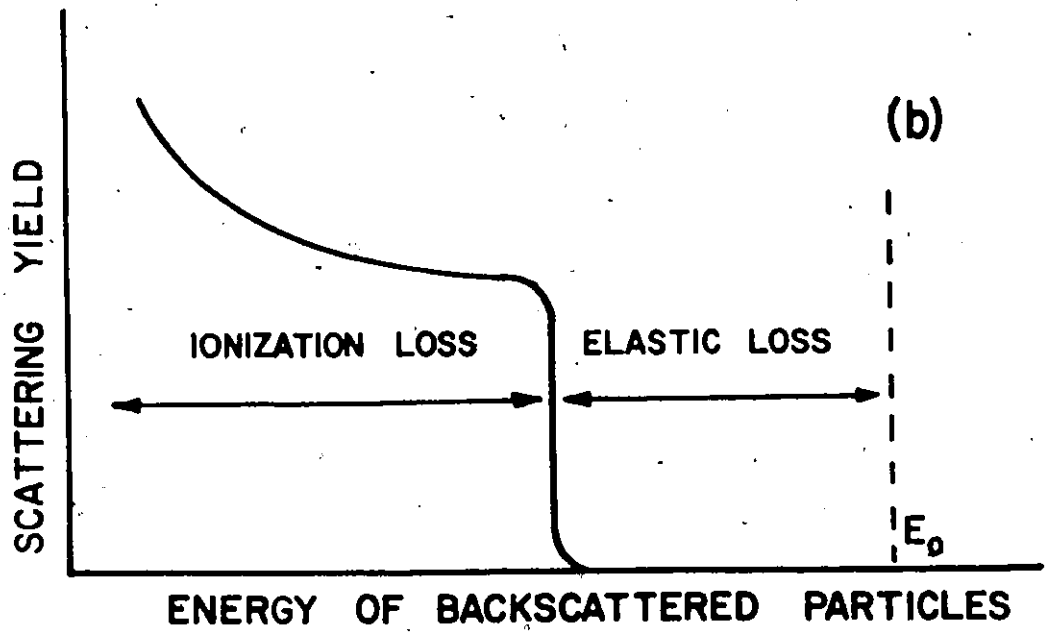

Figure 2.8 A schematic diagram of elastic scattering

(a) The various angles involved in Eqn. (2.25)

(b) The backscattered yield versus energy of the back-scattered particles.

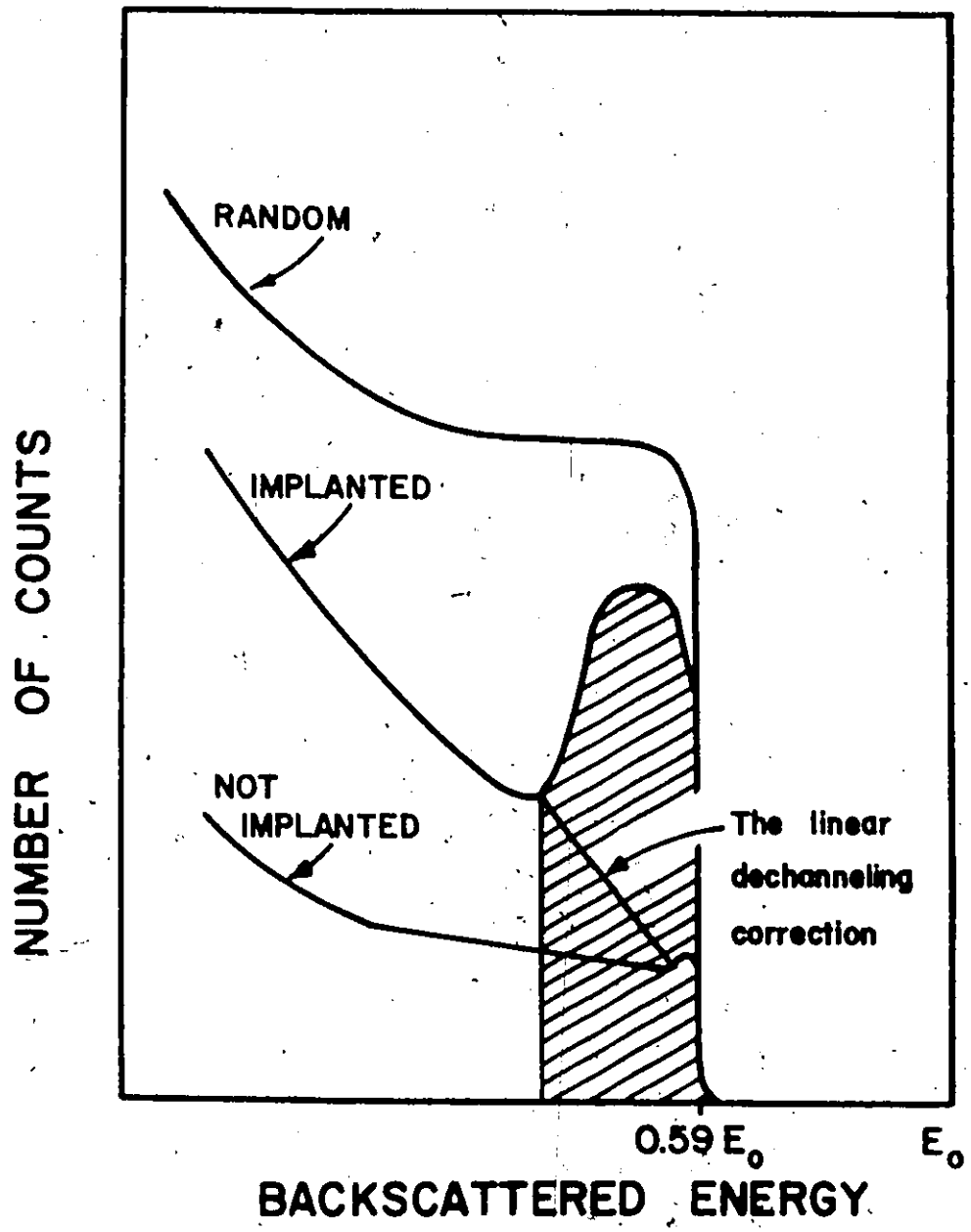

Figure 2.9 The random and aligned backscattered spectra from an implanted silicon crystal. The shaded area gives the uncorrected amount of lattice disorder. The line indicates how the non-channeled component of the aligned beam increases across the implanted region.

that are scattered out of the aligned direction by the damage and subsequently contribute an unwanted background by backscattering from the regular lattice atoms. It is because of this dechanneling that the implanted spectrum does not coincide with the aligned curve at depths below the implanted region. The fraction p(x) of displaced atoms at a given depth x (i.e. the normalized damage) is given by

$$p(x) = \frac{\chi(x) - \chi_R(x)}{1 - \chi_R(x)} \qquad (2.27)$$

where $\chi(x)$ is the normalized yield (i.e. the aligned spectrum divided by the spectrum for random incidence) at the depth x, and $\chi_R(x)$ is the normalized dechanneled fraction of the aligned analysing beam at the same depth. $\chi_R(x)$ may be approximated by a linear dechanneling correction as shown in figure 2.9. This is known to be an oversimplification, however recent work[34] has shown that the error thus introduced is not serious. An excellent account of the backscattering technique for measuring lattice disorder has been presented by Weisenberger et al[35] and more recently by Eisen.[36]

The depth distribution of the damage may be obtained by plotting p(x) versus channel number and subsequently converting the channel number first to an energy scale and then to a depth scale using the known stopping power for He^+ in the given crystal. A detailed description of the conversion of an energy to depth scale has been given by Feldman and Rodgers.[37] As the number of channels containing the damage is usually only a few percent of the total analysable depth, it is usual to assume a constant stopping power for He^+ in the crystal as a function of depth,

and hence a constant thickness Δx_c per channel. However, different stopping power values for the incident (channeled) and scattered parts of the trajectory should be used. The values used for 2 MeV He^+ in silicon were $(dE/dx)in = 14.5$ eV/Å and $(dE/dx)out = 29$ eV/Å. (Note that these values correspond to $S^*(E)$ and $S(E)$ respectively in equation 2.25). Recent work by Eisen et al[38] confirms that these values are reasonable. The values used for the stopping powers in germanium and silicon carbide will be discussed in the appropriate chapters.

2.5.2 Foreign Atom Lattice Location Using Channeling

The channeling behaviour of MeV particles may also be used to obtain information concerning the lattice location of foreign atoms. By comparing the measured yield for an aligned direction to that for the random, the percentage of dopant atoms located on the axial row may be obtained. From symmetry considerations or by measuring down another direction, the substitutional component of the foreign atoms may be deduced. The yields are usually corrected for the fact that in the aligned case, a small fraction of the incident beam is not channeled. With reference to equation 2.24, it can be seen that if the mass of the foreign atom is greater than the mass of the target, the backscattered helium ion suffers a smaller elastic energy loss from it than from the target atom, and the resulting edge of the foreign atom spectrum occurs at a higher energy, as shown in figure 2.10. If the implanted region is relatively thin, the spectrum edge appears as a peak. For the opposite case (i.e. $M_{dopant} < M_{substrate}$), the dopant spectrum will be superimposed on the large substrate background and

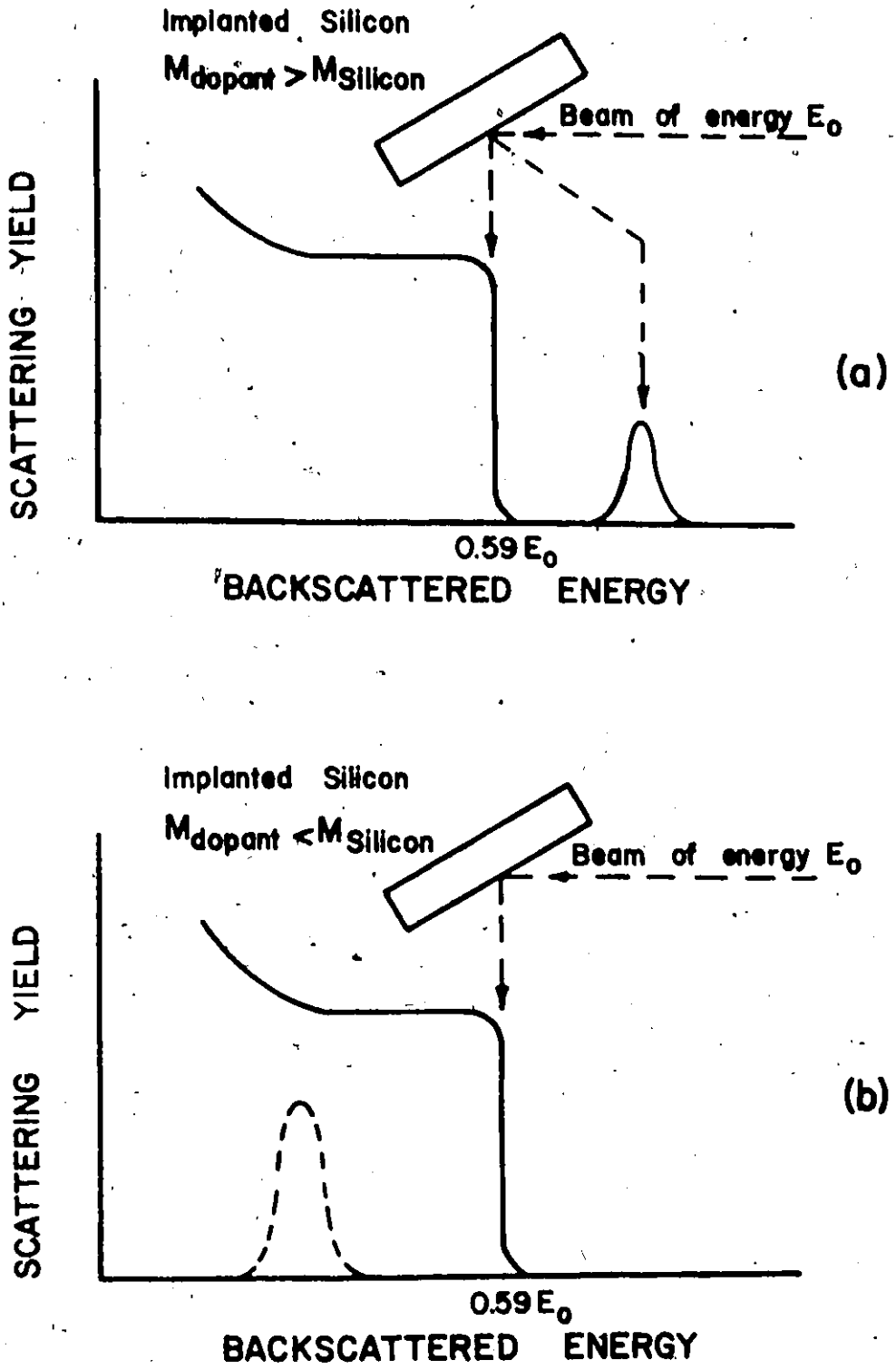

Figure 2.10 A schematic representation of dopant atom detection. In (a) the mass of the dopant atom is greater than the mass of silicon and the dopant spectrum is clearly resolved. In (b) the dopant mass is less than that of silicon, and the dopant spectrum is superimposed on the large substrate background.

cannot be resolved for the dopant concentrations of interest (i.e. $\leq 10^{-3}$ atomic fraction). Unfortunately, this is the case for nitrogen into silicon, germanium and silicon carbide. In the present investigation another close impact process has been used. A collimated beam of deuterium has been used in place of helium, and the alpha particles emitted from the $^{14}N(d,\alpha)^{12}C$ reaction measured. The details of this measurement have been discussed by Amsel et al[39,40] They show that the theoretical sensitivity of the process is 1.1×10^{14} N/cm^2 which agrees well with the experimentally determined value of $\sim 2 \times 10^{14}$ N/cm^2. This sensitivity has allowed measurements to be made on the nitrogen-germanium system but not on the nitrogen-silicon system as discussed in chapters VI and V respectively. The $^{15}N(p,\alpha)^{12}C$ reaction has been used with SiC.

2.6 The Annealing Behaviour of Ion Implanted Samples

Although it is generally recognized that an ion-implanted sample must be annealed following implantation in order to remove the associated radiation damage, very little is known about the fundamental processes involved in such an anneal. In general, the annealing behaviour of an implanted sample will depend on the nature of the damage caused by the implant and those factors that affect the amount of damage (for example, the mass of the ion, the substrate temperature, the total dose and dose rate) will affect the subsequent annealing behaviour of the sample. Although a complete understanding of how each parameter affects the annealing is not known at the present time, there are some generally accepted results. For example, there is evidence that an amorphous layer reorders by epitaxial

growth on the underlying substrate. This has been seen by channeling effect measurements where the damage spectra initially decreases in width from the low energy side before decreasing in height following anneal, indicating regrowth from the substrate-damage interface. Electron diffraction studies[41] have shown that the totally damaged samples regrow with the orientation of the substrate, while thinned samples without a crystalline region underneath (i.e. disordered throughout the total thickness) became polycrystalline following anneal. It is also generally recognized that a totally damaged crystal requires higher anneal temperatures to restore crystal perfection than a sample only partially damaged. In the latter case, the damage is associated with isolated clusters rather than a complete layer.

The most prevalent defect remaining following anneal has been found by electron microscopy to be dislocations.[42] The number of dislocations found represent an amount of damage that is in general below the detectibility level of channeling effect measurements (10^{-3} atomic fraction). For high dose implants, the anneal kinetics may be influenced by the formation of alloy phases, gas bubbles, or polycrystalline regions.

The annealing behaviour of implanted samples is related to the number and motion of defects. As these defects are related to the damage caused by the implant, there has been a great deal of study into the disorder production and annealing behaviour of light and heavy ions in silicon. At 87°K, the disorder production per unit volume has been found to be proportional to the total energy deposited into atomic processes at a given atomic energy density rate.[22] However, at room temperature, the

amount of disorder for equal atomic energy densities depends on the mass of the ion. The ionizing effects of the beam have been used to explain this, and it is now believed that the number and annealing of defects depends on the amount of energy deposited into both electronic and atomic processes. This will be discussed in more detail in chapter IV.

2.7 The Role of Nitrogen as a Donor

2.7.1 Introduction

This section discusses how nitrogen could be expected to behave in silicon, germanium and silicon carbide based on the known chemical properties of nitrogen and of these semiconductor materials. The study of the chemical and physiochemical nature of semiconductors is fairly recent and was motivated by a desire to predict apriori how to prepare compound semiconductor materials with given properties. Although most of the emphasis has been placed on understanding II-VI and III-V compound semiconductors, the parameters found to be important in these materials will also be important in the simple semiconductors.

These physiochemical parameters that have been found to be important in understanding semiconductors are[43]

- the nature of the crystal structure (i.e. the nature of the packing of the atoms in space, considering the shape and dimensions of the cavities between atoms)
- the coordination number - the number of nearest neighbours equidistant from each atom
- the effective radius of the atom (ionic or covalent radius)
- the bond energy and related interatomic interactions

- the possible existence of stable, hard to dissociate molecules or alternate stoichiometries

It is recognized that the role of nitrogen (or any other atom) as a donor relies on the fact that it can substitutionally replace a lattice atom of the semiconductor and give up an electron with a reasonable, well defined ionization energy. The parameters listed above will determine if this is possible. In the discussion to follow, silicon and germanium will be grouped together as they are both elemental semiconductors, and silicon carbide will be treated separately. All three of these semiconductors are characterized by covalent bonding between the constituent atoms.

2.7.2 Silicon and Germanium

Of the five parameters listed in the preceeding section, the last three (atom size, bond energy, and alternate stoichiometries) are the most important in answering the question of whether nitrogen will become a donor in silicon and germanium. The first two parameters are known to be less important, as other group V elements do become donors in silicon and germanium, and hence the crystal structure and coordination number must be such as to allow the formation of substitutional solid solutions. A comparison of the properties of a known donor in silicon and germanium, say arsenic, with those for nitrogen, gives insight into the behaviour of nitrogen.

Sirota[43] has calculated the covalent radius of silicon and germanium, while Pauling[44] has calculated it for silicon, germanium,

nitrogen and arsenic. The covalent radius is that radius associated with the atom when it enters into a covalent bond. It has been shown[44] that the value obtained for a given atom is independent of the molecule or crystal into which the atom is bonded. Table 2.2 compares the sizes of both nitrogen and arsenic to silicon and germanium.

TABLE 2.2

The Covalent Radii of Nitrogen and Arsenic compared to Silicon and Germanium

Silicon

r_{Si}	r_N	r_{As}	r_N/r_{Si}	r_{As}/r_{Si}
1.22°	0.70*	1.18*	0.57	0.97
1.17*			0.60	1.01

Germanium

r_{Ge}	r_N	r_{As}	r_N/r_{Ge}	r_{As}/r_{Ge}
1.45°	0.70*	1.18*	0.48	0.81
1.22*			0.57	0.97

° indicates Sirota[43] data * indicates Pauling[44] data

It is generally accepted[45] that if the size of the two atoms are within 15% of each other, the size factor is favourable for solubility of one component in the other. From Table 2.2, it is readily seen that on the basis of atom size, nitrogen would not be expected to form a substitutional solid solution in either silicon or germanium. The small size of

the nitrogen atom would favour an interstitial position, as it is known to have in metals.[46]

Although silicon and germanium are covalently bonded materials, the predicted bonding energy does not give an accurate measure of the bond energy. An additional energy which arises from a resonance between the covalent bond and an ionic component in the bond, must be considered. This extra energy is predictable from the electronegativity of each element in the bond. (The electronegativity is a measure of the power of an atom to attract electrons, and the relative electronegativity between two atoms is a measure of how similar the atoms are chemically). Pauling[44] has shown that bond energies may be calculated from the expression

$$V_{A-B} = (V_{A-A}\ V_{B-B})^{1/2} + 30\ (x_A - x_B)^2 \qquad (2.28)$$

where V_{A-A} = single bond energies for atom A to atom A bond

x_A = electronegativity of element A

The bond energies have been calculated using this expression and are tabulated in Table 2.3.

TABLE 2.3

Bond Energies
V_{Si-N} = 83.5 kcal/mole
V_{Si-As} = 37.9 kcal/mole
V_{Si-P} = 49.2 kcal/mole
V_{Ge-N} = 81.1 kcal/mole
V_{Ge-As} = 36.0 kcal/mole
V_{Ge-P} = 46.7 kcal/mole

From these results, it is seen that the bond energies for nitrogen in silicon and germanium are not similar to those for arsenic or phosphorus. In general, an atom is observed to be a dopant if the atom-host bond energy is comparable in magnitude to the host-host bond energy. This is not the case for nitrogen. The relationship between the electronegativity difference of the two atoms and the ionic character of the bonds has also been discussed by Hultgren.[47] He shows that an electronegativity difference of 1.2 (for $x_N - x_{Si}$) corresponds to approximately 30% ionic bonding while that of 0.2 (for $x_{As} - x_{Si}$) results in only a 1% ionic character of the bond. Because the electronegativity of silicon and germanium are equal, these results also apply to germanium. Thus, on the basis of bonding, nitrogen would not be expected to be a donor in silicon or germanium.

The question of stable molecules or alternate stoichiometries is a particularly relevant one for nitrogen. Pauling[44] discusses the nature of bonds in materials and shows that atoms contained in the first row of the periodic table - especially nitrogen and oxygen - tend to form stable multiple bonds, especially with themselves. In fact, nitrogen and oxygen are alone among the elements in having their standard states much different in stability from single-bonded states. The N≡N triple bond has an energy of 226 kcal/mole while the O=O double bond has an energy of 118.3 kcal/mole.[44] It is well known that oxygen ions form atomic aggregates of successive composition (SiO_2, SiO_3, SiO_4) and the formation of these aggregates has been used to explain the donor behaviour of oxygen in silicon.[48] The fact that certain of these aggregates approach saturation before others that are electrically inactive, accounts for the

existence of a maximum concentration of donors. The theory of Kaiser, Frisch and Reiss[48] for oxygen in silicon is in good agreement with experiment. It is possible that similar aggregates (Si_xN_y) can form in silicon and germanium and behave in a similar manner. (The nitride Si_3N_4 is known to form.)

2.7.3 Silicon Carbide

The role of nitrogen in silicon carbide is more involved than in silicon or germanium due to the fact that silicon carbide is a compound semiconductor. The five parameters mentioned above will still be important however. Once again, a comparison of the properties of a known dopant in silicon carbide, for example, aluminum[49], to those for nitrogen will serve to give some insight into the behaviour of nitrogen. Unlike silicon and germanium, it is now possible for the dopant atom to replace either the silicon or the carbon atom, and as shown in Table 2.4, the nitrogen atom may quite easily fit into a carbon site, while the other dopant (aluminum) would more easily fit into a silicon site. Thus it is possible that nitrogen may act as a donor in silicon carbide, based on atomic size.

TABLE 2.4

The Covalent Radii for Nitrogen and Aluminum in SiC*

r_{Si}	r_C	r_N	r_{Al}	r_C/r_{Si}	r_N/r_{Si}	r_N/r_C	r_{Al}/r_{Si}	r_{Al}/r_C
1.17	0.77	0.70	1.26	.66	0.60	0.91	1.07	1.64

* All data due to Pauling[44]

The calculation of bond energies for nitrogen in silicon carbide can proceed as in the previous section. The results, which are not too

conclusive, are tabulated in Table 2.5. Nitrogen may replace either a carbon or silicon atom with little difference in energy from that of the Si-C bond.

TABLE 2.5

Bond Energies in SiC	
Bonding Energy for Silicon to Carbon Bond	V_{Si-C} = 73.9
Bonding Energy assuming nitrogen replaces Carbon	V_{Si-N} = 83.5
Bonding Energy assuming nitrogen replaces Si	V_{C-N} = 64.0
	kcal/mole
$\frac{V_{Si-N}}{V_{Si-C}} = 1.13$	$\frac{V_{C-N}}{V_{Si-C}} = .86$

The problem of alternate stoichiometries still exists however. The stability of N_2 and stable nitrides may still prevent large quantities of nitrogen from entering the SiC lattice structure.

2.7.4 Conclusion

The preceding oversimplified physical-chemical approach to the role of nitrogen in silicon, germanium and silicon carbide has shown that nitrogen would not be expected to behave as a true donor in either silicon or germanium, but quite likely could be a donor in silicon carbide. The existence of stable nitrogen compounds formed due to the small size and large electronegativity of nitrogen, may interfere with any donor effects that may be present, or may themselves be responsible for donor-like behaviour.

III

EXPERIMENTAL TECHNIQUES

3.1 The Accelerator Facilities

3.1.1 Introduction

Three accelerator facilities were used in this study - the 150 keV accelerator and 3 MeV Van de Graaff at McMaster, and the 2.5 MeV Van de Graaff at the Chalk River Nuclear Laboratories. With the exception of a few low energy implantations into silicon carbide, all the implantations were performed using the 150 keV accelerator. Most (approximately 80%) of the backscattering work was performed at McMaster, the remainder was done at Chalk River.

3.1.2 The Ion Implantation Accelerator

The ion implantation accelerator was a Texas Nuclear Corporation model 9509 Cockroft-Walton neutron generator that was modified to accelerate nitrogen or other ions derivable from a gas. The analysing magnet limited the maximum energy to 85 keV for nitrogen. For the damage work, single implants at 80 keV were used while implants at 80 and 40 keV in a dose ratio of 3:1 were used for the electrical samples. The beam currents used varied from 40 nanoamperes to 4 microamperes. Doses ranged from 10^{13} N^+/cm^2 to 10^{15} N^+/cm^2 and were measured by means of a current integrator described previously.[50] The beam was defocussed over an area of

approximately eight square centimeters, resulting in an estimated reproducibility of 20% in the total dose. The substrate was tilted several degrees away from normal incidence in order to minimize possible channeling effects along a major axis.

The low temperature target system consisted of a Malaker Corporation Mark VII-C Cryomite cryogenic cooler. This system has previously been described in detail.[51] In the present investigations, the Faraday cup served as a cryo-shield; it was thermally connected to the cold head and completely surrounded the sample except for the beam entrance port, as shown in figure 3.1. The geometry of this cryoshield resulted in a solid-angle trapping efficiency of 96% of 2π steradians. In front of this cryo-shield was a 30-cm beam line trap cooled to liquid nitrogen temperature. This arrangement reduced the rate of condensation of water vapour, hydrocarbons etc. on the cold target surface to a value well below the detectability limit of the helium ion backscattering, which was $\sim$100 Å. Sample temperatures ranged from 30°K to 300°K and were measured with a chromel-Au(0.02% Fe) thermocouple to ±5°K. Secondary electron suppression was obtained by applying a negative 300 volt potential to the electron suppression grid shown in figure 3.1.

3.1.3 The Van de Graaff Accelerators

The helium ion backscattering facilities at McMaster and Chalk River are almost identical. High Voltage Engineering Corporation accelerators employing rf ion sources are used to generate a 2 MeV beam of He^+ ions. Apertures placed in the beam line reduce the beam diameter to 1 mm and ensure that the beam full angle divergence is <0.05°, while energy feedback

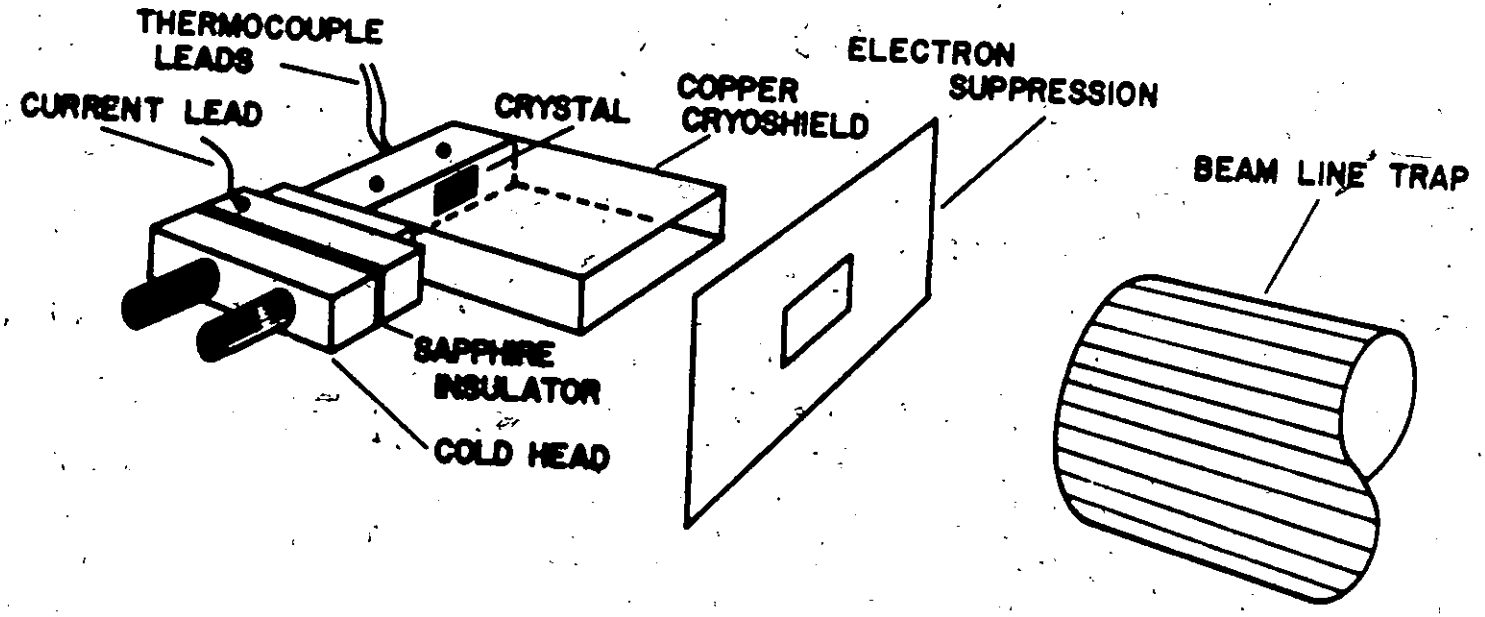

Figure 3.1: The low temperature target system. Secondary electron suppression was achieved by applying a negative 300 volt potential to the suppression grid.

slits ensure that the beam is monoenergetic. He^+ ions scattered ~150° with respect to the incident beam are detected with a silicon surface-barrier detector, and energy analysed with standard nuclear electronics to be described below. Typical detector resolution was 15 keV which corresponds to a depth resolution (in silicon) of approximately 300 Å. A double axis goniometer having an angular resolution of <0.02° was used to align the various channeling directions with the incident beam.

3.2 The Substrate Materials

Crystals produced by various growth techniques and from different sources were used as targets to ensure that the characteristics observed were due to the properties of the implanted ions, and were not influenced by impurities or defects initially present in the crystal.

The silicon was obtained from Monsanto or Texas Instruments and had resistivities ranging from 1 - 150 Ω-cm. Both p and n type Czochralski and float-zoned material was studied. The oxygen content of the float-zoned material was quoted by the supplier as $<2 \times 10^{16}$ O/cm^3. The orientation of the crystals was <111>. In all cases, the p type material was boron doped while the n type was doped with phosphorus.

The silicon carbide was obtained from the Norton Company, the Carborundum Company, and the Westinghouse Astronuclear Laboratory. The Westinghouse material was reported to have a carrier concentration of $\sim 5 \times 10^{17}$ Al/cm^3, while the concentration of aluminum in the other samples was not supplied. The polytype of the silicon carbide samples was unknown.

The germanium samples were obtained from RCA or Sylvania and were

doped with boron, gallium or indium. The resistivities ranged from 1 - 10.5 Ω-cm.

Prior to implantation, the samples were cleaned using the following procedure:

For silicon and silicon carbide

Step 1: 10 minutes in 2 H_2SO_4:1 H_2O_2 at 65°C followed by deionized water rinse

Step 2: 10 minutes in 4 H_2O:1 H_2O_2:1 HCl at 65°C followed by deionized water rinse

Step 3: 30 seconds in a dilute (~8%) HF acid solution

For germanium

Step 1: degrease in hot chloroform for 10 minutes

The deionized water employed in the above procedure had a resistivity of 18 MΩ-cm and was obtained from a Millipore "super-Q" system.

Before each anneal, the samples were cleaned again using the same procedure. The only exception was the silicon samples used for the C-V analysis, where step 3 of the cleaning procedure was omitted.

3.3 Annealing Techniques

The vacuum anneals were carried out in Lindberg furnaces using either a quartz (for silicon and germanium) or mullite (for silicon carbide) tube connected to a liquid-nitrogen trapped oil diffusion pumped vacuum system. Pressures were less than 2×10^{-6} torr. at all temperatures. Two furnaces were used, resulting in possible annealing temperatures as low as 100°C and as high as 1500°C. Except where otherwise mentioned, all samples were subjected to isochronal anneal cycles of 10 minutes at each temperature. Following each anneal step, the samples were measured at

room temperature.

Anneals in ambients other than vacuum were carried out in the same apparatus using a steady flow of the desired gas. The tube was initially pumped out, and then backfilled with the desired gas before the sample was annealed.

3.4 Backscattering Techniques.

3.4.1 Introduction

He^+ ion backscattering techniques have been used to obtain a direct measure of the amount of crystal damage present after an implant or after a subsequent anneal. The theory of this technique has been discussed in Chapter II, and a brief description of the experimental apparatus will be presented here.

The analysis consists of aligning the incident He^+ ion beam along the target crystal channeling direction and comparing the yield of backscattered He^+ ions from the implanted target to that obtained from a non-implanted target. For such a study, the sample is mounted on a goniometer allowing simultaneous rotation about two orthogonal axes. A well collimated beam (typically less than 0.1°) is allowed to strike the sample and particles that are scattered through 150° are detected by a suitable detector. A block diagram of the setup at McMaster is shown in figure 3.2. This diagram may be thought of as consisting of two parts; (a) that required to accurately align the crystal with the incident beam, and (b) that required to compile the data. Each of these two parts is

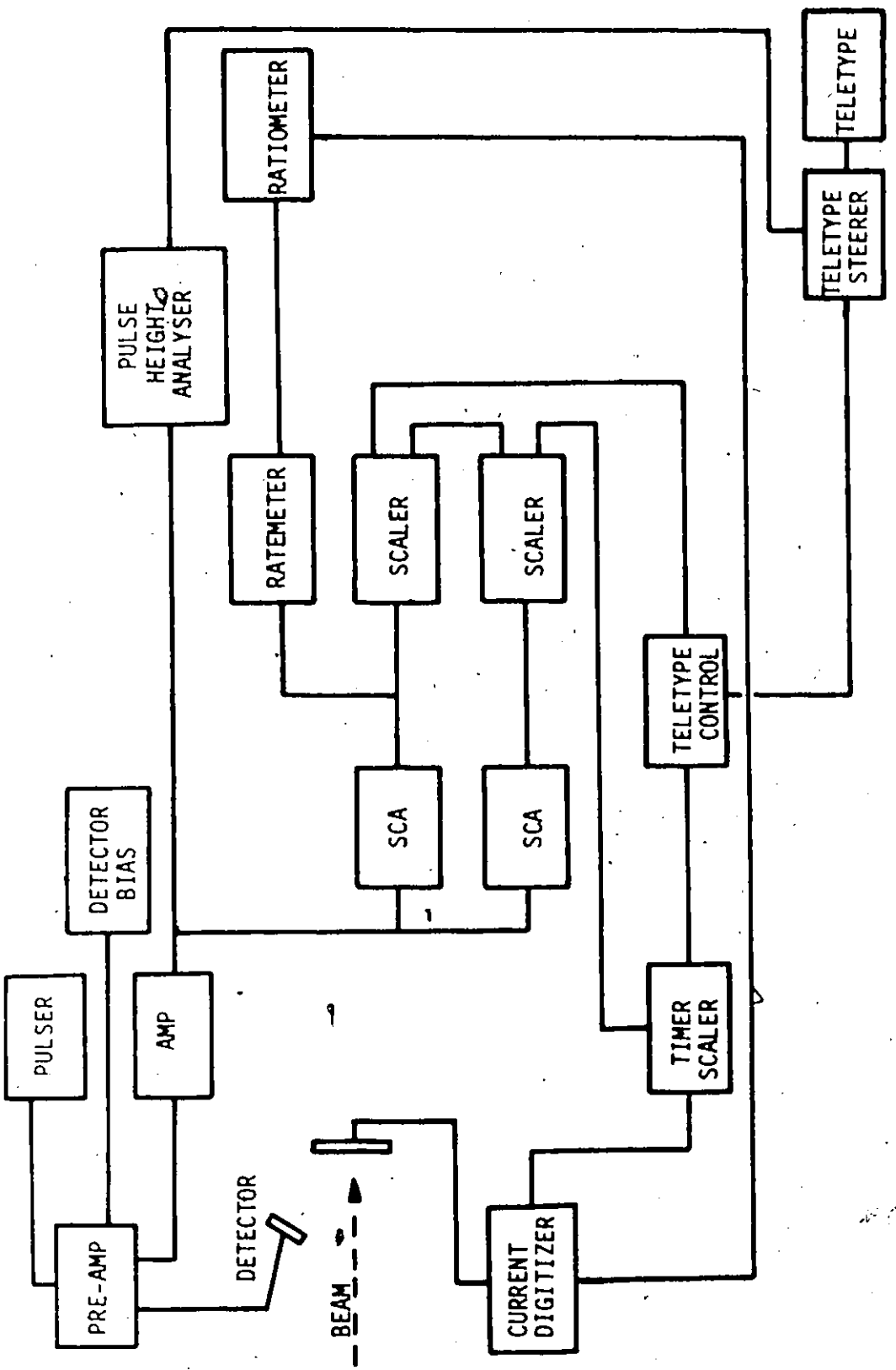

Figure 3.2: A block diagram of the backscattering facilities at McMaster University.

discussed below.

3.4.2 The Crystal Alignment

Those parts of the system utilized to align the crystal are shown in figure 3.3(a). The backscattered particles are detected by a silicon surface barrier detector. This detector is a reverse biased p-n junction constructed in such a way as to allow all the incident particles to be stopped in the depletion region. When a charged particle enters the detector it creates free electron-hole pairs and loses energy at a rate of 3.6 eV/pair (for a silicon detector). This rate of charge carrier formation has been found to be nearly independent of particle energy and particle type over a wide range of energies, provided the sensitive depth of the detector exceeds the range of the particle and provided the electric field in the depletion region is sufficiently large to separate the charge carriers before they recombine. The field strength and sensitive depth can be controlled by the external bias applied to the detector. The current pulse resulting from the carrier creation will be proportional to the energy of the incident radiation. The pre-amplifier and amplifier serve to amplify the detector output, while the single channel analyser(SCA) allows the operator to set a "window" in the backscattered energy spectrum. For an ion implanted sample, this window is usually set to correspond to particles backscattered from the region immediately below the implanted damaged area (see figure 3.4). The output from the single channel analyser is fed to a ratemeter whose output is proportional to the rate at which pulses arrive at the input. The ratio between this signal and the

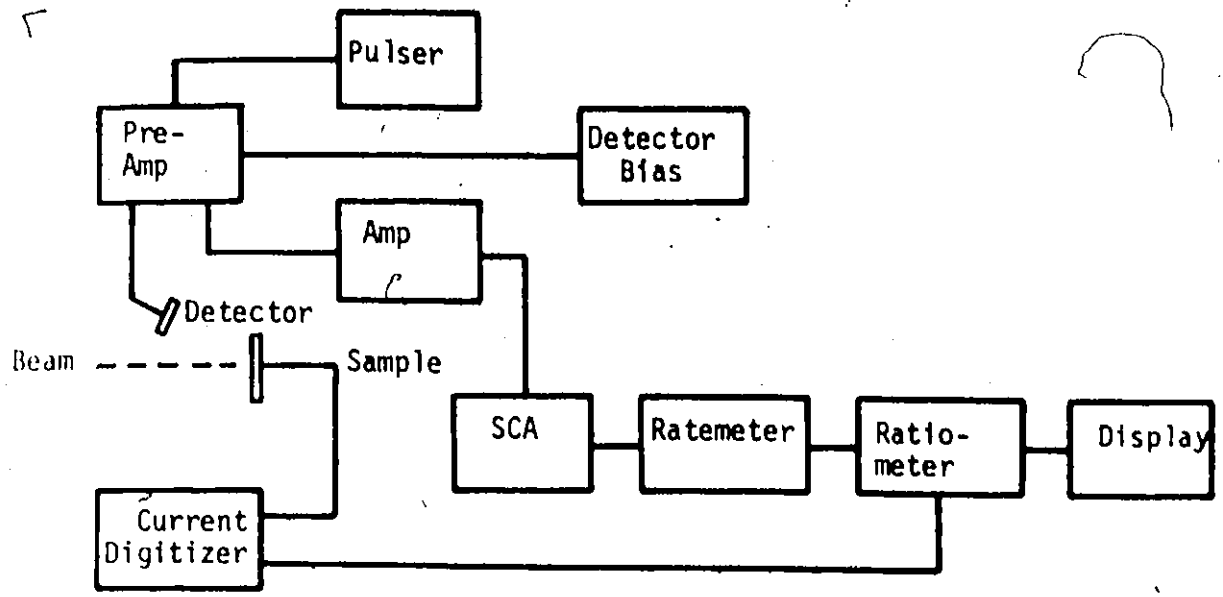

Figure 3.3(a): The backscattering equipment used for crystal alignment.

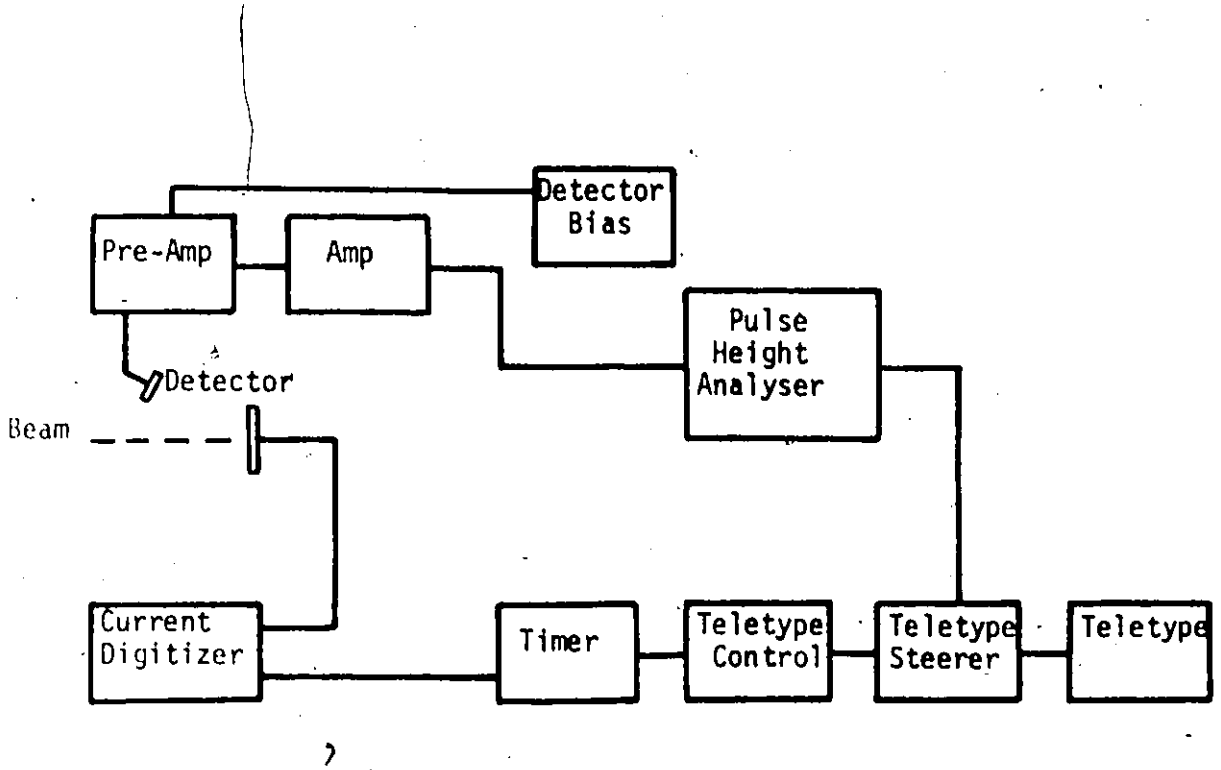

Table 3.3(b): The backscattering equipment used for data acquisition.

current as measured at the target is displayed on a large meter. This ratio is used to allow for beam current fluctuations. If the beam current drops, the output from the ratemeter will necessarily drop, but the ratio should remain constant. In practice, to align a crystal, the operator selects a convenient tilt angle and rotates the crystal through 360° while watching the ratiometer. As the beam intersects with low order crystallographic planes, the beam will be channeled and the back-scattered yield will fall, resulting in a dip on the ratiometer. The angle corresponding to these dips may be plotted on a standard stereogram from which the relative angular orientation of the crystal may be determined, as shown in figure 3.4. Lines are drawn connecting opposite points (which correspond to planar dips) on the stereogram and the common intersection of the three lines is the channeling direction. The channeling direction is found more accurately by scanning the tilt and azimuth angles through the values read from the sterogram and collecting data with a single channel analyser as shown in figure 3.5.

3.4.3 Data Acquisition

Figure 3.3(b) shows the equipment used to compile the data. As before, the detector output is amplified and fed to the single channel analysers and also to a pulse height analyser. A timer-scaler connected to the current digitizer serves as a control for the system. This scaler is preset to terminate the data acquisition when the total integrated charge reaches a preset level which corresponds to the desired statistical accuracy. This integrated charge is usually kept constant for all samples

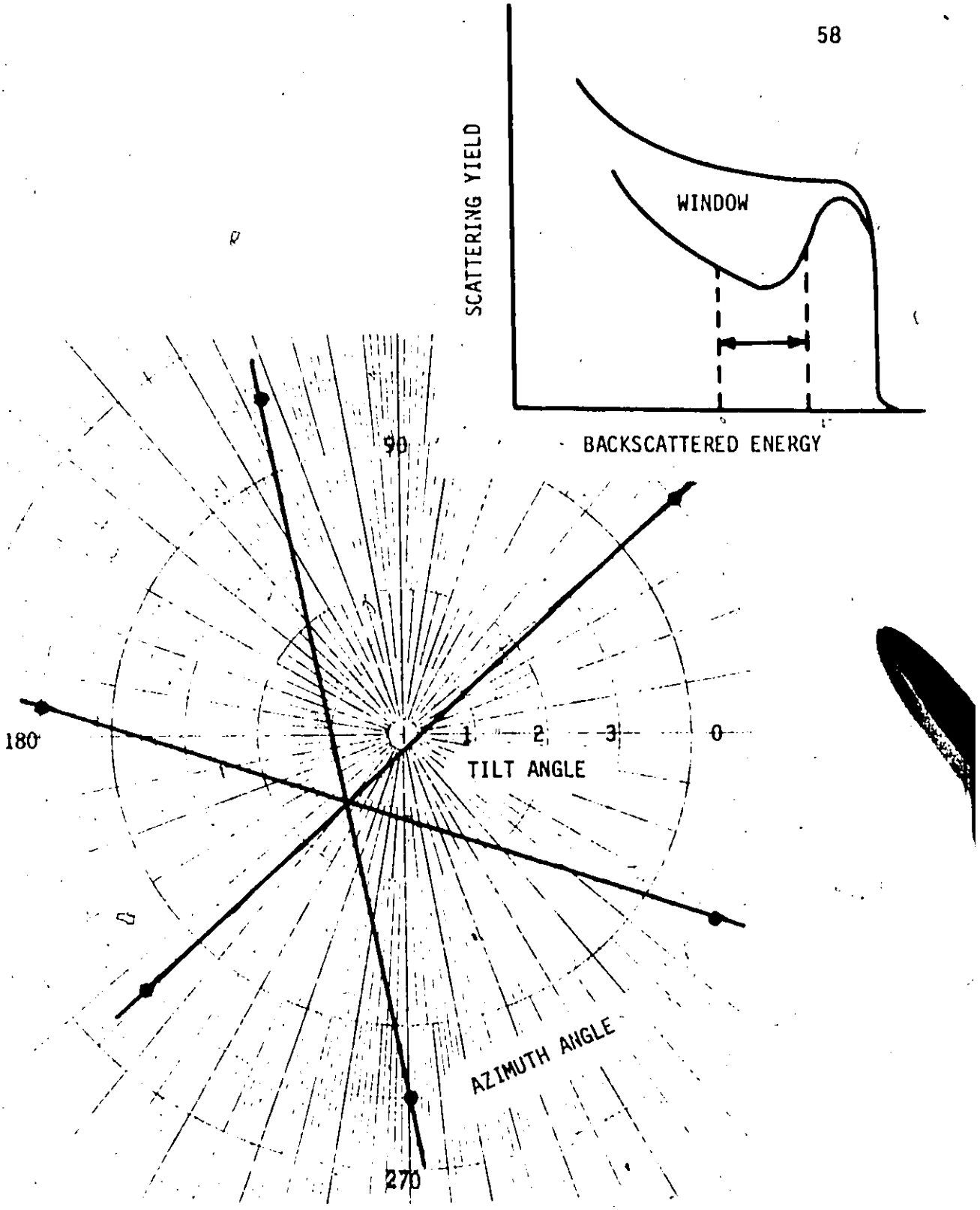

Figure 3.4 An actual stereogram obtained during initial crystal alignment. The inset shows the location of the energy limits of the single channel analyser used to obtain the data.

```
INITIAL ALIGNMENT OF PJ 88 SI
PICK TILT OF 1.2 AND SWEEP AZIM
210

 001379 000632 000673 001000
215

 001134 000537 000560 001000
220

 000681 000397 000405 001000
225

 000331 000215 000199 001000
230

 000215 000144 000162 001000
235

 000314 000159 000183 001000
240

 000544 000335 000363 001000
245

 000991 000521 000531 001000
250

 001296 000603 000616 001000

PICK AZIM AS 233 VARY TILT
0.6

 001082 000604 000550 001000
0.8

 000818 000489 000519 001000
1.0

 000375 000216 000246 001000
1.2

 000241 000134 000179 001000
1.4

 000693 000354 000377 001000
1.6

 001269 000618 000712 001000

PICK TILT OF 1.1 AZIM OF 233
```

INITIAL VALUE OF TILT TAKEN FROM STEREOGRAM (FIG. 3.4)
APPROX. ALIGNED VALUES:
TILT 1.2°
AZIM. 230°

AZIMUTH VARIED IN 5° STEPS FROM 210° TO 250°

AZIMUTH OF 233° SELECTED AS OPTIMUM

TILT VARIED IN 0.2° STEPS FROM 0.6° TO 1.6°

OPTIMUM ALIGNED VALUES
TILT 1.1° AZIMUTH 233°

Figure 3.5 Actual data obtained by varying the azimuth and tilt angles through the values obtained from the stereogram shown in figure 3.4.

or annealing conditions during a given experiment, to allow the data to be readily normalized. The output from the pulse height analyser is printed out by means of the teletype, as shown in figure 3.3(b).

3.5 Electrical Techniques

3.5.1 Room Temperature Hall Measurements

Room temperature Hall measurements were performed on silicon and germanium samples as a function of anneal temperature following the procedure of Johannson et al.[52] This technique uses the space charge region of the p-n junction formed by the implantation to electrically isolate the implanted region from the substrate. The Van der Pauw patterns used for these measurements were mesa etched in the sample following anneal using a 1 HF:20 HNO_3 acid etch. Aluminum was used to contact the implanted area. In all cases, the measuring current was kept an order of magnitude larger than the reverse leakage current. A Keithley model 225 constant current source and a Hewlett-Packard 3450 digital voltmeter were used to make the measurements. A magnetic field strength of 5000 Gauss was used. A detailed description of the technique, together with the formulae and assumptions used, is given in Appendix A.

For silicon carbide samples, aluminum was evaporated on the surface of the sample and a Van der Pauw pattern etched out of the aluminum using photolithographic techniques. The remaining aluminum acted as a mask for the beam during the implantation and was removed prior to annealing. Some of the silicon carbide samples were alloyed to tungsten prior to implantation

in order to electrically contact the substrate.

3.5.2 Low Temperature Hall Measurements

Hall measurements were performed on nitrogen implanted silicon samples at various temperatures using an automated system described in the literature.[53] The system measures the conductivity and Hall voltage of the sample between 4.2°K and room temperature, and punches the data out on paper tape. The data is then used to calculate the concentration, mobility, and resistivity of the sample as a function of temperature. The ionization energy of nitrogen in silicon was calculated from the data.

The Hall samples were fabricated by thermally growing approximately one micron of silicon dioxide on the surface and then diffusing phosphorus contact areas into the silicon through holes opened in the oxide using photolithographic techniques. Following the diffusion, a standard "spider" pattern was opened up between the contacts. The oxide masked the area other than the spider from the beam. Following implantation and anneal, aluminum was used to contact the diffused areas. A sample ready for measurement is shown in figure 3.6.

3.5.3 The C-V Technique

The MOS capacitor (C-V) technique was used to measure the carrier concentration in the silicon samples as a function of anneal temperature to check and confirm the room temperature Hall measurements. In this method, a thin ($\sim$2000 Å) layer of SiO_2 was deposited on the silicon surface by means of the decomposition of a mixture of silane and oxygen. The

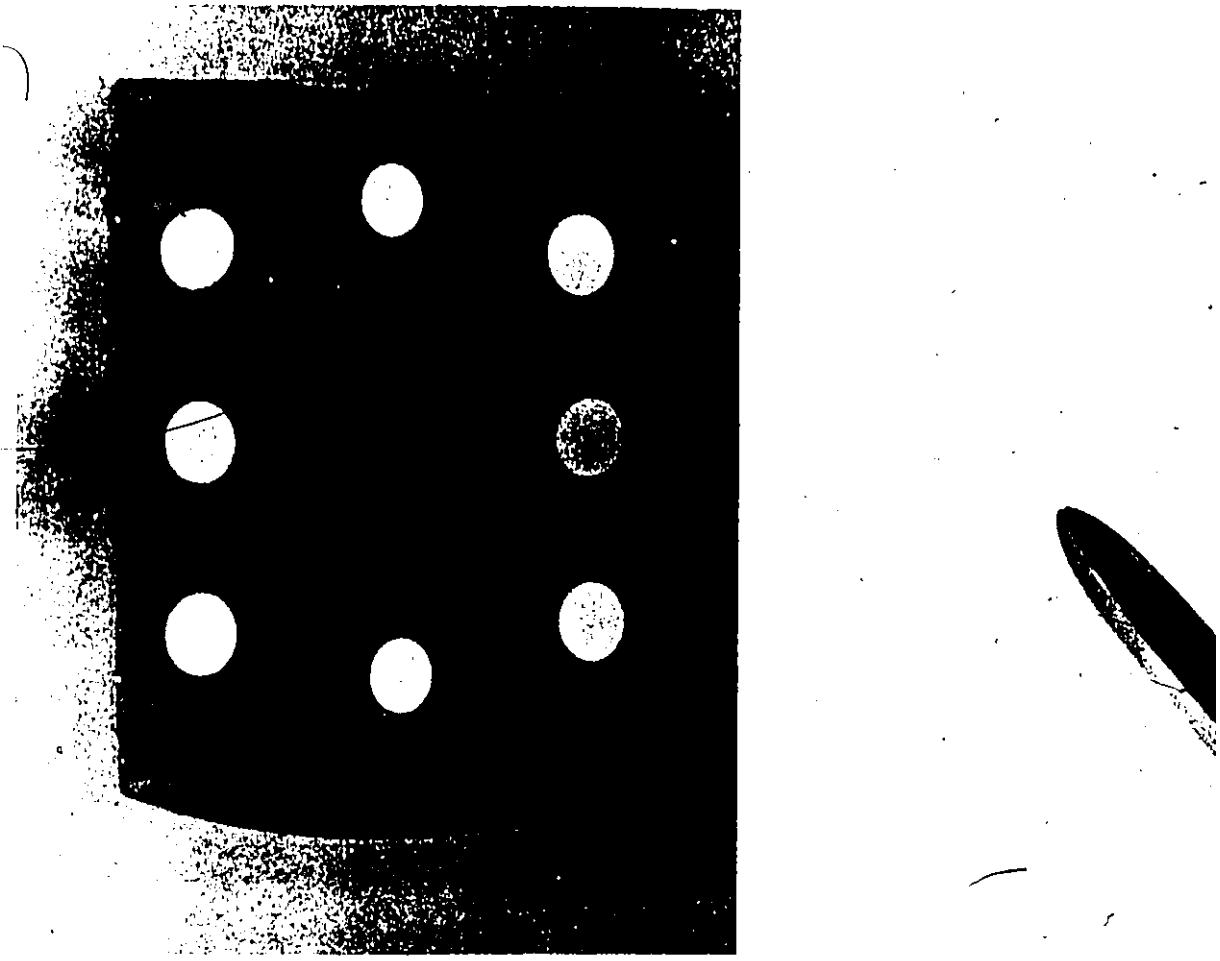

Figure 3.6: A diffused contact Hall Sample

sample temperature was approximately 300°C during this deposition. Aluminum dots 0.020 inch in diameter were evaporated on the oxide surface and the capacitance-voltage relationship of the metal-oxide-semiconductor device was measured. This measurement involves detecting the high frequency small signal capacitance as the dc bias is varied from a region of strong accumulation to strong depletion. The capacitance varies from that of the oxide only, C_{ox} under conditions of strong accumulation, to that of the series combination of the oxide capacitance and the depletion capacitance, denoted C_{min}. A typical capacitance-voltage curve for a sample used in this investigation is shown in figure 3.7. The normalized minimum capacitance (C_{min}/C_{ox}) has been calculated as a function of oxide capacitance (or thickness) with the concentration of the ionized dopant as a parameter. The oxide thickness was determined from the measured value of C_{ox}, the known area of the capacitor, and the dielectric constant of the oxide. Non-implanted samples were oxidized and measured under the same conditions as a control, and the results agreed well with the known concentration of the substrate. This measurement averages the carrier concentration over the maximum depletion width obtained, which is ~1200 Å for nitrogen implanted silicon, assuming $N_D = 10^{17}$ N/cm^3.[54] The technique, which has been fully described in literature[55], and in Appendix B, not only affords a non-destructive method of determining the carrier concentration, but also gives a rapid check on beam uniformity. This is accomplished by measuring the C-V relationship over the implanted area, which can be easily covered with aluminum dots by evaporation through a suitable mask.

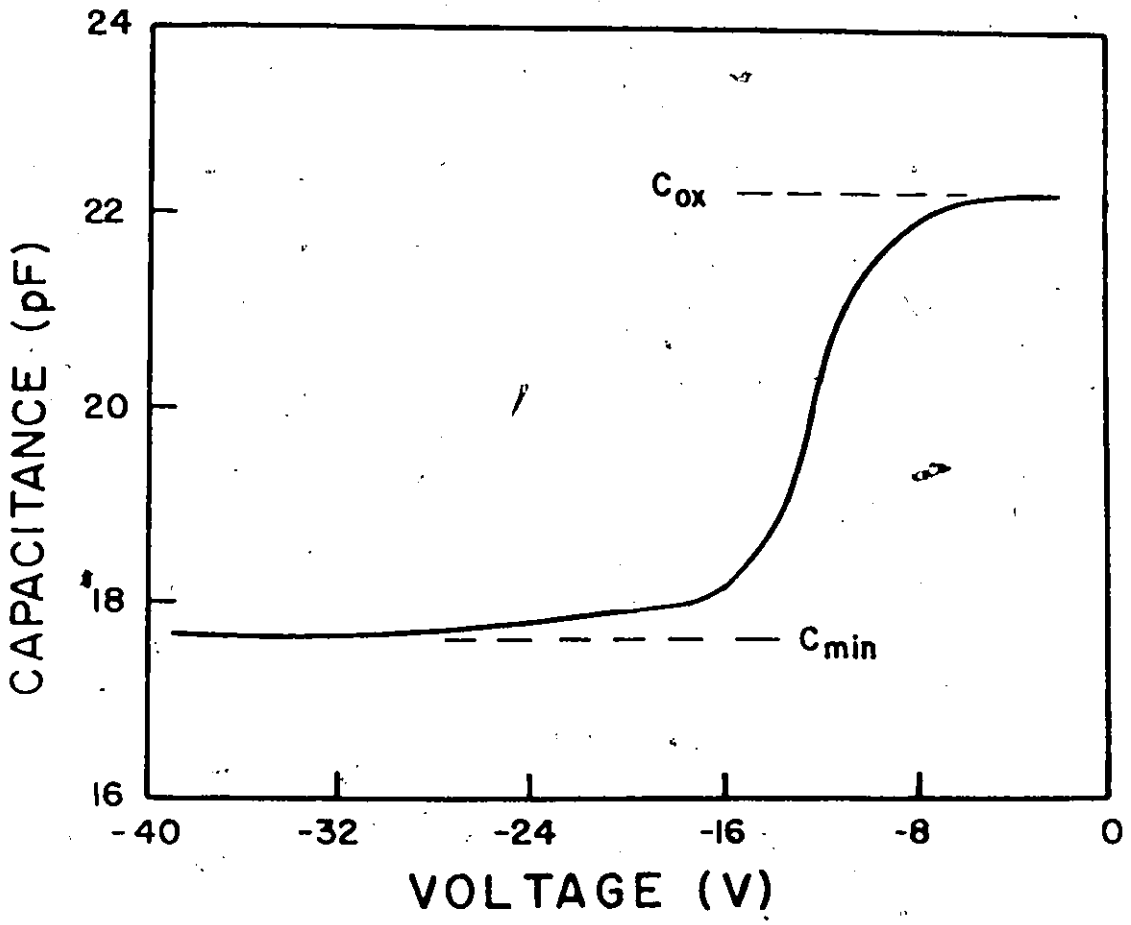

Figure 3.7: A typical capacitance-voltage plot for a nitrogen implanted silicon sample.

3.5.4 Anodization and Stripping Techniques

In order to determine the depth dependence of the dopant nitrogen ions in silicon, anodization and stripping combined with room temperature Hall runs were carried out. The techniques used have been adequately described in the literature[56], and consist of growing an anodic oxide on the silicon surface which is subsequently removed using dilute HF acid.

A circular Van der Pauw pattern was mesa etched in the silicon and contacted with evaporated aluminum. The sample was then mounted in a Teflon holder similar to that described by Crowder.[57] This holder uses a viton "O" ring to define the anodization area, and holds the sample for both the anodization and Hall experiments. Anodization was carried out using a current density of 5 ma/cm^2 in a solution of ethylene glycol, H_3BO_3, KNO_3 and aluminum nitrate to a constant forming voltage of 120 volts. The resulting oxide was stripped in an 8% HF solution. The step thickness was measured by stripping ten layers, measuring the total thickness removed, and calculating the average step size. Reproducible layers of 250 Å could be obtained in this way. Although the step thickness will vary somewhat with the doping of the layer (which usually varies considerably with depth for an implanted layer) it was felt that this was a sufficiently accurate technique for the present investigation.

IV

THE DAMAGE PROPERTIES OF NITROGEN IMPLANTED SILICON

4.1 Introduction

A continuing interest in low temperature ion implantation has appeared in the literature during the past few years. The original motivation for such studies in semiconductors has been the observed correlation between the amount of crystal damage introduced by the implantation and the resulting electrical conversion efficiency following a suitable high temperature anneal. In general, the more extensive the damage in the implanted region (i.e. the closer it approaches an "amorphous" layer), the more effective is the subsequent conversion efficiency during annealing.

Early studies of lattice disorder in the boron-silicon system[5,58] indicate that the dependence on implantation temperature extends well below room temperature. They also show that, for such light ions as boron, rapid annealing can occur during implantation and that this annealing markedly affects both the lattice location of the implanted dopant and the distribution of compensating centers. Eisen and Welch[59] have shown that low-temperature boron disorder depends not only on the total dose, but also on the dose rate.

This chapter presents the results of a damage study on nitrogen implanted silicon. The total amount of lattice disorder and its depth distribution has been measured as a function of implantation temperature (25 - 300°K) and of dose rate (5 - 500 nA/cm^2). Single implants at 80 keV

were used. Since these results were to be compared with the theory of damage distribution presented in chapter II, and since this theory inherently precludes saturation effects, a dose which does not cause total damage was required. Preliminary measurements at 28°K and room temperature for doses of 10^{14} N/cm^2 and 10^{15} N/cm^2, which will also be presented, indicated that 10^{14} N/cm^2 did not cause saturation damage and annealed well. Since this dose complemented the electrical measurements, it was chosen for this study.

It should be mentioned that the damage results presented in this chapter were obtained after the samples had been allowed to return to room temperature, and therefore after some annealing had taken place. Picraux et al[60] have shown that, for the silicon-antimony system, low temperature implantations analysed at room temperature exhibit considerably less damage than when the data are taken in-situ at the implantation temperature. Similarly, studies with boron implants[59] indicate that significant annealing occurs on warming up to room temperature, unless the dose is high enough to render the sample almost totally amorphous. The nitrogen-induced damage behaviour is expected to be quite similar to that induced by boron. Most samples were analysed within twelve hours of the implantation, but in a few cases, several days annealing at room temperature occurred before the backscattering analysis. The data is first presented and compared with theory and then discussed in detail.

4.2 Results

The dependence of the total amount of disorder on implant temperature over the temperature range 30° - 300°K at three different dose rates, 5, 50 and 500 nA/cm^2 is shown in figure 4.1. At all dose rates, the amount of retained damage increases as the implantation temperature is decreased below room temperature, but eventually reaches a maximum around 100 - 140°K and then falls off. This temperature of maximum damage is seen to depend quite strongly on dose rate. For the 50 and 500 nA/cm^2 implants, there is also a suggestion of a second peak at still lower temperatures (i.e. <40°K). These results imply that at least one significant annealing process is occurring during these implantations, even at the lowest temperatures.

Somewhat similar reverse-annealing effects have been observed by Picraux and Vook[22] in their annealing studies of low-temperature (38°K) 100-keV oxygen implants in silicon.

In the temperature range of 60 - 100°K, the total amount of damage retained at low dose rate is considerably greater than for a similar implant at higher dose rate. The relative widths of the disorder peaks do not follow any dose rate pattern, however this may be partly due to room temperature annealing effects, since some samples were kept at room temperature longer than others before analysis. In particular, the scatter in the data for the 50 nA/cm^2 dose rate may be due to annealing effects, since this data had the longest delay between implantation and analysis.

In order to test how well the experimental damage profiles agreed

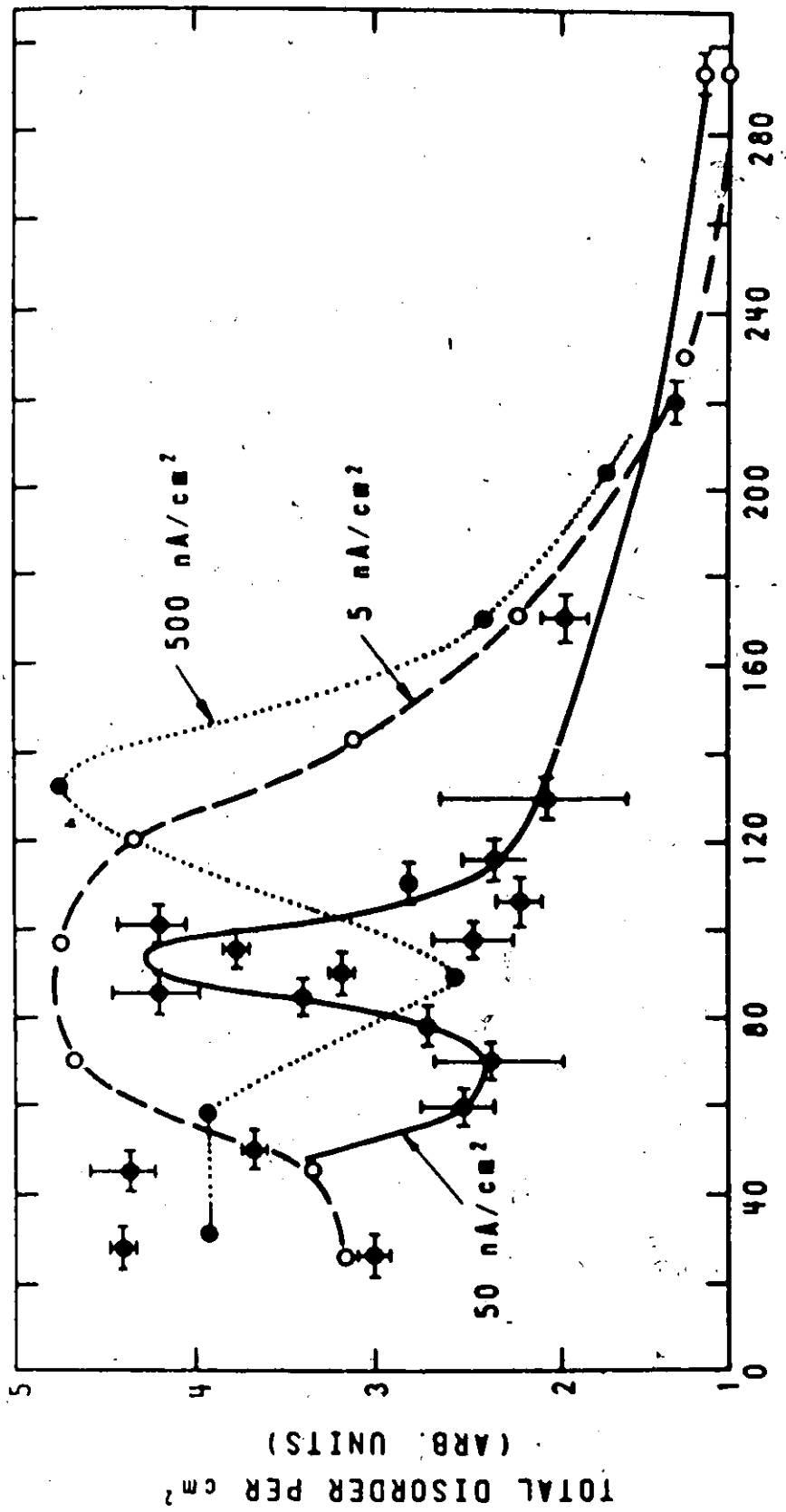

Figure 4.1 The total amount of disorder versus implant temperature at three dose rates: 5, 50, and 500 nA/cm^2.

with the atomic collision theory presented in chapter II, the data for the 5 nA/cm^2, 95°K implant was compared to the damage distribution and nitrogen-ion range distribution as calculated by Winterbon.[16] This particular experimental profile was the most reasonable choice to compare with theory, as these implantation conditions resulted in the greatest amount of retained damage (and hence the least amount of annealing) on warming up to room temperature, as shown in figure 4.1. The results are presented in figure 4.2 where data from two different analysed positions on the sample are shown (• and o). This data was collected and analysed as discussed in chapter III. There is good agreement between the two sets of data, and also between the observed and theoretical distributions, especially near the region of maximum damage. The damage distribution calculated by Brice[19] is also shown in figure 4.2. The two theoretical curves are nearly identical except at shallow depth, where the discrepancy is mainly due to Brice's assumption that secondary recoil atoms have negligible range. Both theoretical curves are based on the energy deposited into atomic processes and do not allow for any annealing.

Although the nitrogen atom distribution is slightly deeper than the maximum in the damage distribution as shown in figure 4.2, most of the implanted ions come to rest well within the limits of the damage produced by the implantation. This has important implications for device fabrication, where maximum damage in the region of the implanted ions may result in enhanced carrier conversion efficiency following anneal.

Figure 4.3 shows the normalized damage profiles at high dose

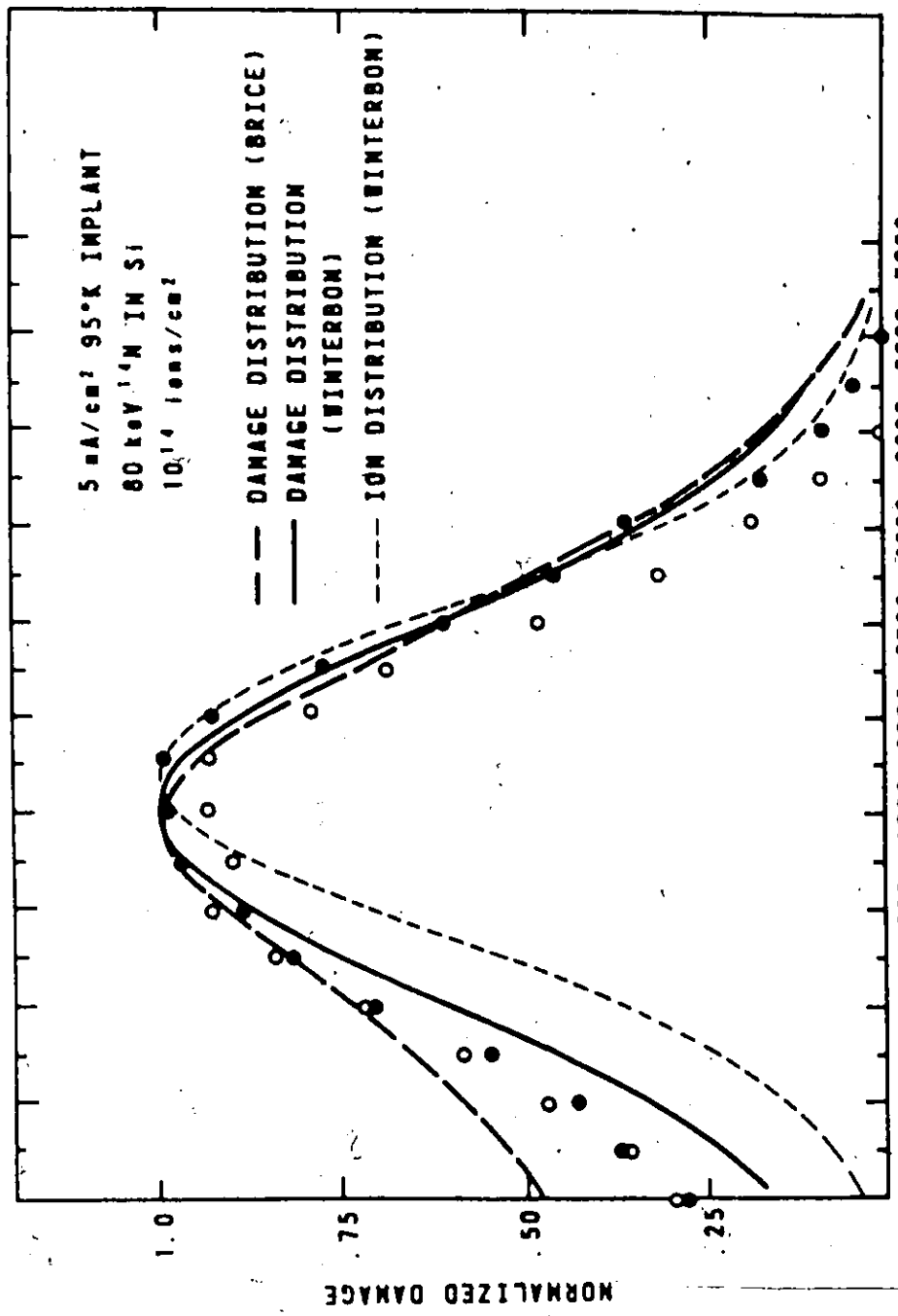

Figure 4.2 Theoretical and experimental damage distribution curves for 80 keV nitrogen ions in silicon.

rate (500 nA/cm^2) for various implantation temperatures. This figure shows that the reduction in total damage when reverse annealing occurs (i.e. the 90°K curve) is not symmetric, but is accompanied by a large truncation of the profile on the surface side of the distribution. (The 30°K and 60°K curves are equivalent, within experimental accuracy.) If this annealing were due strictly to thermal effects, a symmetrical reduction of the damage profile would be expected with little shifting of the peak position. It is true, of course, that annealing effects near the surface may differ somewhat from the bulk and thus create a small asymmetry in the profile. However, the damage level in these samples is so heavy (even near the surface) that the mean path length for a mobile defect to find a damage cluster is no more than ~10 - 20 Å, therefore any perturbation in the profile due to the proximity of the surface should be restricted to a much shallower depth than that observed in figure 4.3.

The profile data at 5 nA/cm^2 (figures 4.4 and 4.5) show quite clearly that this asymmetric truncation of the damage profile is not a surface phenomenon, but that it is associated in some way with the reverse annealing region. At high implantation temperatures (i.e. ≥95°K, figure 4.4), no significant peak shifting can be detected, even though much of the damage has annealed away during the implantation. On the other hand, at 26°K (figure 4.5) a similar amount of annealing produces a very pronounced peak shift and the damage profile does not approach the theoretical distribution until a depth of ~2200 Å.

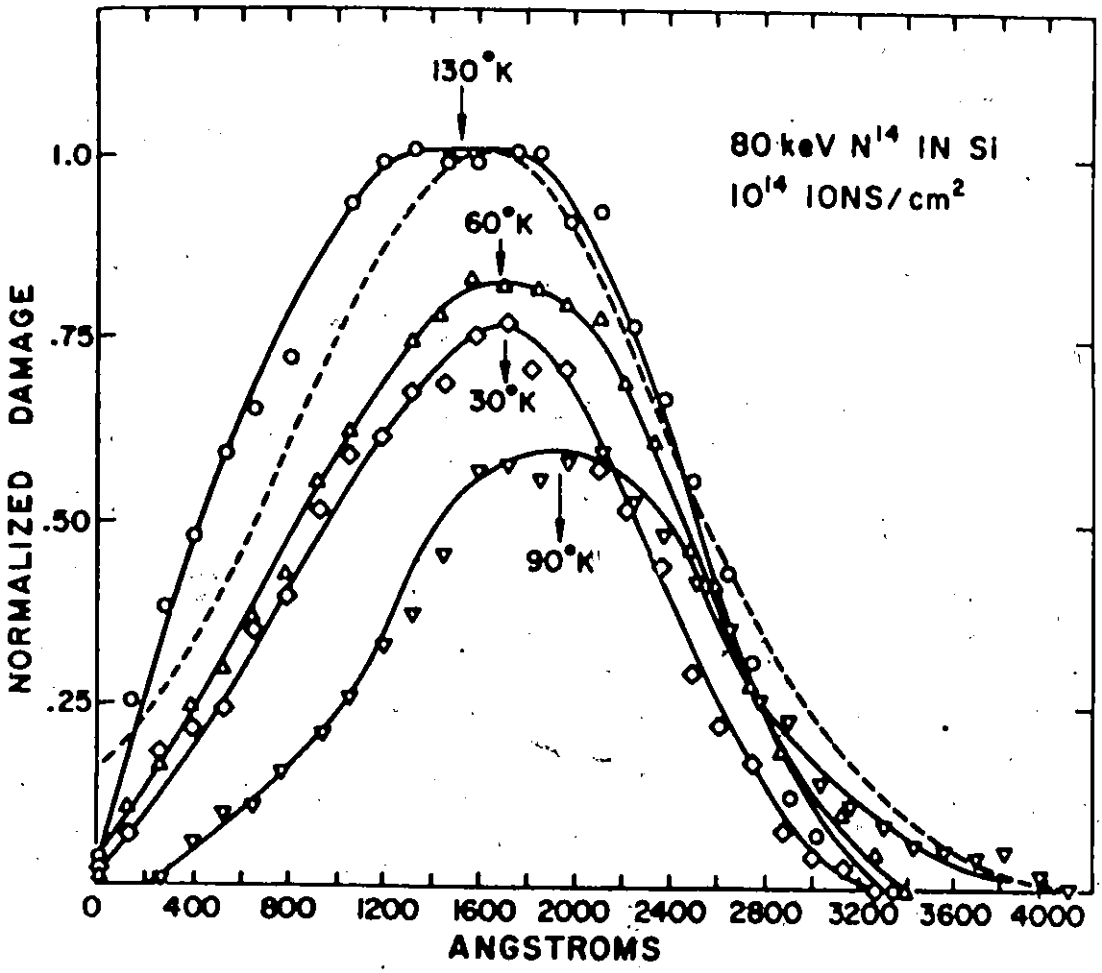

Figure 4.3 The normalized damage profile for the 500 nA/cm^2 implant, as measured by backscattering analysis with 2-Mev helium.

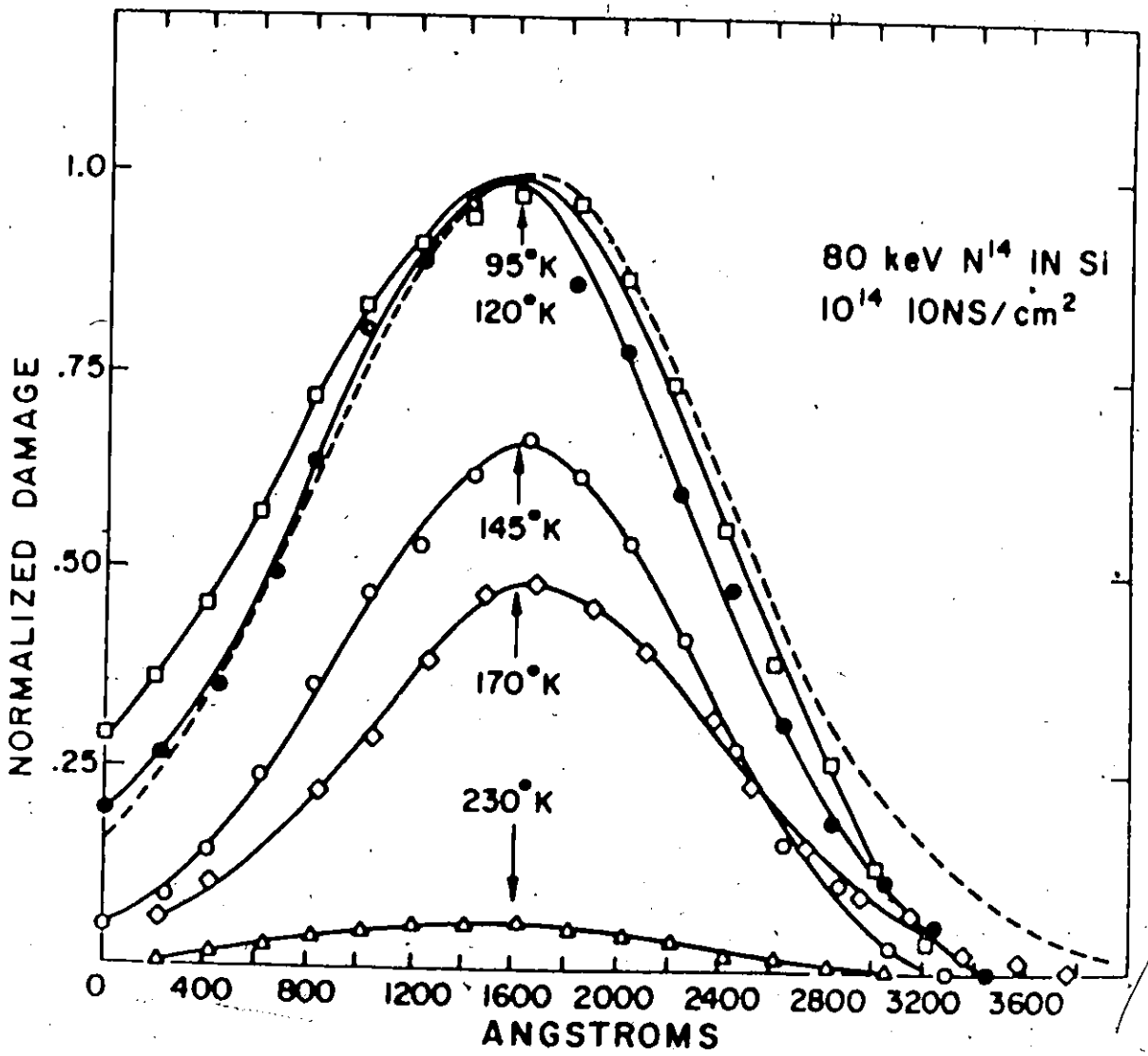

Figure 4.4 The normalized damage versus depth for the 5 nA/cm^2 implant, as measured by backscattering analysis with 2-MeV helium.

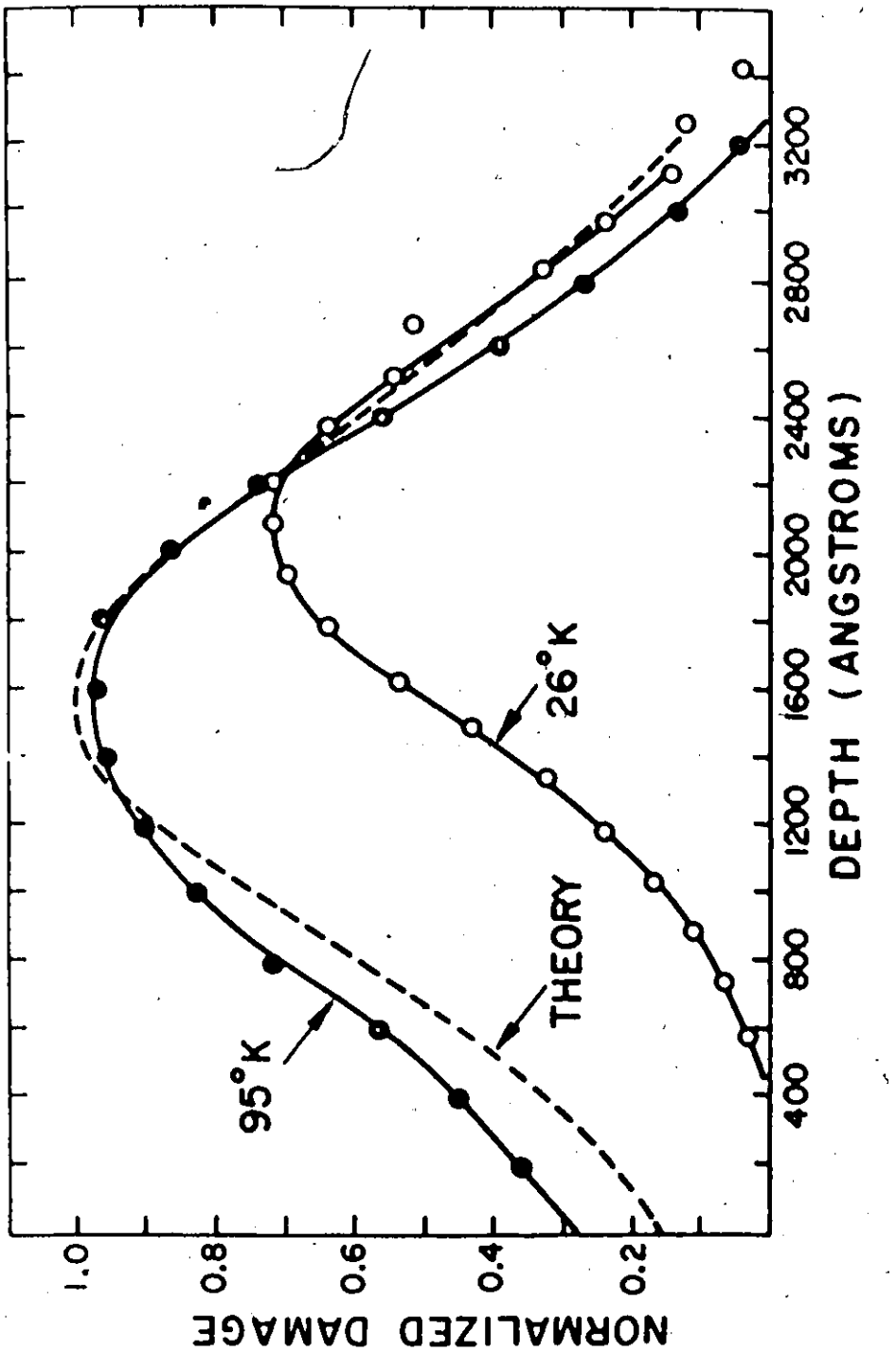

Figure 4.5 A comparison of damage profiles for 5 keV/cm^2 implants at 95°K and at 26°K. The theoretical profile is due to Winterbon.

4.3 Discussion

There are several models[61,62] from which the total amount of ion bombardment damage of silicon can be estimated. In all cases, these models predict that the total amount of damage will increase as the temperature is lowered until a maximum value is achieved, whereupon the observed damage should remain constant for any further reductions in temperature. The maximum disorder is expected to occur at that temperature where the migration of vacancies or other defects is no longer possible.

The present study of nitrogen implantations in silicon has shown that the amount of retained damage increases as the implantation temperature is lowered, but that it eventually reaches a maximum in the temperature region 80 - 150°K and then decreases for lower temperatures (figure 4.1). Also, the character of the maximum and the associated decrease in damage at lower temperatures depend strongly on the dose rate. Consequently, some sort of mobile defect(s) exists in this 30 - 70°K temperature range. Picraux and Vook[22] have described various defects known to occur in silicon and have discussed which of these might be responsible for beam-enhanced annealing. They suggest that negative vacancies (V^-), formed during implantation from ionization phenomena, are directly involved in the low-temperature lattice reordering†.

† EPR measurements in silicon have shown that the isolated vacancy can exist in several different states: the neutral state V°, positive state V^+, negative state V^-, and the double negative state $V^=$[63]. Each of these states has its own activation energy for migration, with the V^- and $V^=$ states being more mobile than V°.

An enhancement of the annealing due to the ionization created by the beam would have an important influence on the relative amount of lattice reordering which occurs during implantation. Such an effect would strongly influence the dose rate and implantation temperature dependence of the disorder.

The main features of the damage profile versus temperature curves shown in figure 4.1 can be explained, at least qualitatively, using some of the known properties of V^0 and V^- vacancies in silicon. The high temperature side of the main peak could be attributed to the freeze-out of the neutral V^0 vacancy, while the corresponding side of the lower-temperature peak (seen in the 50 and 500 nA/cm^2 implants) could be a similar freeze-out of the more mobile negative vacancy. The reverse annealing behaviour on the left hand side of the main peak may be attributed to thermal instability of the mobile (V^-) defect: for example, in this temperature region the negative vacancy may dissociate rapidly into a neutral (immobile) vacancy and an electron before it is able to accomplish much annealing. Since the rate of formation of V^- depends not only on the neutral V^0 concentration but also on the ionization density during implantation, one might expect the relative importance of V^--assisted annealing to increase strongly with dose rate. This in turn would cause the temperature region for reverse annealing (i.e. the low-temperature side of the main peaks in figure 4.1 to increase with dose rate - as is indeed the case.

One interesting test of the importance of such ionization-induced annealing effects is to examine the depth distribution of the

damage profiles. An example of this is given in figure 4.5 for two cases (i) at 26°K where ionization induced annealing is thought to dominate and (ii) at 95°K where it is assumed to be absent. As each 80 keV nitrogen ion penetrates the silicon crystal, a certain fraction of its incident energy is expended in electronic excitation; the remainder goes into nuclear collisions, producing recoil atoms which in turn create more electronic excitation, more nuclear collisions and so on. The amount of energy lost in electronic processes $\eta(E)$ dominates at higher energies (i.e. in the early stages of slowing down), but eventually the energy lost into atomic recoil processes $\nu(E)$ becomes the major energy loss process. The ratio of energy loss in these processes $(\eta(E)/\nu(E))$ for 80 keV nitrogen in silicon as a function of depth has been shown in chapter II, figure 2.6. It can be seen from this figure that near the surface of the crystal, a much larger amount of energy is deposited into electronic excitations, but that at depths greater than $\sim$1000 Å, atomic recoil processes dominate.

Thus, if ionization phenomena were responsible for the enhanced annealing, a much stronger reduction of the damage distribution should occur near the surface. This preferential reduction of the surface side of the distribution will result in a skewing of the damage profile in such a way as to make the peak position of the damage appear to move towards deeper depths, as was indeed observed in figure 4.5 for the 5 nA/cm^2 implants and in figure 4.3 for the 500 nA/cm^2 implants.

No further interpretation is offered at this time. Additional measurements, with the backscattering analyses being made "in-situ" at the implanted temperature, are required before a more detailed explanation is attempted. This is not possible with the present accelerator facilities.

4.4 The Annealing Characteristics of Nitrogen Damaged Silicon

The results presented in the previous sections have shown how the amount of damage caused by the implantation of nitrogen into silicon varies as a function of implantation temperature and dose rate. It is also important, especially for device fabrication, to have some knowledge of how the silicon crystal recovers following high temperature annealing treatments. To obtain this information, silicon samples were implanted at 28°K and room temperature to total doses of 1×10^{14} and 1×10^{15} N/cm^2 using a dose rate of 5 nA/cm^2. The damage caused by the implantation prior to anneal and as a function of anneal temperature was measured by the backscattering technique. All anneals were conducted in vacuum for 10 minutes.

Figure 4.6 presents the results for the 1×10^{14} N/cm^2 implants at both 28°K and room temperature. To within the sensitivity of the backscattering technique (10^{-3} atomic fraction), good regrowth of the damaged layer is accomplished by anneals to ~700°C, for both the 28°K and the room temperature implantations.

The results obtained for samples implanted at 28°K to a total dose of 1×10^{15} N/cm^2 are shown in figure 4.7. The damage caused by

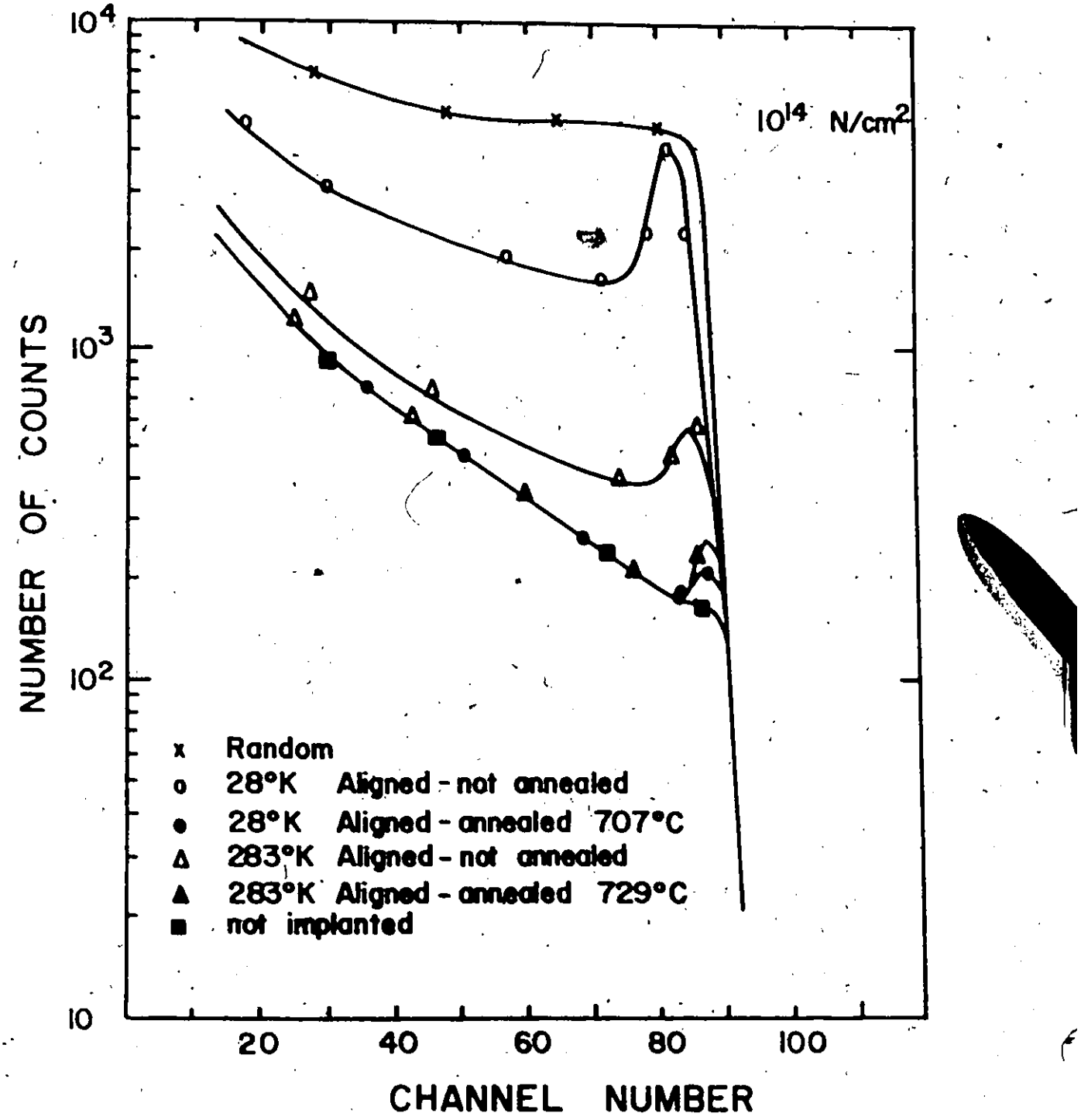

Figure 4.6 The backscattering spectra for 10^{14} N/cm^2 implanted into silicon at 28°K and 283°K.

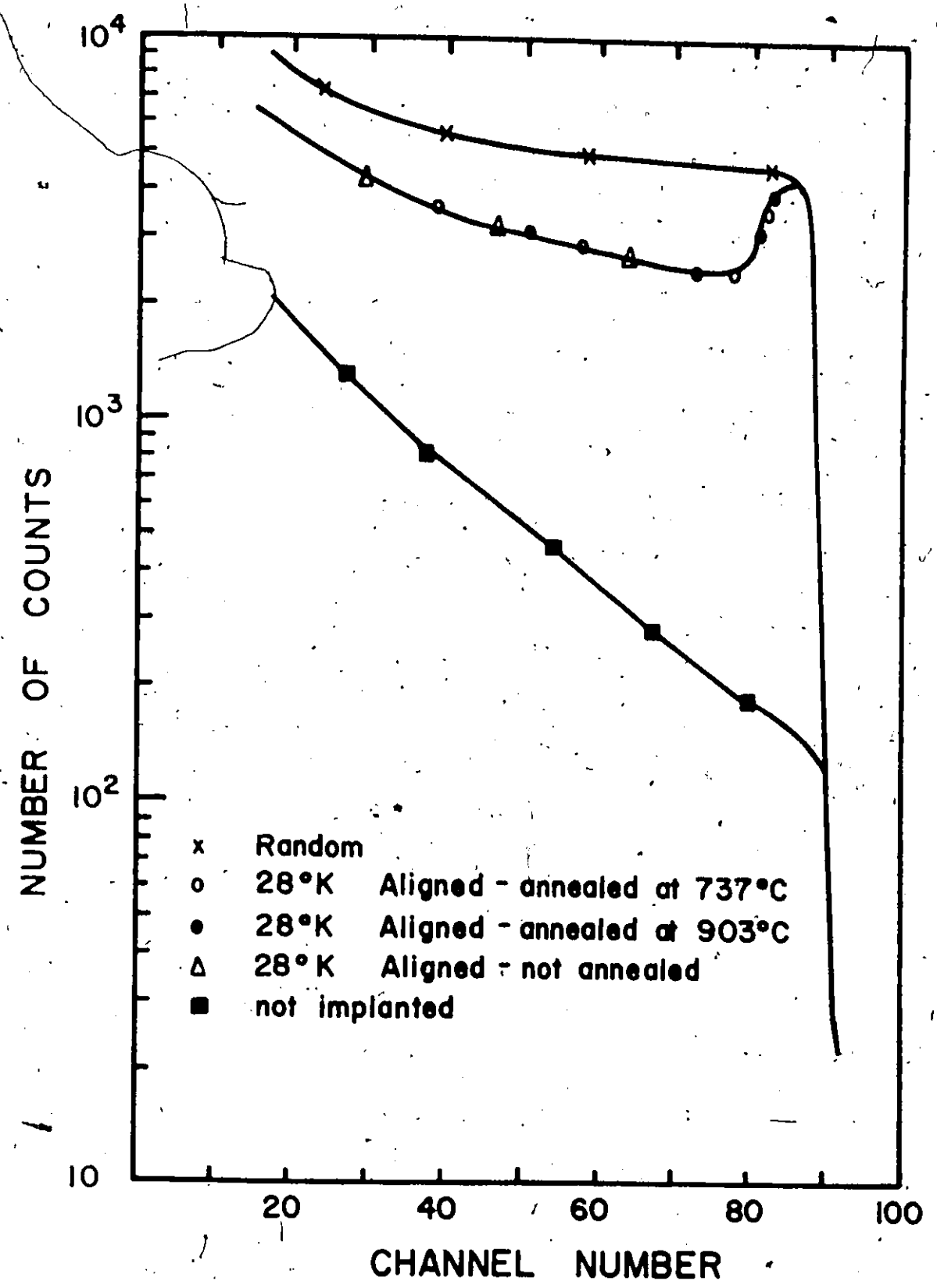

Figure 4.7 The backscattering spectra for 10^{15} N/cm^2 implanted into silicon at 28°K.

these implantation conditions does not anneal even following anneals to ~900°C. The results for room temperature implants to the same dose are shown in figure 4.8. The damage is observed to anneal well following anneals at 737°C, with a peak remaining in the region of maximum damage. However, annealing at higher temperatures causes this damage peak to regrow. This suggests that poor crystal structure, perhaps caused by a different stoichiometry, exists at the mean nitrogen damage depth.

The results of these annealing experiments indicate that any electrical behaviour observed in nitrogen implanted silicon may depend critically on the implantation and annealing conditions, especially for doses higher than 1×10^{14} N/cm^2.

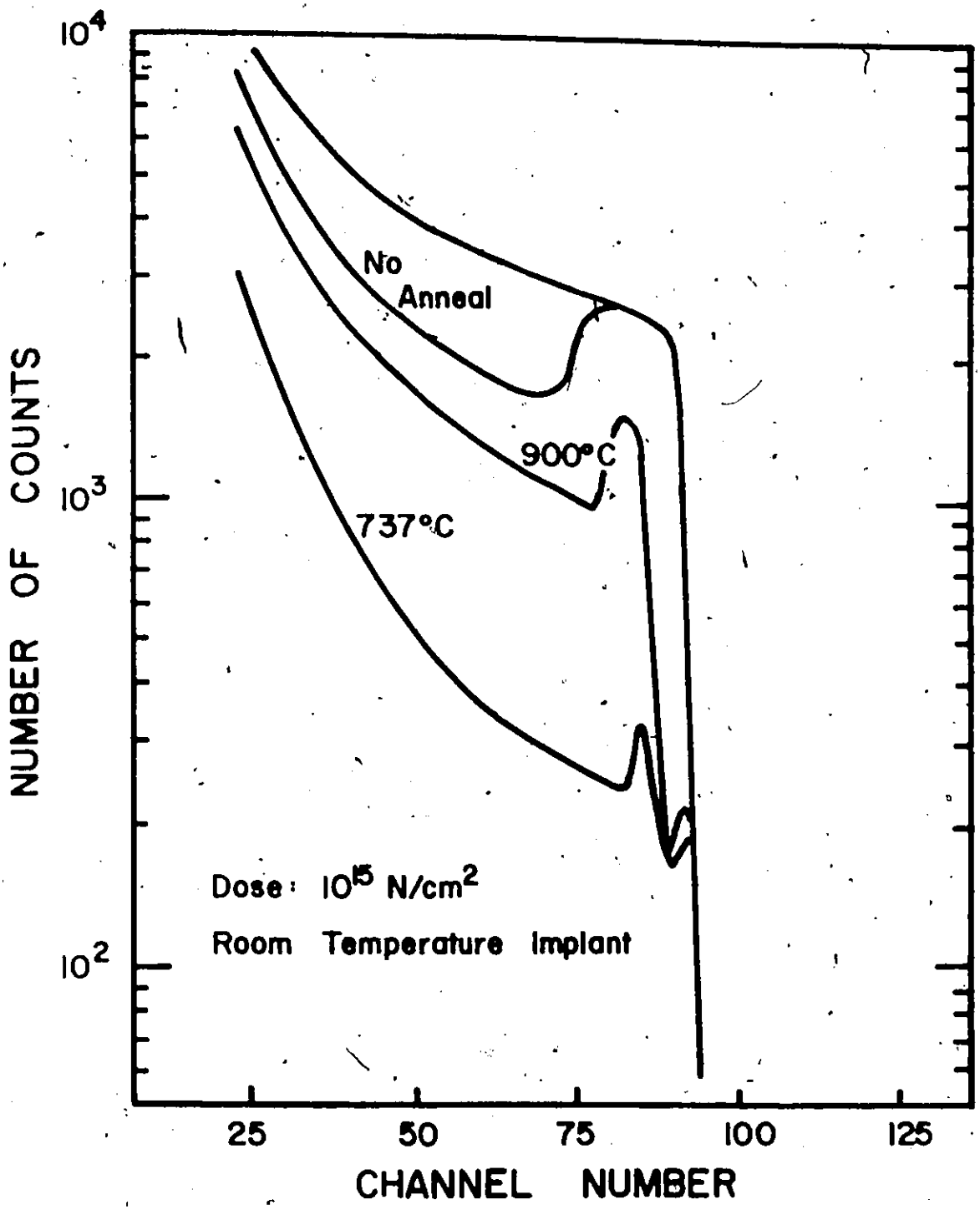

Figure 4.8 The backscattering spectra for 10^{15} N/cm^2 implanted into silicon at 283°K.

V

The Electrical Properties of Nitrogen Implanted Silicon

5.1 Introduction

This chapter presents the results of electrical measurements performed on nitrogen implanted silicon. Following a review of previous work on the nitrogen-silicon system, the data will be presented and then discussed.

The most extensive experiments with nitrogen implanted silicon to date have been those of Zorin et al.[3] They examined 15 ohm-cm silicon implanted at room temperature to a total dose of 6.2×10^{14} N/cm^2 and observed donor-like activity following anneals in the temperature range of 700-900°C. Zorin et al attributed the observed activity to the donor behaviour of nitrogen, although the measured concentration never exceeded 1% of the implanted nitrogen ions. By fitting a theoretical curve to their concentration data, a donor ionization energy of 0.045 eV was obtained. Roughan et al[2] have examined 100 ohm-cm <111> silicon implanted with nitrogen to doses from 10^{12} to 5×10^{14} ions/cm^2. The implants were performed at room temperature and they obtained donor ionization energies of 0.033 to 0.044 eV, in good agreement with Zorin et al. Roughan states that their annealing conditions gave 100% carrier conversion efficiency at 1200°C; however, for temperatures below this, they were unable to get the carrier concentration to approach the implanted nitrogen concentration.

Kleinfelder[64] has examined hot implants (625°C) of nitrogen in 1 ohm-cm material, and found a donor activation energy of 0.142 eV. Schwuttke et al[4] have examined high energy implants (2 MeV) where the nitrogen formed a buried layer about 2 microns from the surface. They observed polycrystalline and amorphous regions for doses of 6.5×10^{16} ions/cm^2 and report pockets of Si_3N_4 in the implanted region. This highly strained and disordered layer commences some rearrangement for anneal temperatures of about 1000°C. Roosild et al[65], have examined the formation of junctions in silicon using nitrogen ions in the energy range from 1 to 2.5 MeV. They found the implanted region to be n-type by using a thermal probe and observed junction depths by means of junction staining. The conductivity of the nitrogen implanted region was found to be low, although they did not state how many of the implanted ions had become electrically active. Cianfrone[66] has measured junction depths for nitrogen implanted silicon following 300°C anneals, while Roosild et al have monitored the junction depth for anneal temperatures of 700°C and 900°C, and found large junction movement to occur in the implantation direction between the two annealing conditions. Recently, Nii et al[67] have stated that they have "confirmed" the existence of an n-type layer following nitrogen implantation into silicon at 10 keV. Table 5-1 summarizes the previous work on nitrogen implanted silicon.

This review of the published results on nitrogen implanted silicon indicates that the electrical behaviour of this ion is not well understood. Although quite a few investigators have studied the nitrogen-silicon system, none has made any attempt to understand the role of nitrogen in silicon, and

TABLE 5.1

PREVIOUS WORK ON NITROGEN IMPLANTED SILICON

Author	n-Type Activity Observed - Attributed to	Dose (cm^{-2})	Implant Temp	Ionization Energy	Anneal Range (°C)	Substrate
Ferber [68] (1963)	Yes	10^{13}-10^{15}	R.T.-300°C	---	500	1Ω-cm
Zorin et al [3] (1966-68)	Yes-Subst. N	6.2×10^{14}	R.T.	0.045 eV	700-900	15Ω-cm <111>
Kleinfelder [64] (1967)	Yes-Subst. N	4×10^{14}-10^{15}	625°C	0.142 eV	625	1Ω-cm <111>
Schwuttke et al [4] (1967)	Yes-Subst. N	$\leq 10^{15}$	R.T.	---	600-1000	2Ω-cm <111>
Cianfrone [66] (1968)	---	10^{15}-10^{16}	R.T.	---	300	3-50Ω-cm <111>
Roughan et al [2] (1968)	Yes-Subst. N	10^{12}-5×10^{14}	R.T.	0.033-0.044 eV	$\leq$ 1200	100Ω-cm <111>
Niu et al [67] (1972)	Yes-Subst. N	6×10^{14}	R.T.	---	850	20-30Ω-cm <111>

in particular, to determine whether it is substitutional nitrogen or a nitrogen induced defect that is responsible for the observed electrical behaviour. All the investigators have assumed that the nitrogen is substitutional, and quote an ionization energy which is supposed to justify this assumption. None however, present either the data or calculation of this ionization energy, with the exception of Zorin et al, who calculates the ionization energy by fitting a theoretical curve to data obtained from measurements performed from 100°K to 300°K. This is much too small a temperature range to determine the ionization energy with any accuracy. All the previous work does however have some results in common: (a) the implantation of nitrogen into silicon does produce a layer with donor-like characteristics and (b), the number of resulting "carriers" is much less than the number of implanted ions. These two results are all that can be reliably inferred from the previous work.

To electrically characterize an ion-implanted system, it is usually sufficient to determine the following information:

- -the anneal temperature at which the number of carriers/cm^2 reaches a maximum
- -the relation between the maximum number of carriers/cm^2 and the implanted dose (the electrical conversion efficiency)
- -the carrier mobility and the "activation energy" of the implanted ion.
- -the influence of the substrate temperature during implantation on the subsequent annealing behaviour
- -the depth distribution of the free carriers

For the nitrogen-silicon system, it is also necessary to determine whether the electrical activity in the implanted layer is due to substitutional nitrogen or to damage centers or trap levels which may be created and electrically active as a result of the implantation and anneal. This

chapter presents the results of measurements performed on nitrogen implanted silicon to determine this information.

The most common technique for measuring the carrier concentration and mobility in ion implanted layers is room temperature Hall effect and sheet resistivity measurements. This technique has been fully described by Johannson et al[52], and consists of implanting ions of one conductivity type into the opposite conductivity type substrate and using the space charge region of the p-n junction so formed to electrically isolate the implanted layer from the substrate. Since good quality, low leakage diodes must be produced in order to use this technique, the characteristics of diodes formed by implanting nitrogen into p-type substrates were initially investigated. Not only does this determine whether or not the layer isolation technique may be applied, but the study of the junction characteristics may also help in understanding the electrical properties of the layer.

Once diode behaviour was observed and it was realized that implanted nitrogen did produce electrical activity, MOS capacitor-voltage measurements were performed. The implantation conditions for these samples were those found in Chapter IV to produce maximum damage. The motivation for selecting these implantation conditions was to determine whether total damage resulted in enhanced electrical activity following anneal. The results of these C-V measurements were confirmed with room temperature Hall effect and sheet resistivity data. Similar measurements were performed using the same implantation conditions but with float-zoned silicon to determine if the oxygen content was affecting the results. If an oxygen complex or the presence of oxygen is affecting the electrical behaviour of the implanted

nitrogen, lowering the oxygen concentration from $10^{18}/cm^3$ (Czochralski silicon) to $2 \times 10^{16}/cm^3$ (float-zoned silicon) should show this. Various resistivity p and n type substrates were used in order to determine if the position of the Fermi level in the substrate or the size or other properties of the substrate dopant atom was influencing the observed behaviour of the implanted nitrogen. MOS capacitor-voltage measurements were also performed on samples implanted with neon under identical conditions to those mentioned above for nitrogen, to ensure that the electrical activity observed (even if it is due to defects) was unique to nitrogen implantation. Low temperature Hall measurements were used to obtain an ionization energy for the conduction mechanism and to gain information about the amount of compensation present in the implanted layer. Implantation to a fixed dose for various implantation temperatures was performed to see whether the amount of damage caused by the implantation affected the electrical conversion efficiency. The results of these measurements along with I-V and C-V data for ion implanted diodes will be presented in the sections to follow, and an interpretation of the role of nitrogen in silicon will be presented in the conclusion.

5.2 Junction Characteristics

P-N junctionswere formed in 1 and 10 ohm-cm boron doped silicon. The implantations were performed under conditions found from the damage study to produce maximum damage - i.e. at 100°K and a dose rate of 5 nA/cm^2. Sequential implants at 80 and 40 keV in a dose ratio of 3:1 were used in

order to produce a broad, fairly uniform distribution of nitrogen. Diode behaviour was monitored as a function of anneal temperature, and it was found that the junction characteristics did not change for anneals above ~750°C. The I-V relations for diodes annealed at 825°C are shown in figure 5.1 (for a 5-10 ohm-cm substrate) and figure 5.2 (for a 1 ohm-cm substrate). In both cases, the reverse breakdown occurs at either ~90 volts or ~50 volts, which agrees with the expected value for avalanche breakdown in the bulk 5 - 10 or 1 ohm-cm substrates.(54) Although the reverse leakage current of the diode formed in the 10 ohm-cm material shown in Fig. 5.1 does not saturate well, this is not true for all the diodes formed with this material. Fig. 5.1 represents a diode selected at random. The 1 ohm-cm diode reverse current saturates before breakdown, as shown in figure 5.2. The electrical contact to both the implanted layer and the bulk substrate was made with evaporated aluminum, and although good ohmic contacts could be made to both the 10 and 1 ohm-cm substrates, it was much easier to form reproducibly good contacts to the more heavily doped 1 ohm-cm material. For this reason, the 1 ohm-cm material was used to form diodes for C-V measurements and for a more detailed I-V study.

The forward and reverse current-voltage characteristics of a diode formed by implanting nitrogen into 1 ohm-cm silicon measured at 77°K and room temperature are shown in figure 5.3 and figure 5.4 respectively. At room temperature, the forward current-voltage behaviour is closely approximated by

$$J = J_s(\exp \frac{qV}{nkT} - 1) \qquad (5.1)$$

where $n = 2$ and J_s is the saturation current density. The value of 2 for n

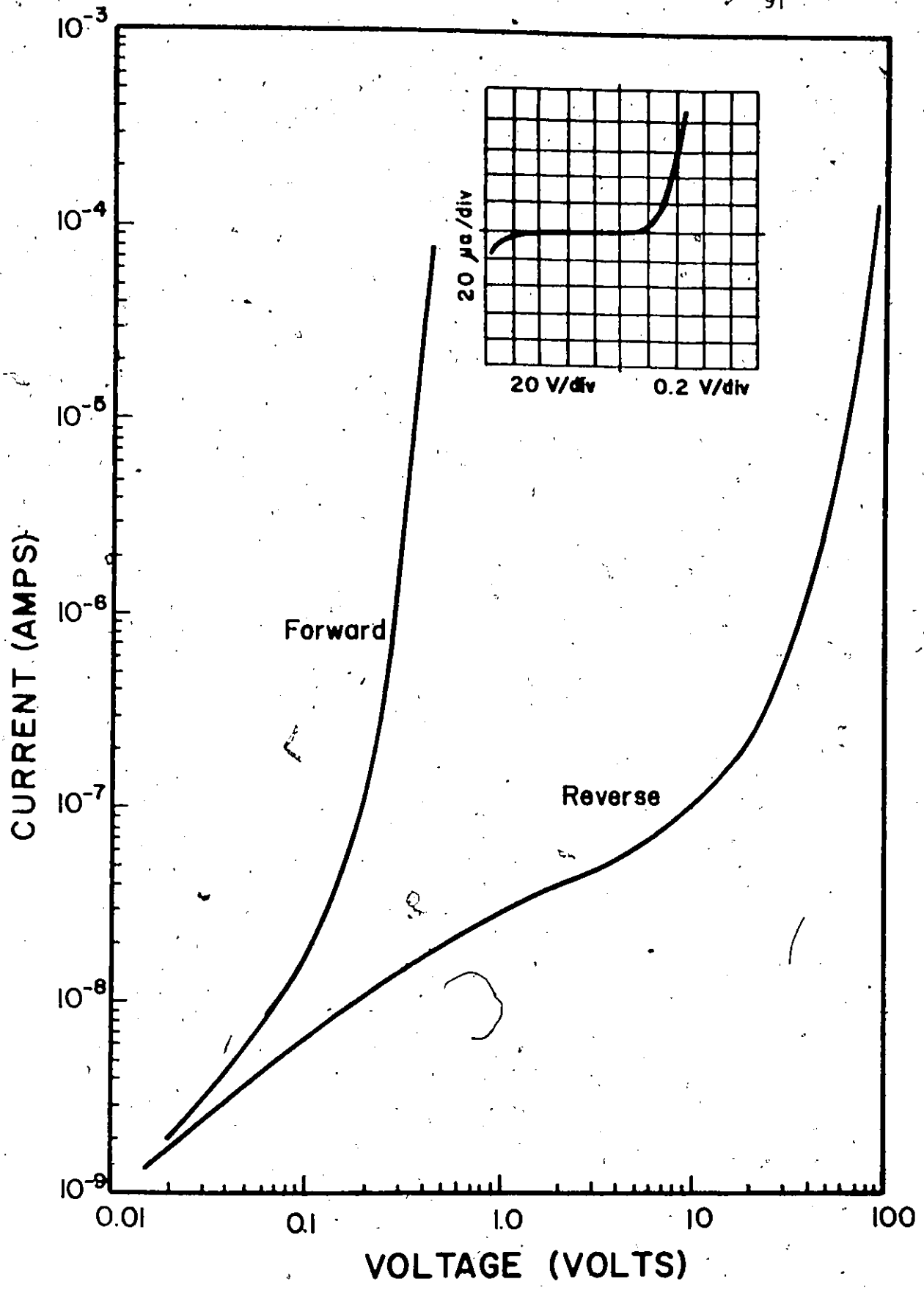

Figure 5.1 The I-V Characteristics of a nitrogen implanted diode. The substrate is 5 - 10 ohm-cm silicon. The dose is 1.4×10^{14} N/cm^2.

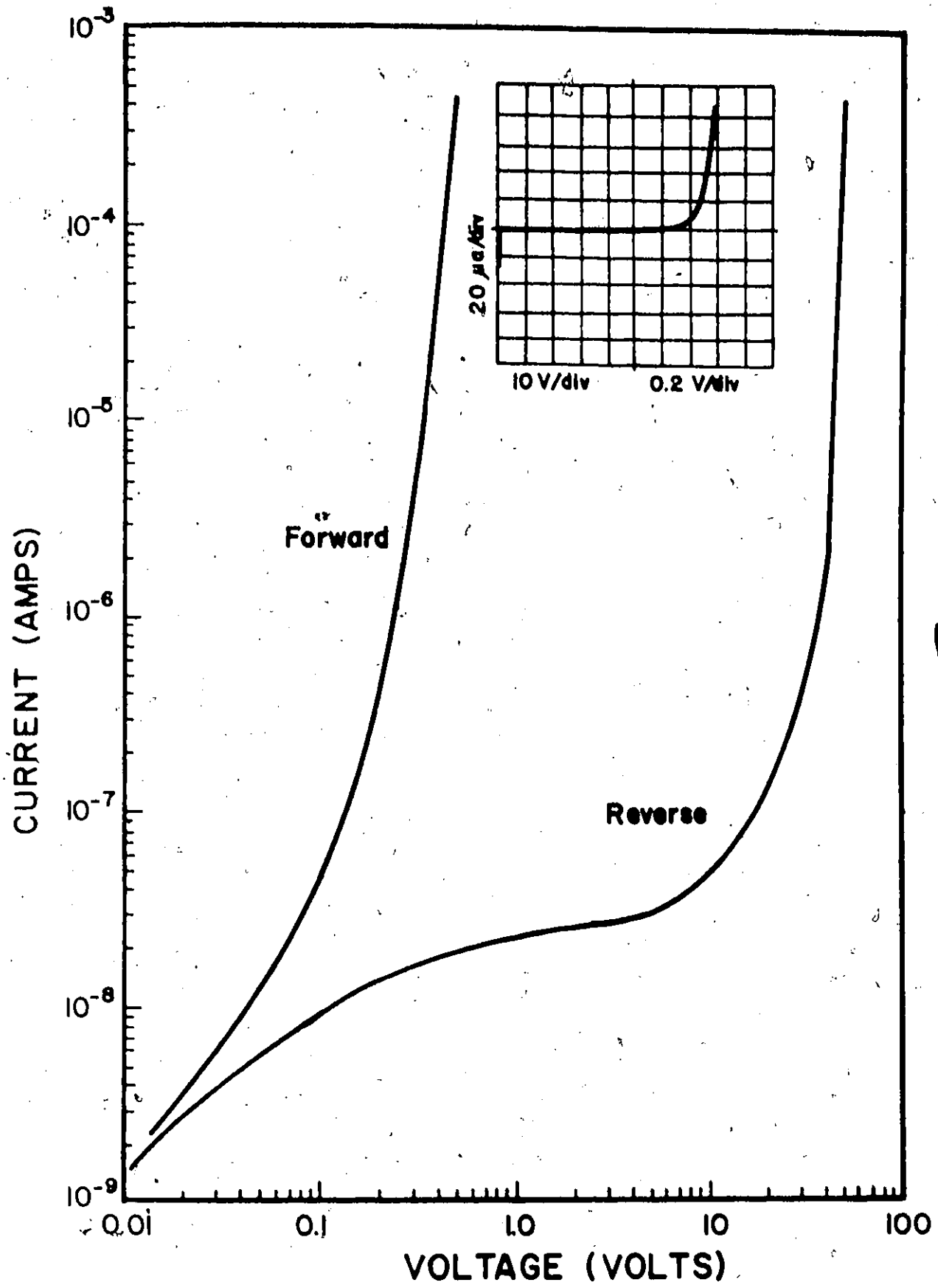

Figure 5.2 The I-V characteristics of a nitrogen implanted diode. The substrate is 1 ohm-cm silicon. The dose is 1.4×10^{14} N/cm^2.

implies that the current flow is predominantly due to recombination in the space charge region. Extrapolation of the straight line approximation to the curve at zero voltage yields a value of 10^{-7} A/cm^2 for the saturation current density at room temperature. The data at 77°K shows a much higher value of n($\sim$5). Although these diodes are mesa etched and show considerable reverse leakage, as shown in figure 5.4, it would be expected that the diode would behave well at low temperatures. It is possible that contact effects at low temperatures are introducing a significant series resistance which causes n to appear high.*

The reverse characteristics for the nitrogen diode are shown in figure 5.4. The leakage current is much lower at 77°K than at room temperature, as would be expected, and the breakdown voltage does not depend significantly on temperature, but is slightly lower, as expected.

The capacitance-voltage characteristic of a diode fabricated in one ohm-cm material is shown in figure 5.5. The curve shows a linear $1/C^2$ versus voltage dependence which is characteristic of an abrupt junction. A $1/C^3$ versus voltage dependence, which is characteristic of a linearly graded junction, was also attempted, but the result did not yield a straight line. The abrupt nature of the junction agrees well with what would be expected from the electrically active carrier profile to be presented later.

A calculation of the carrier concentration of the bulk substrate material from the slope of the $1/C^2$ versus V plot indicates an acceptor concentration of $\sim 6 \times 10^{15}$ /cm^3 corresponding to a resistivity of $\sim$2.5 ohm-cm. No tolerances on the one ohm-cm resistivity were given by the crystal supplier. The capacitance of the diode at zero volts and at 10 volts confirms

*This effect may also be caused by surface effects.

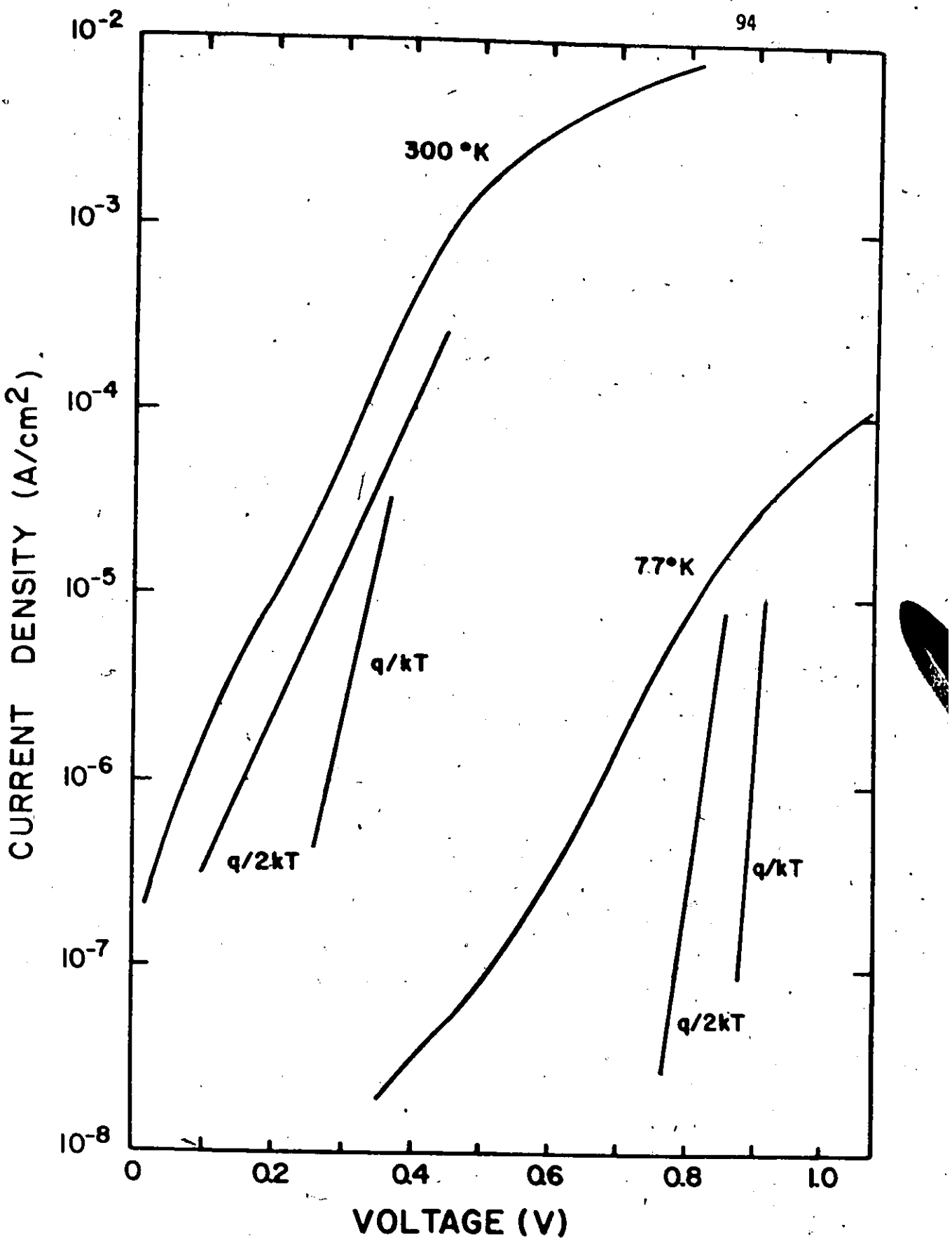

Figure 5.3 The forward biased I-V relationship for a nitrogen implanted diode measured at 300°K and 77°K. The substrate is 1 ohm-cm silicon.

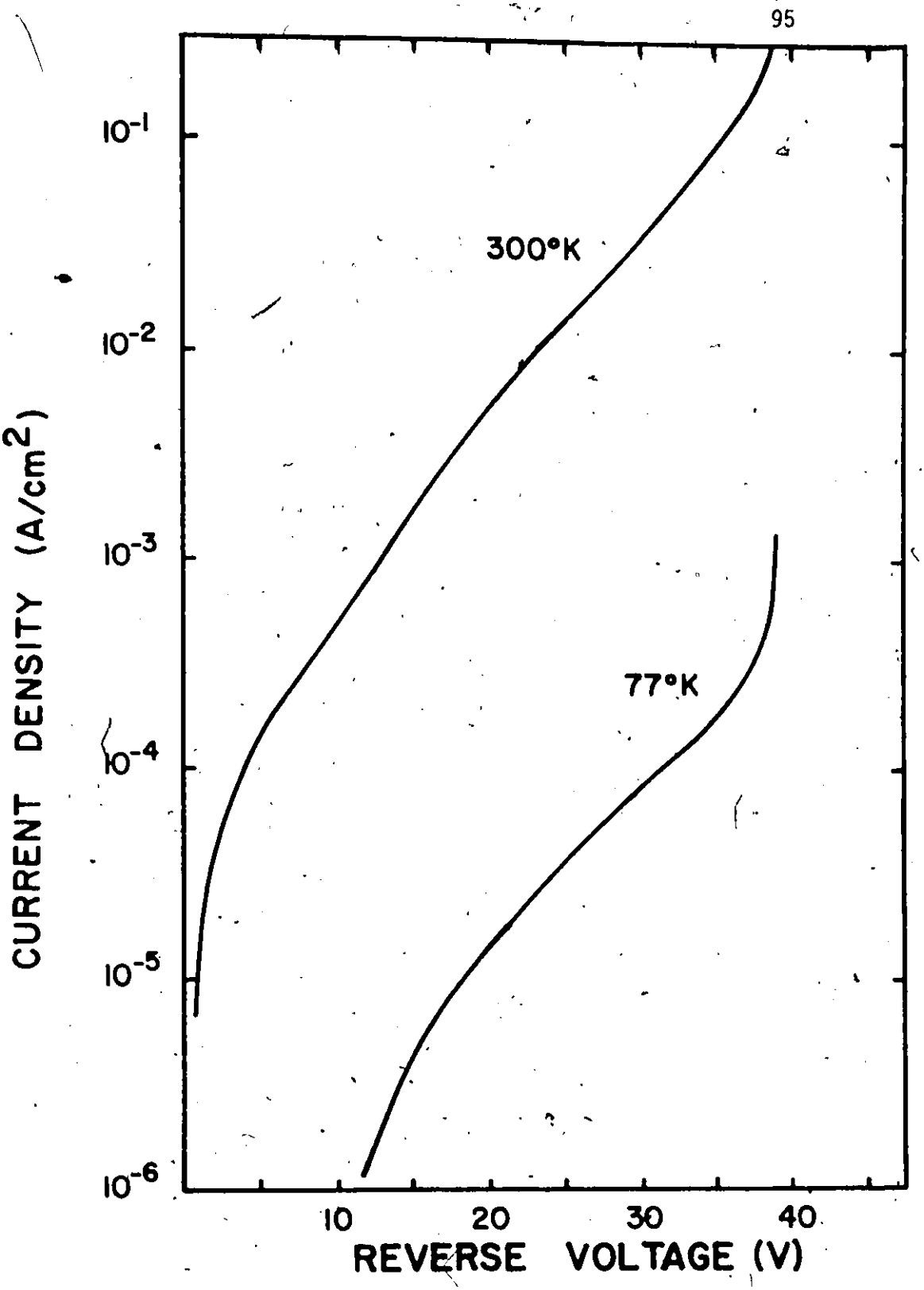

Figure 5.4 The reversed biased I-V relationship for a nitrogen implanted diode measured at 300°K and 77°K. The substrate is 1 ohm-cm silicon.

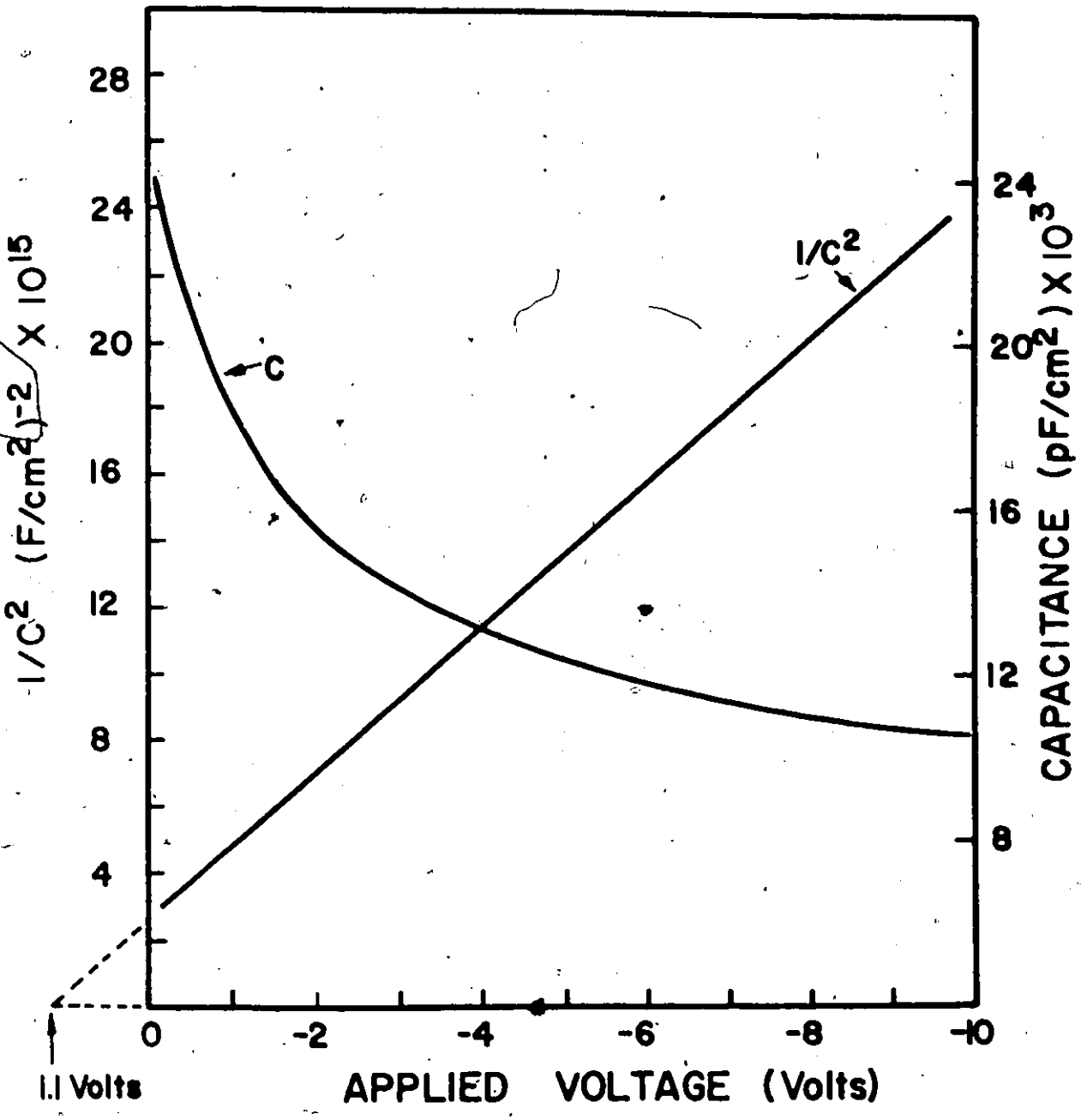

Figure 5.5 The capacitance-voltage characteristics of a nitrogen implanted diode.

this value of $6 \times 10^{15}/cm^3$. The voltage intercept of the curve at 1.1 volts yields a build-in voltage of $(1.1 - 2kT/q) = 0.94$ volts. Although this value agrees well with that expected[54] for an abrupt one-sided junction where the n-type region is degenerate, it does not agree with the value calculated by subtracting the sum of the absolute values of the Fermi potentials from the bandgap. This calculation yields a value of 0.71 V.

The results of these measurements on nitrogen implanted diodes indicate that although rectification is taking place, the theory of the p-n junction is not being well obeyed as the temperature dependence of the I-V characteristics and the C-V data deviate from the theoretically predicted behaviour.

5.3 Room Temperature Measurements

5.3.1 MOS Capacitance-Voltage Measurements

The diode characteristics described in the previous section showed that n-type behaviour can be obtained in nitrogen implanted silicon. Preliminary room temperature Hall measurements indicated a low carrier conversion efficiency, and a problem was encountered in electrically contacting the implanted layer at low anneal temperatures. For this reason, the MOS capacitance-voltage technique was used.

MOS C-V measurements were performed on samples implanted at 100°K at a dose-rate of 5 nA/cm^2 to total doses ranging from 5×10^{13} N/cm^2 to 8×10^{14} N/cm^2. As shown in Chapter IV, this implantation temperature and

dose rate was found to produce the maximum amount of damage as measured by backscattering when the sample was returned to room temperature. If enhanced electrical conversion is to be observed following the anneal of a totally damaged layer, then it should be observed for some dose in this range. The results of these measurements on 10 ohm-cm Czochralski grown silicon are shown in figure 5.6. There are three temperature regions of interest for this data: below 725°C where the layer does not exhibit n-type behaviour, between 725°C and some maximum temperature at which the n-type behaviour is lost, and above this maximum temperature where the layer has become p-type.

For anneal temperatures below 725°C, the implanted region is highly resistive. This resistive region acts as an effective capacitance in series with that of the deposited oxide. Using the known oxide thickness, and assuming a dielectric constant of 11.7 for the resistive material, the implanted region was calculated to be approximately 2500 Å thick, in good agreement with the depth of the implanted nitrogen, as shown in figure 2.3.

For all doses, the n-type conversion takes place quite rapidly at ∿725°C. The maximum carrier concentration obtained depends on the dose up to a dose of ∿1 x 10^{14} N/cm^2, and then saturates at 8 x 10^{16} carriers/cm^3, as shown in figure 5.7. For doses higher than ∿6 x 10^{14} N/cm^2, the capacitance-voltage plots fail to behave in the expected manner. The change in capacitance from accumulation to depeletion was very small, and the samples showed light sensitivity under both polarities of applied bias. Under normal conditions, the sample should only show light sensitivity when biased into depletion. The value of capacitance obtained was lower for these heavily doped samples

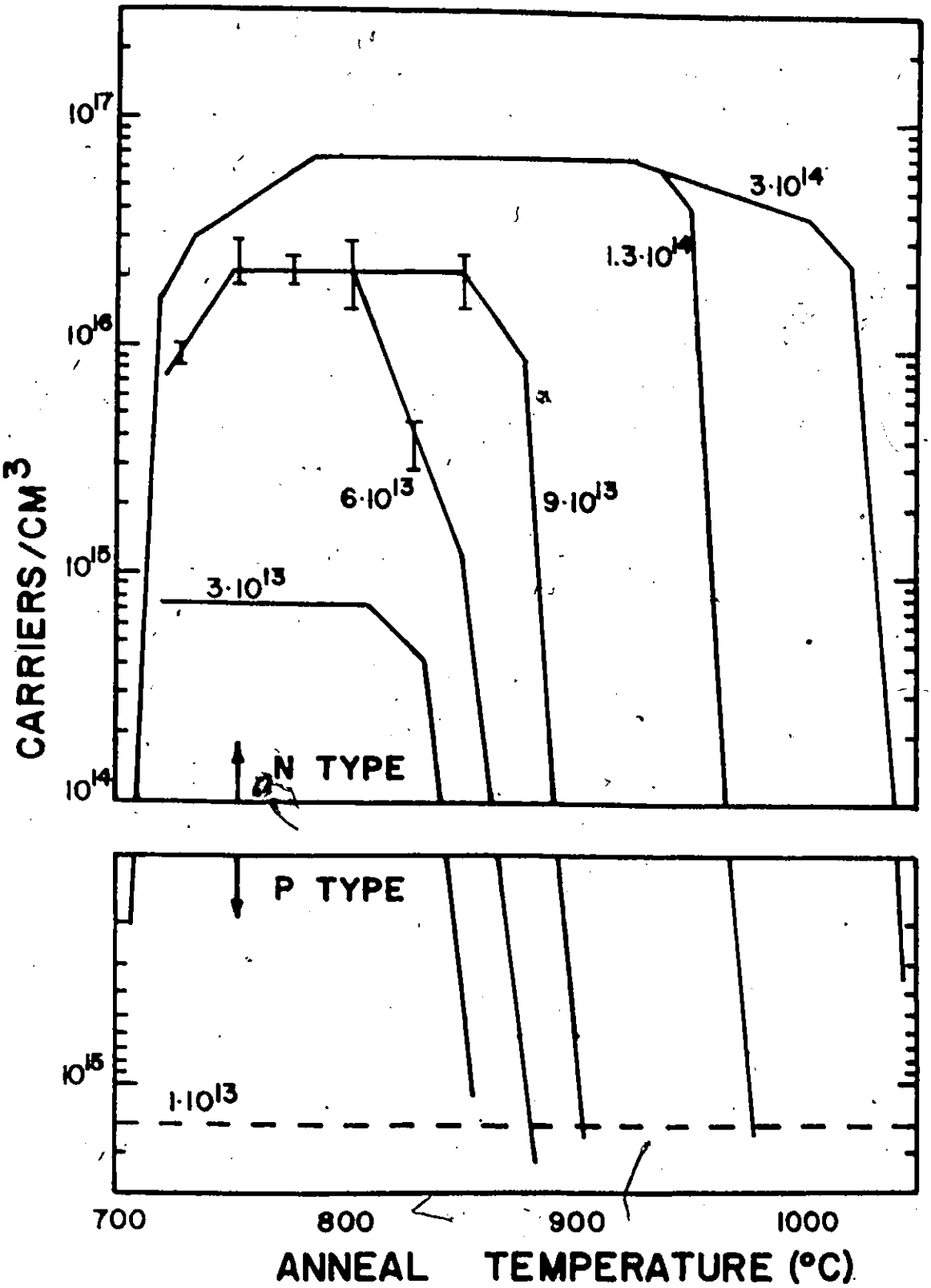

Figure 5.6 The results of MOS capacitance-voltage measurements for various implantation doses as a function of anneal temperature. The substrates are 10 ohm-cm Czochralski grown silicon.

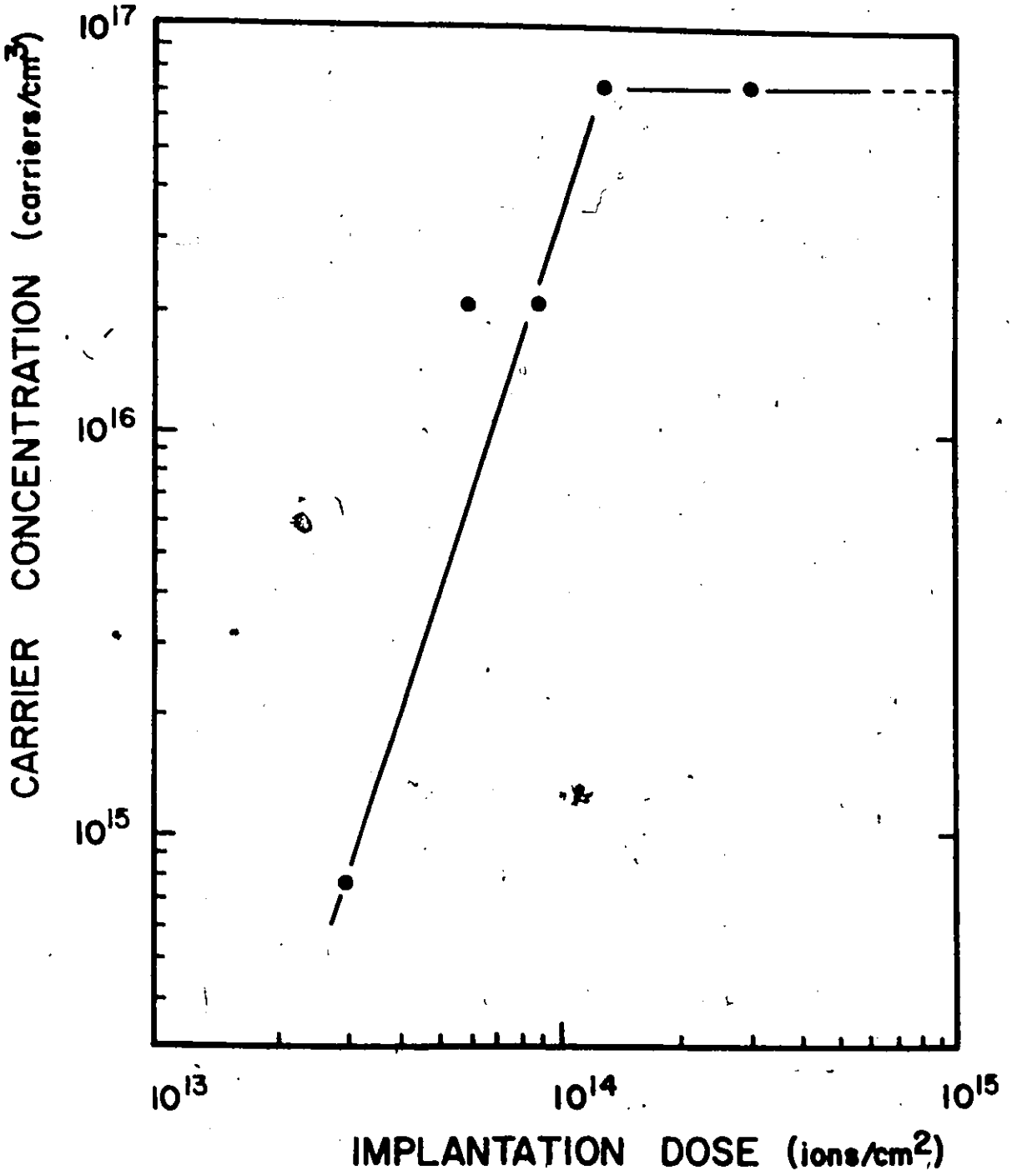

Figure 5.7 The number of carriers produced in nitrogen implanted silicon as a function of implantation dose.

than for the samples that showed well-behaved C-V characteristics. It is believed that, although the sample is relatively well annealed as observed by backscattering, some damage remains which acts as a capacitance in series with the oxide capacitance. Capacitance-voltage curves for a 1×10^{14} N/cm^2 implant and a 6×10^{14} N/cm^2 implant annealed at 800°C for 10 minutes are shown in figure 5.8. For implantation doses lower than $\sim 6 \times 10^{14}$ N/cm^2, the results were reproducible and typical of n-type behaviour. Each of the curves on figure 5.6 was obtained using approximately 3 different samples, and error bars are shown on one of the curves to illustrate the reproducibility achieved.

Figure 5.6 shows that as the annealing temperature is increased, the n-type behaviour is eventually lost, and the material reverts to p-type. Between 725°C and this type conversion temperature (which depends on the dose and is between 850°C and 1050°C) the carrier conversion efficiency is very low (<1%).

In order to determine whether the observed electrical activity was dependent upon the oxygen content of the Czochralski crystals used for the above experiments, float-zoned material of various resitivities was implanted at 100°K using a dose-rate of 5 nA/cm^2 and measured by the MOS capacitance-voltage technique as a function of anneal temperature. Both p and n-type substrates were used. The results for the p-type crystals are shown in figure 5.9. There is little difference in the behaviour of nitrogen in the float zoned and Czochralski crystals, and the poor electrical conversion efficiency is independent of substrate resistivity. Nitrogen implanted into n-type crystals caused the substrate to become more n-type, but the carrier

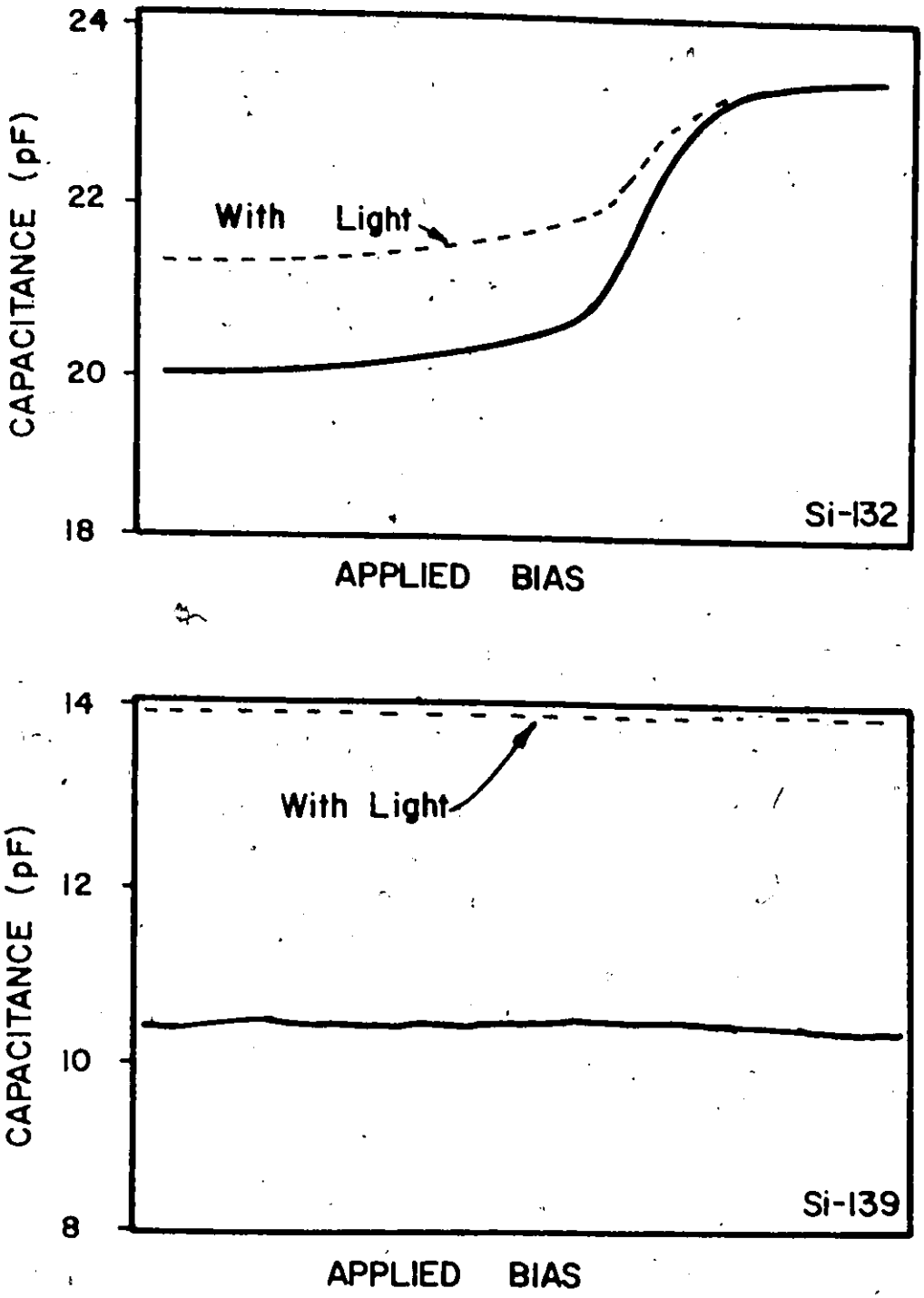

Figure 5.8 C-V plots for nitrogen implanted silicon following 10 minute anneals at 800°C (a) the results for a dose of 1.8×10^{14} N/cm^2. (b) the results for a dose of 6.0×10^{14} N/cm^2.

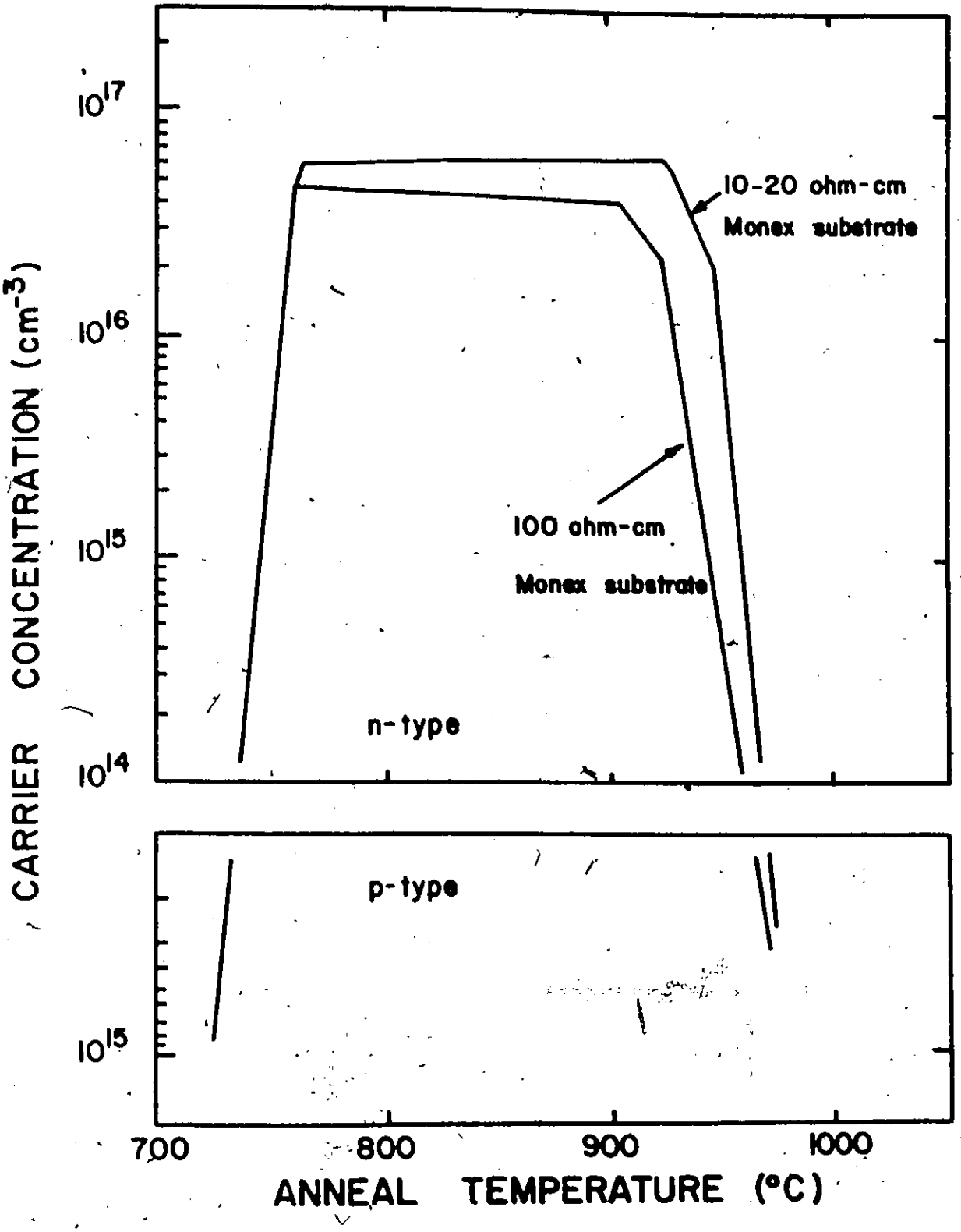

Figure 5.9 The MOS capacitance-voltage results for nitrogen implanted into float-zoned silicon.

conversion efficiency was still less than 1%.

One problem with such a low carrier conversion efficiency is that the conduction observed may not be due to the substitutional position of the implanted ion, but may be due to damage centers or trap levels that are electrically active. In an attempt to determine whether the observed electrical behaviour was unique to nitrogen, neon was implanted into n and p-type silicon under similar conditions as for nitrogen and the resultant electrical behaviour monitored as a function of anneal temperature by the MOS C-V technique. The analysing magnet limited the maximum implantation energy to 50 keV. Following implantation of neon into n-type silicon, the implanted region remained n-type, but the layer was insensitive to light in the apparent inversion layer. For neon implanted into p-type silicon, the layer remained p-type following anneals to 800°C, whereupon it lost sensitivity to light regardless of the polarity of the applied bias. Above 850°C, the implanted region was readily depleted and was slightly n-type. These results for neon implanted into n and p-type silicon are shown in figure 5.10(a) and 5.10(b) respectively. The results imply that the n-type properties observed in the nitrogen implanted layer are unique to nitrogen, and if damage centers are responsible for this n-type behaviour, then nitrogen is playing an important role in the production of such defects.

The suggestion that a nitrogen induced defect is accounting for the observed donor behaviour is not totally unfounded. It is known[48] that atomically dissolved oxygen introduced during the initial growth of the silicon crystal reacts when the silicon is heated, to form a sequence of oxygen aggregates until finally silica (SiO_2) is formed. Only those aggregates which

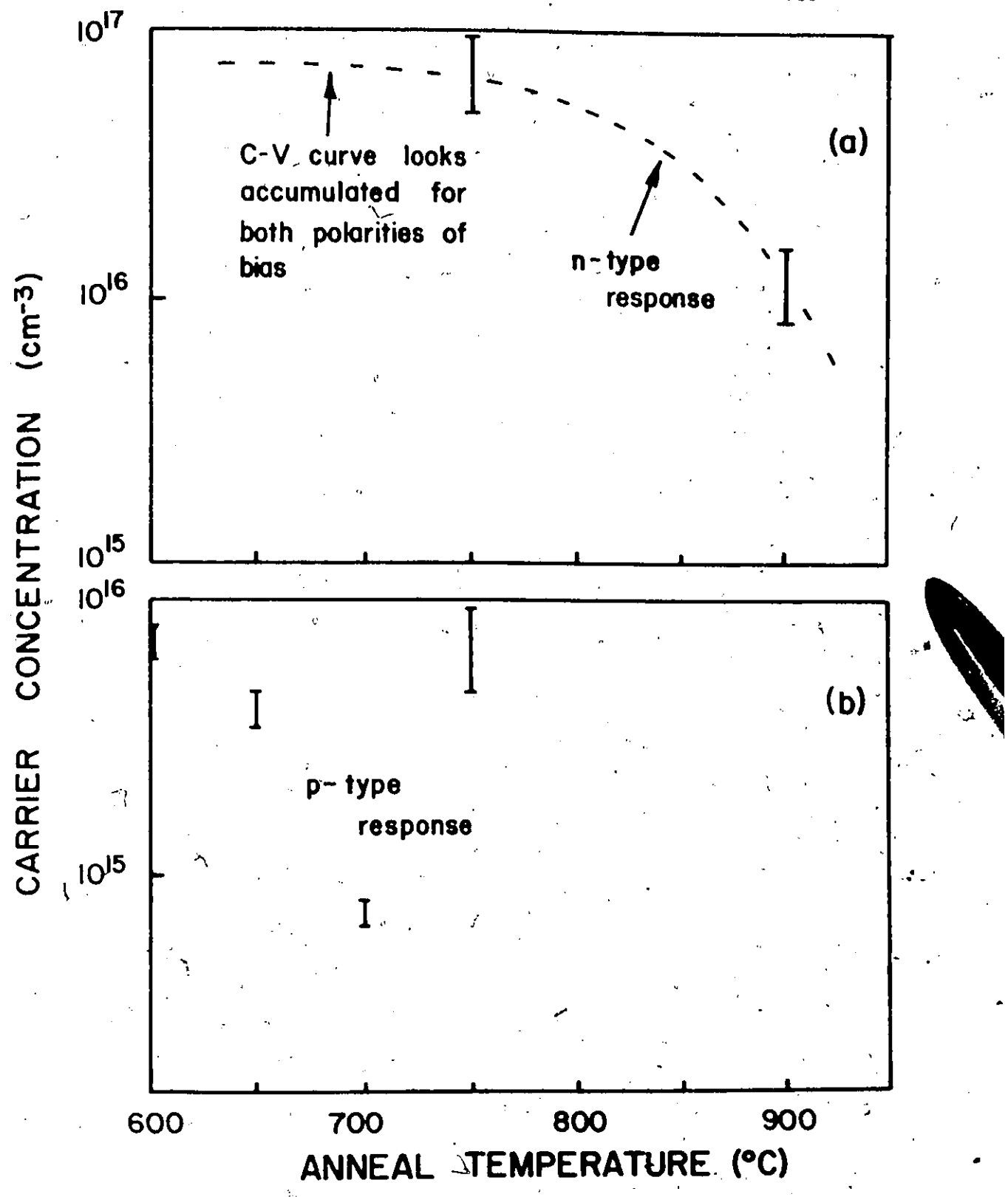

Figure 5.10 (a) 50 keV Ne^+ implanted into n-type silicon.
(b) 50 keV Ne^+ implanted into p-type silicon.

possess fewer than five bound oxygen atoms appear to act intensively as donors at room temperature. In particular, the donor states produced following heat treatment at 450°C appear to consist principally of a donor SiO_4 complex. The fact that only certain of the aggregates formed act as donors is used to explain the saturation of the number of donors regardless of the initial amount of dissolved oxygen. No extensive donor activity is observed after heating the silicon at 1000°C; however, the donors reappear if the sample is reheated to ~450°C, following the high temperature anneal.

A similar nitrogen induced defect may be responsible for the observed donor behaviour following anneals in the range 700-900°C. Again, only certain defects may act as donors and this could explain the observed saturation of donor activity. The fact that the donor activity is lost at high anneal temperatures may be due to a thermal breakup of these defects. The nitrogen "donors" do not reappear if the sample is reannealed in the 700-900°C range after an anneal at a temperature sufficiently high to lose the donor-like behaviour. This may be due to out-diffusion of the nitrogen or to the formation of other defects. These points will be discussed in more detail at the end of this chapter and in Chapter VIII.

5.3.2 Room Temperature Hall Measurements

The results of the C-V measurements presented in the last section have been confirmed by room temperature Hall effect and sheet resistivity measurements. The results of these measurements are shown in figure 5.11, and confirm the low electrical conversion efficiency obtained with the MOS

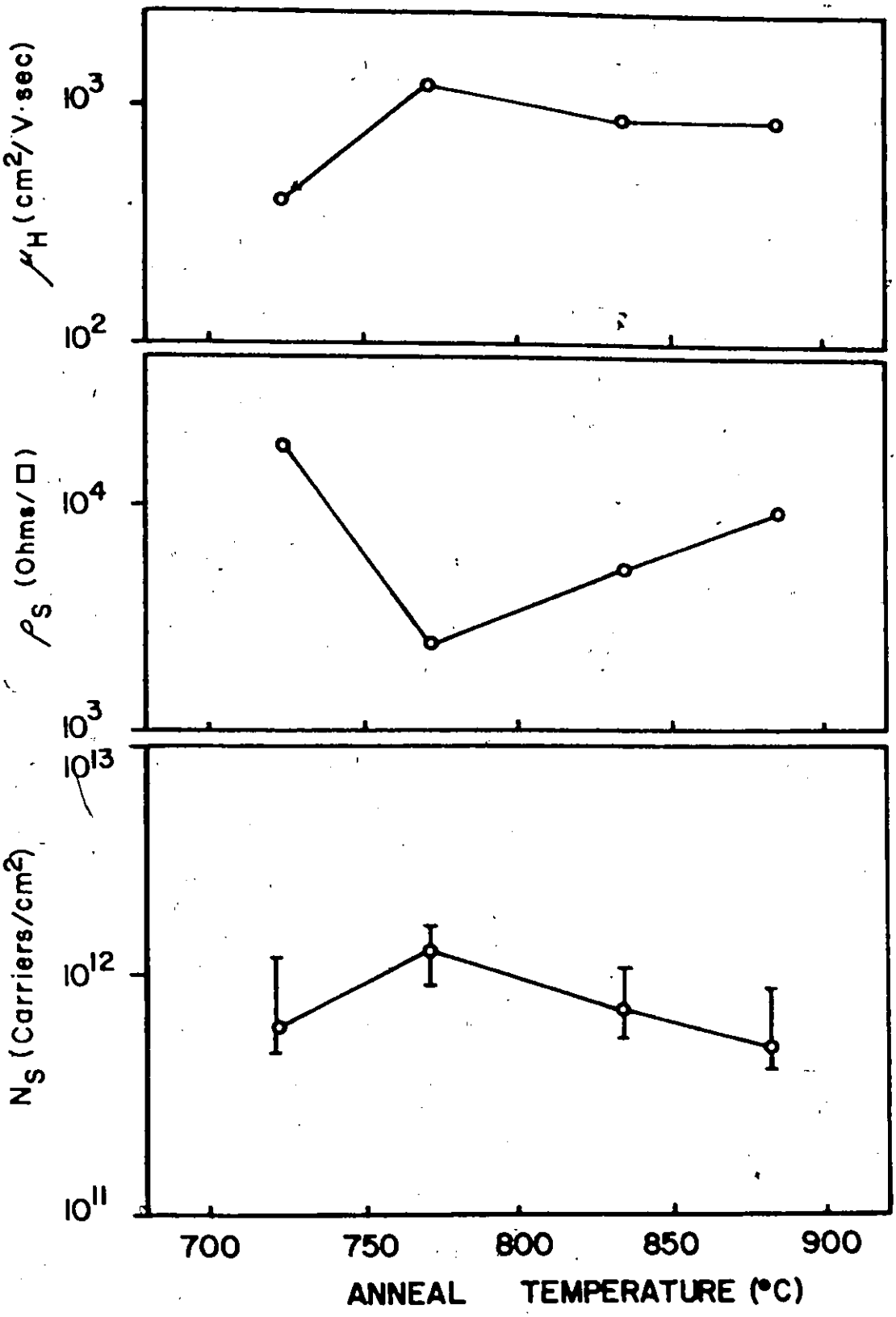

Figure 5.11 The results of room temperature Hall effect and sheet resistivity measurements performed on nitrogen implanted silicon

capacitor technique. It should be pointed out that both the C-V and Hall effect measurements give the weighted average of the measured property over the thickness of the measured layer, i.e. over the maximum depletion depth for the MOS capacitor technique as discussed in Chapter III and Appendix B, and over the distance from the surface to the junction for the Hall effect technique. To determine how the carrier concentration varied with depth from the crystal surface, room temperature Hall effect measurements were combined with anodization and HF acid stripping. The resultant concentration profile for such measurements conducted on nitrogen implanted silicon is shown in figure 5.12. The concentration is virtually constant as a function of depth to depths of ~1500 Å at which point the resistivity is too high to allow measurements to be performed, which implies that the region between 1500 Å and the edge of the depletion region in the n-type material is quite thin. An estimate of the junction depth can be obtained from the profile data and the known abrupt nature of the junction. The profile data indicates that the concentration is flat and equal to $\sim 7.5 \times 10^{16}$ ions/cm^3, while the room temperature Hall effect shows that the weighted average from the surface to the edge of the depletion region is $1 - 1.5 \times 10^{12}$ ions/cm^2. Assuming that the concentration is flat at 7.5×10^{16} from the surface to the depletion layer edge, then a distance $x = 10^{12}/7.5 \times 10^{16} = 1350$ Å to $1.5 \times 10^{12}/7.5 \times 10^{16} = 2000$ Å is obtained. The width of the depletion region in the n-type material would be ~260 Å.[54] This would give a metallurgical junction depth of 1610-2260 Å. For the low temperature Hall measurements to be described in the next section, it was assumed that the junction depth was 2000 Å.

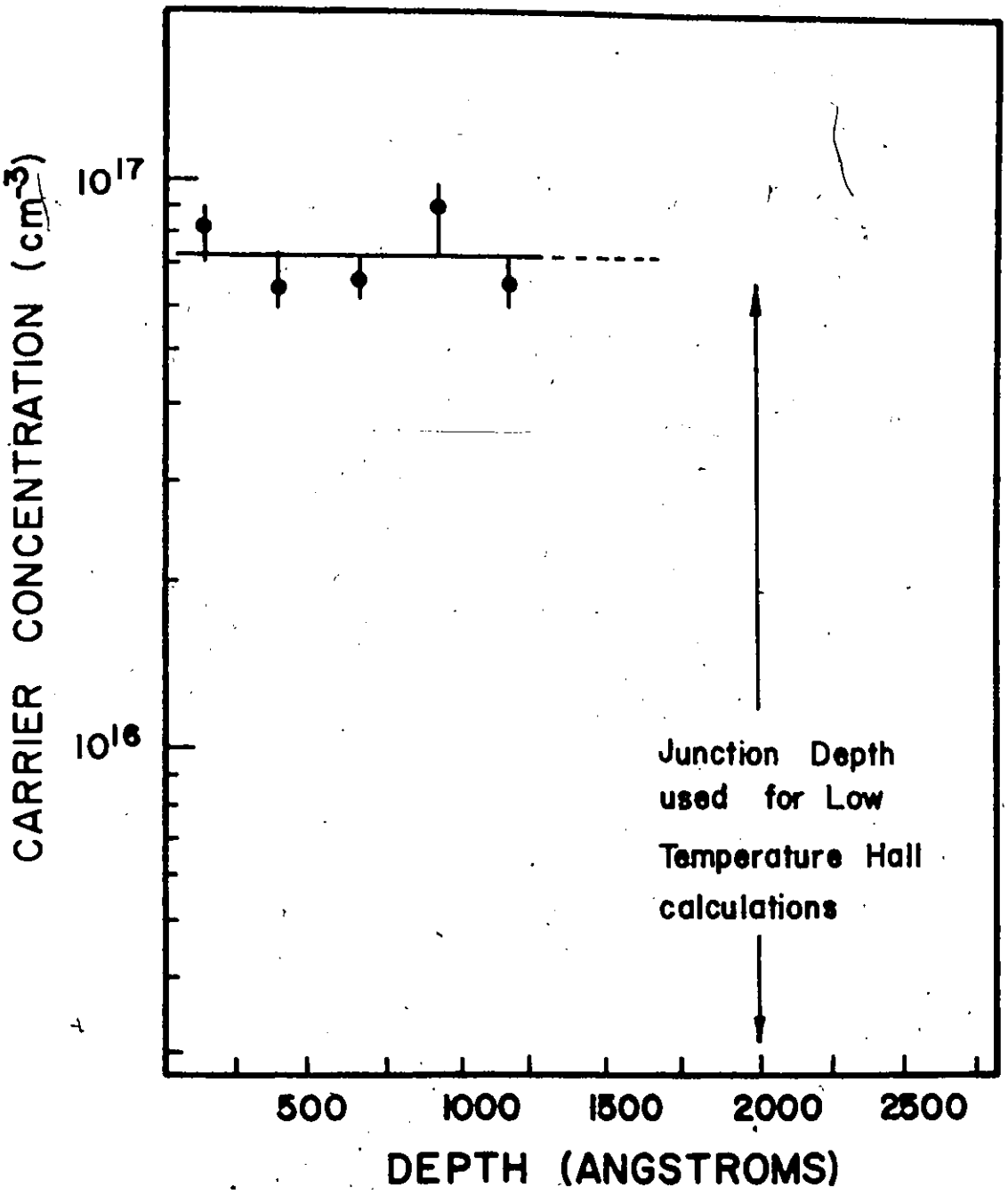

Figure 5.12 The carrier profile for 1.4 x 10^{14} N/cm^2 implanted into 10 ohm-cm silicon. The anneal temperature was 825°C.

All the measurements that have been described in the sections above have been conducted on samples implanted at 100°K using a dose rate of 5 nA/cm^2. To determine if the implantation temperature, and hence the amount of damage caused by the implantation, was influencing the observed electrical characteristics, implantations at this dose rate to a fixed dose were performed at various temperatures, and the electrical activity following 20 minute vacuum anneals measured at room temperature using the Hall effect technique. The results are presented in figure 5.13 and show that the observed electrical activity is independent of the implantation temperature.

To ensure that a 10 minute anneal was neither too long nor too short for optimum electrical behaviour, an isothermal anneal was performed. A 10 ohm-cm silicon sample with diffused phosphorus contacts was implanted at 100°K and 5 nA/cm^2 to a dose of 1.4 x 10^{14} N/cm^2 and annealed for various times in vacuum at 825°C. The resultant electrical behaviour as determined by room temperature Hall effect measurements is presented in figure 5.14. The concentration reaches a maximum of 1.1 x 10^{12} carriers/cm^2 after 50 minutes and then decreases. Increasing the anneal temperature to 850°C causes the concentration to decrease at a more rapid rate, as shown in figure 5.14.

The possibility exists that the implanted nitrogen may outdiffuse during the anneal following implantation. This effect would be observed if the diffusion was not controlled by the bulk diffusion coefficient, but for example, by a surface effect, and would be more pronounced in a vacuum anneal than in an nitrogen ambient anneal, and for this reason, anneals in nitrogen were performed. The observed electrical behaviour was independent

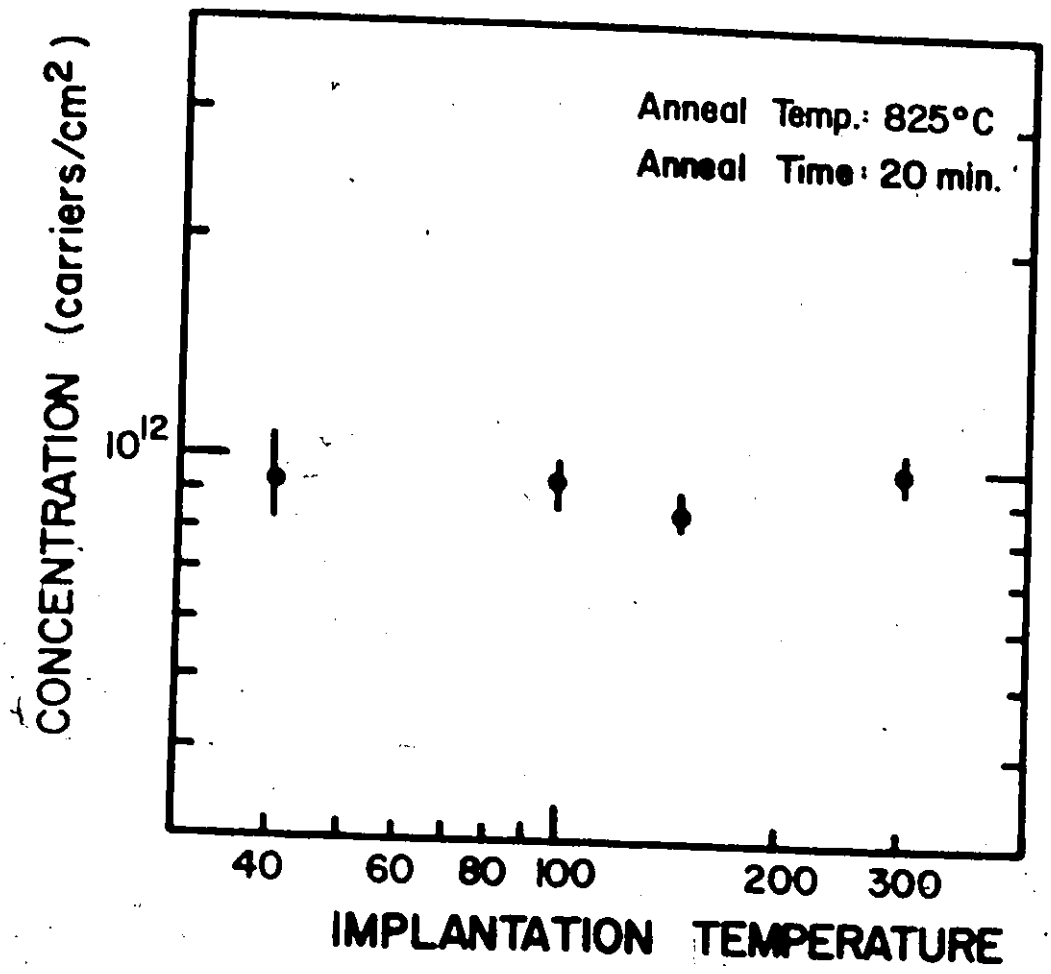

Figure 5.13 The observed carrier concentration for 1.4×10^{14} N/cm^2 implants into silicon for various implantation temperatures.

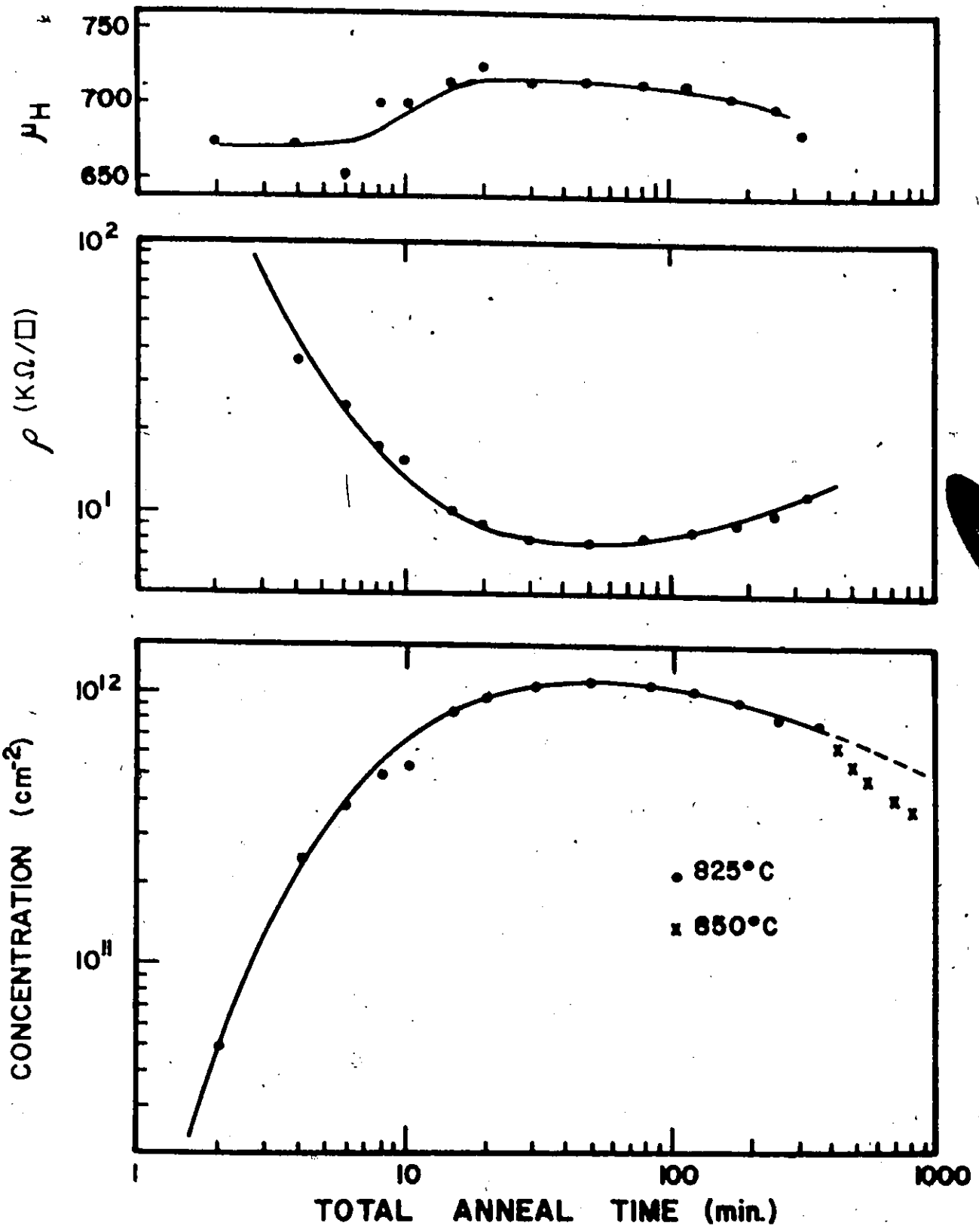

Figure 5.14 The results of an isothermal anneal for silicon implanted with 1.4×10^{14} N/cm^2.

of the annealing ambient. The backscattering results as a function of annealing temperature presented in the last chapter also imply that the nitrogen is not outdiffusing.

5.4 Low Temperature Hall Measurements

In order to determine the ionization energy, temperature dependence of mobility, and degree of compensation present in the nitrogen implanted silicon samples, Hall effect and conductivity measurements were made as a function of temperature. Ideally, the dose used for such a measurement should be low enough to prevent degeneracy and band spreading conditions. A dose of 1.4×10^{14} N/cm^2 was found to be the lowest dose for which reproducible data could be obtained. The diffused contact silicon samples shown in figure 3.6 were implanted at 100°K and room temperature using a dose rate of 5 nA/cm^2. Energies of 80 and 40 keV were used in a dose ratio of 3:1. Following implantation, the samples were annealed at 825°C for a total of 30 minutes, in 10 minute steps, and Hall and conductivity measurements as a function of temperature were performed at each step. The annealing temperature was selected on the basis of the earlier MOS capacitor and room temperature Hall measurements.

In partially compensated n-type silicon, the number of free carriers n, at a temperature T is given by

$$\frac{n(n + N_A)}{N_D - N_A - n} = \frac{N_c}{g_D} \exp\left(\frac{-E_D}{kT}\right) \qquad (5.2)$$

where N_A = number of acceptors
N_D = number of donors

g_D = donor degeneracy factor = 2
E_D = the donor ionization energy
N_c = the density of states in the conduction band

and $$\frac{N_c}{g_D} = 2.694 \times 10^{15}\ T^{3/2} \qquad (5.3)$$

Substituting (5.3) into (5.2) yields

$$\frac{n(n + N_A)}{N_D - N_A - n} = 2.694 \times 10^{15}\ T^{3/2} \exp\left(\frac{-E_D}{kT}\right) \qquad (5.4)$$

It is clear from equation (5.4) that the ionization energy of a dopant impurity (E_D) may be obtained from the gradient of a plot of $nT^{-3/2}$ vs 1/T or $n^2T^{-3/2}$ vs 1/T. The plot of $nT^{-3/2}$ vs 1/T is used at very low temperatures where $n << N_D-N_A$ and $n << N_A$ while that of $n^2T^{-3/2}$ vs 1/T is used at intermediate temperatures when $N_A < n << N_D - N_A$. The assumptions used for the first method are much more easily satisfied that those for the second, and hence the $nT^{-3/2}$ vs 1/T method gives a more reliable estimate of the ionization energy. Unfortunately, the previous results obtained for the ionization energy of nitrogen in silicon[3] were obtained at fairly high temperatures (~100°K) and as a result, are probably not too accurate. The present study has used temperatures as low as 20°K, and the ionization energy was obtained from the gradient of the $nT^{-3/2}$ versus 1/T plot.

The normalized carrier concentration as a function of temperature for the room temperature implanted samples is presented in figure 5.15. The corresponding resistivity and mobility are shown in figure 5.16. Two curves are shown on each graph, corresponding to 20 and 30 minute total anneal times. The data of Zorin et al[3] has been included on figure 5.15,

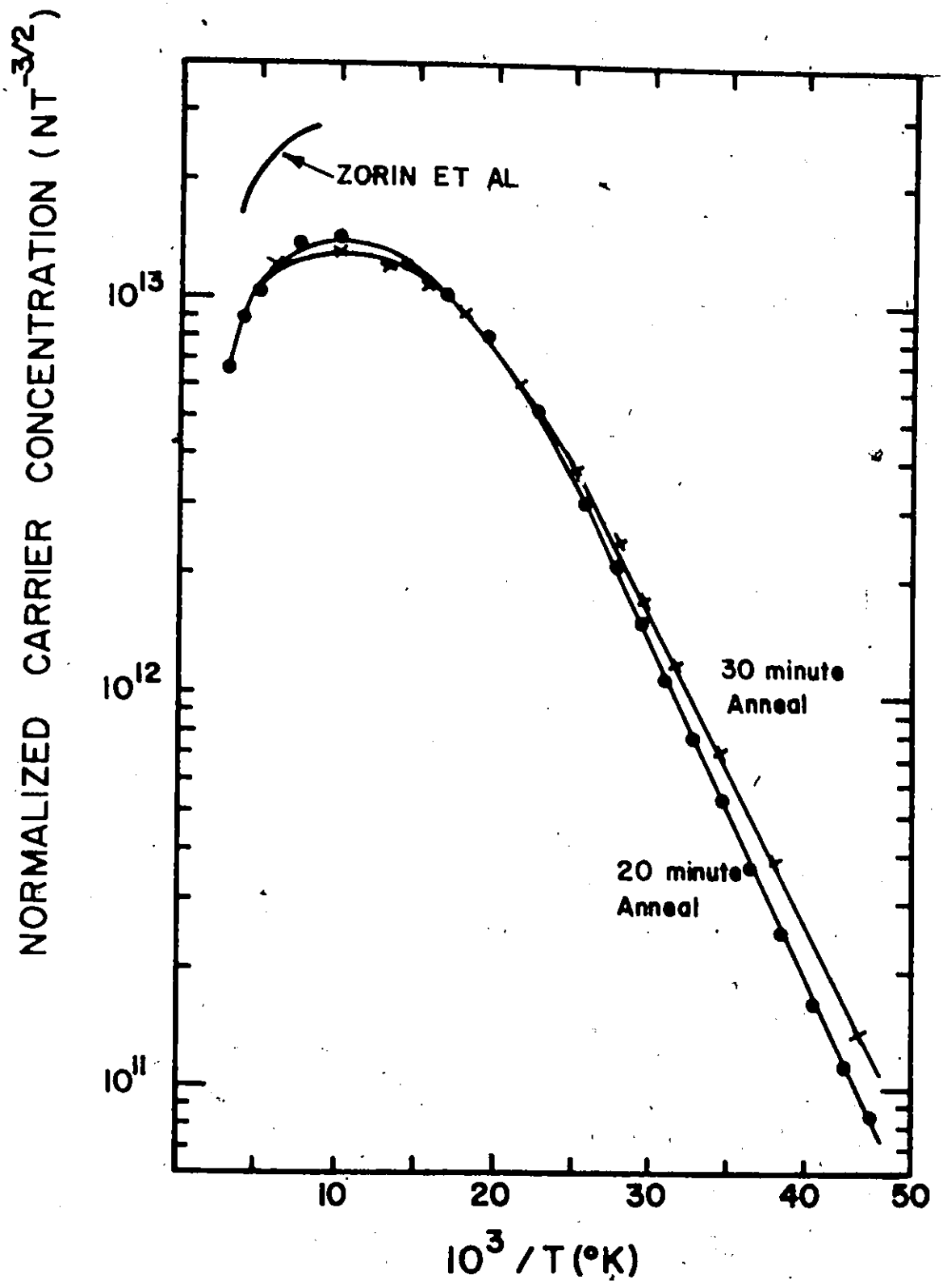

Figure 5.15 The normalized carrier concentration as a function of reciprocal temperature for silicon implanted at room temperature with 1.4×10^{14} N/cm^2.

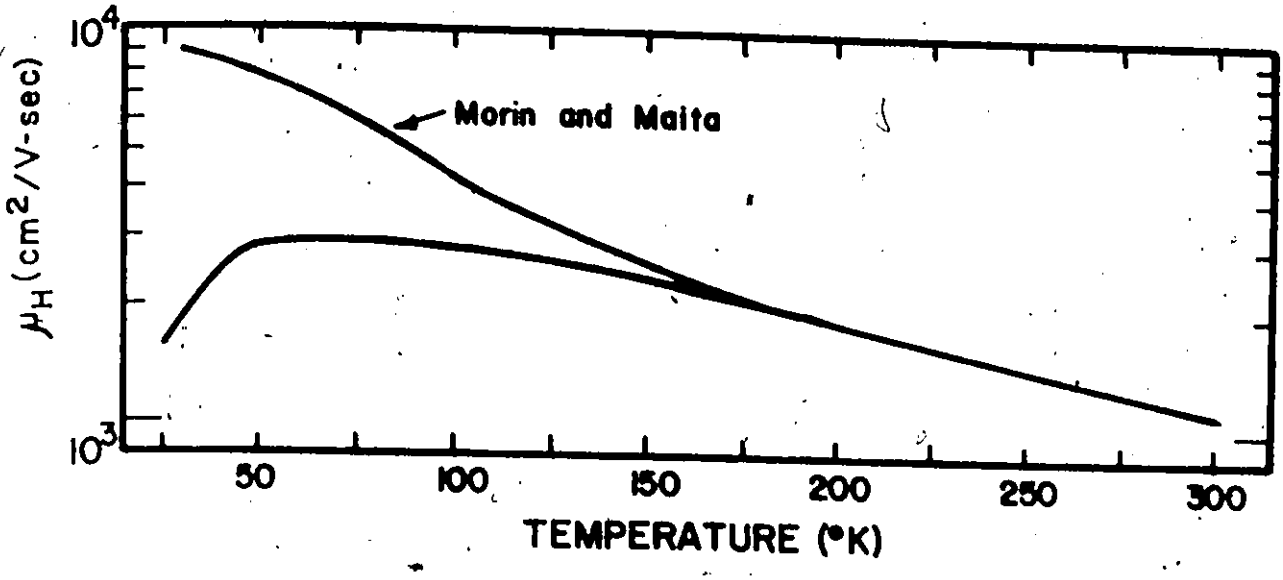

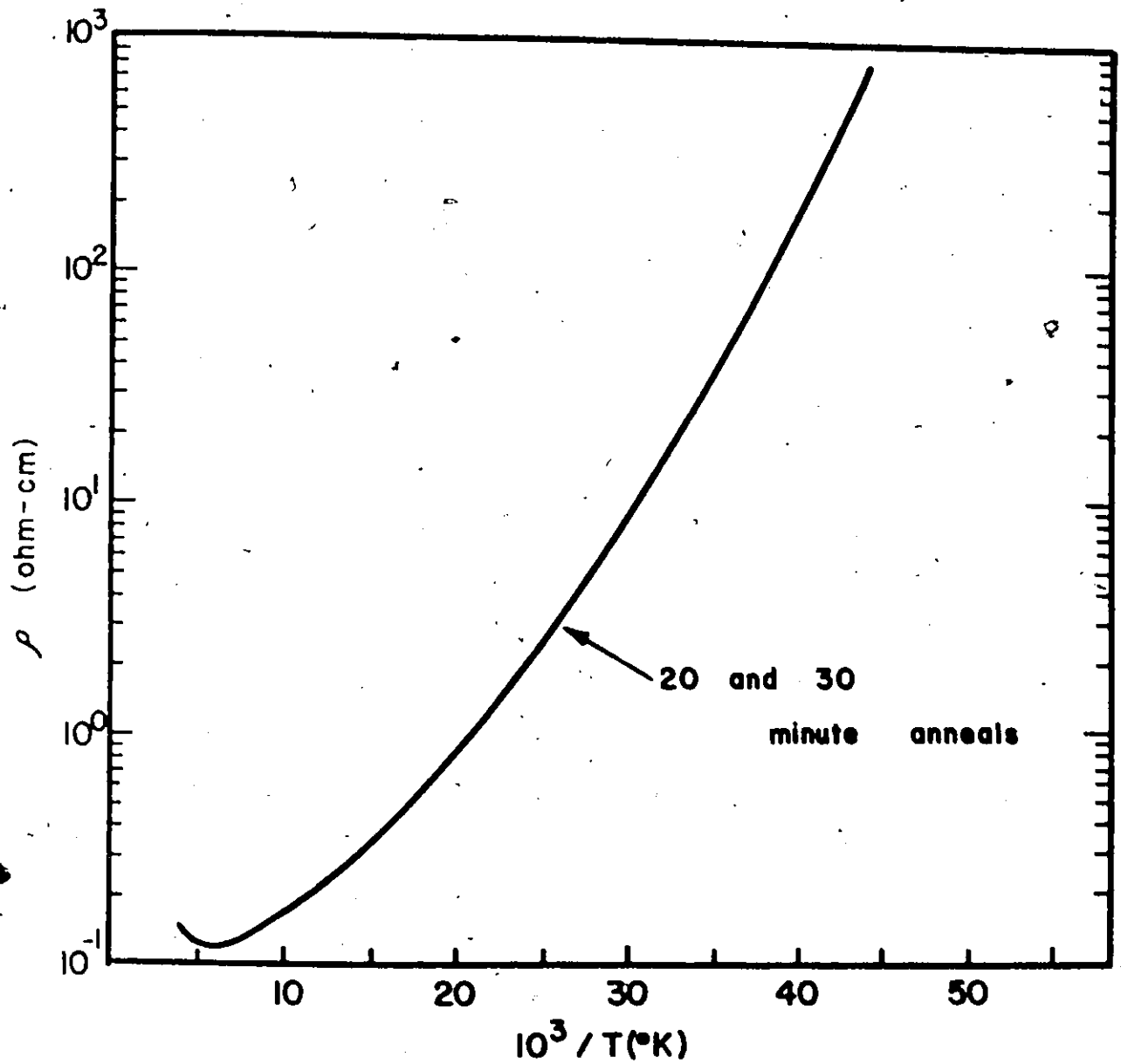

Figure 5.16 The resistivity and Hall mobility for the sample shown in fig. 5.15. The mobility of a bulk arsenic doped sample as determined by Morin and Maita[69] is shown for comparison

from which it is seen that the temperature range over which their data was accumulated was rather limited. Using the gradient of these curves, the ionization energy for the 20 minute total anneal time sample was found to be 0.017 eV while 0.015 eV was found for the 30 minute total anneal time sample. These results are equal within experimental error, as the temperature accuracy is ±1°K, which would superimpose the two curves.

The mobility of an arsenic doped bulk sample as measured by Morin and Maita[69] has been included on figure 5.16 for comparison with that of the ion implanted samples. These results will be discussed further following the presentation of the data obtained for samples implanted at 100°K.

Figure 5.17 presents the normalized carrier concentration data obtained following 10, 20 and 30 minute total anneal time of a sample implanted at 100°K. The accompanying mobility and resistivity are shown in figure 5.18. In order to ensure that the equipment was calibrated and working well, a bulk boron doped silicon sample was measured as a function of temperature using the same procedure as for the nitrogen implanted samples. The results are included on figure 5.17. The ionization energy for the bulk boron doped sample was calculated to be 0.044 eV in good agreement with the generally accepted value of 0.045 eV.[54] Values of 0.017 eV, 0.016 eV and 0.016 eV were found for the ionization energy of the nitrogen implanted samples following total anneals of 10, 20 and 30 minutes.

Using expression 5.4, it should be possible to fit the curve once the ionization energy E_D is known. In this way, a measure of the compensation (N_A) can be determined. Attempts to fit these curves using a single dopant ionization energy failed, as the shape of the experimental curve

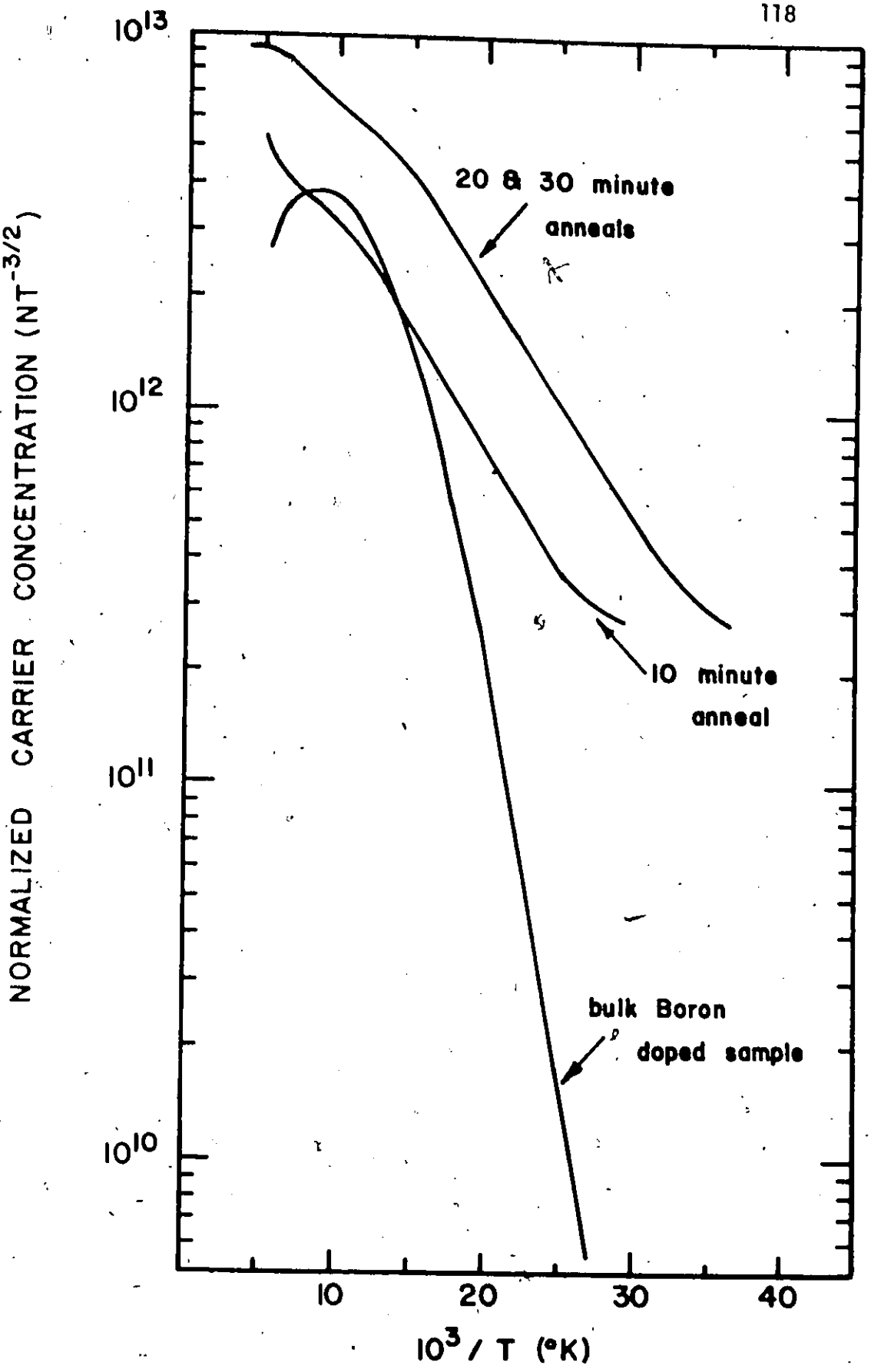

Figure 5.17 The normalized carrier concentration as a function of reciprocal temperature for silicon implanted at 100°K with 1.4×10^{14} N/cm^2. A bulk boron doped sample is shown for comparison.

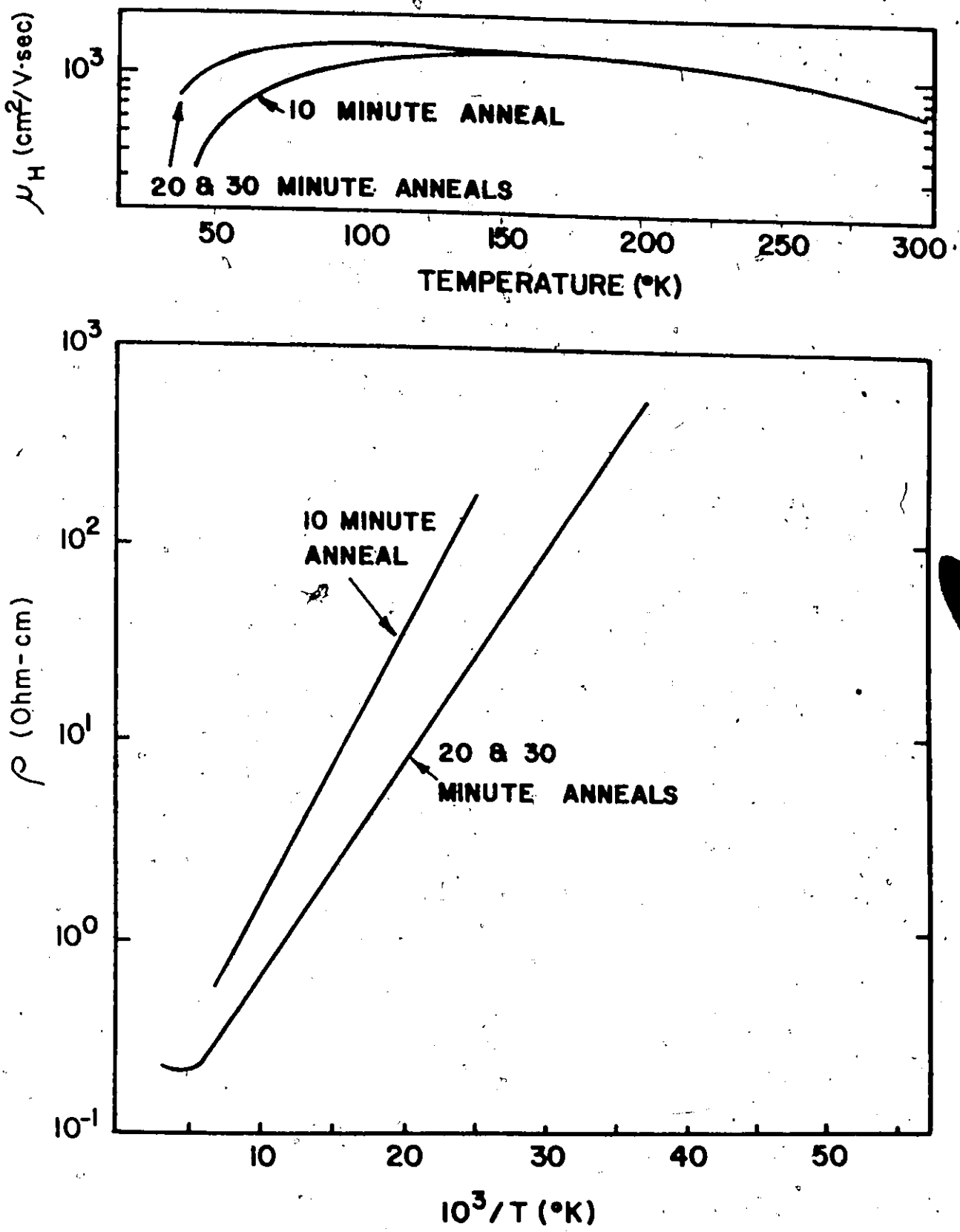

Figure 5.18 The resistivity and Hall mobility for the sample shown in figure 5.17.

near 100°K is not predicted by theory. Figures 5.16 and 5.18 show the carrier concentration for samples implanted at room temperature and 100°K, and show that the shape of the curve changes as the sample is annealed for longer times. Although all the curves are characterized by the same, ionization energy at low temperatures, another energy level may be present and be responsible for this observed behaviour.

5.5 Conclusions

The preceding sections have presented the results of electrical measurements performed on nitrogen implanted silicon. It has been established that the impurity levels in the silicon used for these investigations, the amount of damage caused by the implantation, the implantation temperature, the dose rate, the annealing time or the annealing ambient have little effect on the resultant n-type behaviour of the layer, provided the dose is kept below $\sim 6 \times 10^{14}$ N/cm^2. Thus either nitrogen has a very low substitutional solid solubility in silicon or defects are responsible for the n-type behaviour.

The question of what happens to the nitrogen after it is implanted is a difficult one to answer. The difficulty lies in the fact that there are very few experimental techniques available to measure the amount and position of nitrogen in silicon. For example, emission spectrographic analysis is not applicable because nitrogen does not yield lines in the visible part of the spectrum. Mass spectrographic analysis is not applicable because the doubly-ionized nitrogen falls exactly on the peak for silicon

at mass 28. Electron spin resonance could in principle yield the net nitrogen concentration. Neutron activation analysis is impractical because of the short lifetimes of nitrogen isotopes. In the next chapter, a nuclear reaction technique using the $^{14}N(d,\alpha_1)^{12}C$ reaction will be described that finds some possible use as a lattice location tool; however, the sensitivity is too low to allow it to be used with the nitrogen-silicon system. The possibililty of nitrogen out-diffusing from the silicon is not supported by backscattering data as mentioned earlier; it cannot be tested by gas-release experiments[70] as the quantity of nitrogen is very low and, as nitrogen is a residual gas in most vacuum systems, a small release would not be detected.

Zorin et al[71] have shown that the nitrogen initially present in the silicon may be made electrically active by bombardment with neon. These results do not agree with the results of the present investigation, and the reason is probably that the crystals used in the present study contain much less dissolved nitrogen than those used by Zorin et al. The Monsanto Company was unable to specify the amount of nitrogen in the crystals used for this investigation, and they have no technique for measuring it. The importance of nitrogen in bulk silicon has been virtually ignored in a recent review paper on the quality of silicon.[72]

Until recently, the amount and nature of nitrogen in bulk silicon had received little attention with the work of Kaiser and Thurmond[73] being the most authoritative. Recently, however, Yatsurugi et al[74] have studied the concentration, solubility, and equilibrium coefficient of nitrogen in silicon by means of charged particle activation analysis. They found that

commercial semiconductor silicon containsless than 1×10^{15} atoms/cm^3 of nitrogen in the un-ionized state and the solubility in solid silicon is $4.5 \pm 1.0 \times 10^{15}$ atoms/cm^3. From resistivity measurements corrected by considering the amount of boron and phosphorus present in the sample, they found that less than 1% of the nitrogen present in the sample was ionized.

It is unlikely, in view of the solid solubility of $4.5 \pm 1 \times 10^{15}$/cm^3 quoted above for nitrogen in silicon, that the observed donor behaviour is due to the substitutional position of nitrogen in the silicon lattice. This is supported by the inability to obtain a normalized carrier concentration, versus reciprocal temperature curve that can be fitted with the single donor theory, and by the fact that damage removes or obscures the observed electrical effect for doses exceeding $\sim 6 \times 10^{14}$ N/cm^2. The relatively constant resultant concentration could be explained as it is for oxygen in silicon - a stable defect is responsible for the conduction and breaks up at the higher temperatures.

There are some reasons for believing that nitrogen is acting as a donor. The unique ionization energy, which is independent of the implantation conditions, supports this idea. Although the diodes formed by implanting nitrogen into silicon do not behave in the expected manner at low temperatures, the room temperature characteristics are well behaved. It is possible that the low solubility of nitrogen in silicon may be responsible for forcing the nitrogen into substitutional sites, if the concentration of nitrogen is high enough.

In order to determine whether substitutional nitrogen or a defect

level (or some combination of the two) is responsible for the observed n-type behaviour, experiments using techniques other than those in the present study would have to be used. A more complete discussion of the role of nitrogen as a donor will be reserved until the final chapter.

VI

THE DAMAGE, LATTICE LOCATION AND ELECTRICAL PROPERTIES OF NITROGEN IMPLANTED GERMANIUM

6.1 Introduction

This chapter presents the results of damage, electrical and lattice location measurements performed on nitrogen implanted germanium. Initially, the annealing behaviour of nitrogen introduced into germanium at room temperature and a randomly selected low temperature (50°K) to total doses of 10^{14} and 10^{15} N/cm^2 was studied. Electrical measurements were then performed on samples implanted under the same conditions. Preliminary results of a lattice location study using the $^{14}N(d,\alpha)^{12}C$ nuclear reaction have been related to these electrical measurements. The next section presents the results of the damage study, followed by the electrical and lattice location results.

The damage properties of 40 keV indium implanted into germanium at room temperature were studied by Mayer et al[75] in 1967. They found that totally damaged samples annealed at 380°C while samples not totally damaged annealed at much lower temperatures (~180°C). These temperatures represent the midpoint in a 10 minute isochronal anneal curve. For indium, a dose of ~10^{14} ions/cm^2 was sufficient to cause saturation damage. No earlier work on the damage and annealing properties of nitrogen implanted germanium has been reported. Consequently, the results of these indium experiments will

be compared with those obtained for nitrogen in the present study.

The electrical properties of nitrogen implanted germanium were studied by Cussins in 1955.[76] This work used polycrystalline material and poor quality single crystals and was performed prior to the damage studies mentioned above. As a result, the author did not have the knowledge of the damage and annealing characteristics of implanted germanium to use as a guide. Cussins was unable to get nitrogen to act as a donor, following anneals to 500°C. Pavlov et al[77] have implanted 1 ohm-cm germanium with nitrogen to a dose of 1000 micro-coulombs (6.25×10^{15} ions/cm^2) and observed "donor" behaviour following anneals at 500°C. For doses less than this, they were unable to get the implanted nitrogen to become electrically active.

Alton and Love[78] implanted germanium with boron (B), aluminium (Al), gallium (Ga), germanium (Ge), phosphorus (P), arsenic (As), and antimony (Sb), and studied the resultant electrical behaviour. Phosphorus was observed to go electrically active following an anneal at 450 - 475°C, arsenic at 500°C, and antimony at slightly above 500°C. They studied <110>, <111>, and <100> crystals and found that higher anneal temperatures were required for type conversion in the <111> samples, than for the other orientations.

To date, the lattice location studies on implanted germanium have applied the backscattering technique[79,80] for cases where the mass of the dopant is greater than that of the substrate. Mayer et al[75] found that indium went into substitutional sites following 10 minute anneals at 400 - 500°C. Björkquist et al[81,82] have studied the lattice location of

heavy group III (indium, thallium) and group V (antimony, bismuth) elements in germanium at various implantation temperatures (25 - 600°C) using the backscattering of a 1.8 MeV carbon beam. At temperatures below 400°C, they found that antimony and bismuth occupy substitutional lattice sites, while at higher temperatures, there is a decrease in the substitutional fraction. The present study uses a channeled beam of deuterium to study the lattice location of implanted nitrogen, as discussed below.

A summary of the implantation studies in germanium is shown in Table 6.1. It is apparent from this table that the role of nitrogen in germanium has not been investigated in much detail. The early work of Cussins' is not too authoritative as the quality of the germanium used in his study was not as good as that presently available. The work of Pavlov is questionable as 6.25×10^{15} N/cm^2 is quite a high dose. Parsons [83] found that a dose of 1.4×10^{15} O/cm^2 required an anneal temperature of 665°C to restore the germanium lattice. Consequently, Pavlov's "donors" may very well be due to damage effects. It is unlikely that nitrogen would behave well as a donor in germanium if it does not behave well in silicon.

6.2 The Damage Study

Prior to performing electrical measurements on nitrogen implanted germanium, the damage and annealing behaviour was studied. If the damage caused by the implantation fails to anneal properly, the electrical measure-

TABLE 6-1

PREVIOUS WORK ON IMPLANTED GERMANIUM

Author	Ion	Dose	Energy (keV)	Implant Temp.	Anneal Range	Substrate
Cussins(76)	N	6 $\mu c/cm^2$	5-90	RT	500°C	30 Ω-cm
Alton & Love(78)	B,Al,Ga, Ge,P,As, Sb	5×10^{14} 1×10^{14}	40	RT	50-700°C	10-40 Ω-cm
Mayer et al (75)	In	6.3×10^{12} 2.3×10^{13} 6.2×10^{14}	40	RT	600°C	20 Ω-cm
Pavlov et al (77)	N	6.25×10^{15}	57	RT	500°C	1 Ω-cm
Björkquist et al (81,82)	In,Tl, Sb, Bi	2.4×10^{14}	30	25-600	600°C	10 Ω-cm
Parsons (83)	O^-	1×10^{12} - 1.4×10^{15}	100	30°K RT 320°C	665°C	48 Ω-cm 0.01 Ω-cm 0.001Ω -cm

ments will be seriously affected, and the observed behaviour may not be due to a substitutional position of the implanted ion. For these damage-anneal studies, four representative implantation conditions were selected - 50°K, 10^{14} and 10^{15} N/cm^2 and 300°K (room temperature) 10^{14} and 10^{15} N/cm^2. All implantations were performed at 80 keV, using a dose rate of 50 nA/cm^2. This dose rate was chosen for convenience and was held constant for all samples. Following implantation, the amount of damage was determined by backscattering measurements, and then the samples were annealed for 5 minutes in vacuum to temperatures as high as 650°C. The amount and distribution of damage following the anneal was again determined by backscattering. The results of these measurements are shown in figure 6.1, where it is seen that the most heavily damaged sample is that implanted at 50°K to a dose of 10^{15} N/cm^2, while the least damaged case is the room temperature low dose implantation. The width of the disorder peak for the 50°K 10^{15} N/cm^2 implant suggests that the damage extends over the whole implanted depth, while the 10^{14} room temperature disorder peak does not reach the random level, indicating that a dose of 10^{14} nitrogen ions/cm^2 is not sufficient to cause saturation damage. Using the annealing temperatures for indium in germanium as a guide,[75] it would be expected that the damage caused by the 10^{14} N/cm^2 implant should anneal at fairly low temperatures(i.e. between 180 - 380°C) which is seen to be the case. A non-implanted spectrum is shown in figure 6.1(a), and indicates that the germanium crystals were not of particularly good quality, as χ_{min}, the ratio of the aligned yield to the random yield, was 0.09. A value of ≈0.03 would be expected for this orientation germanium crystal.[84] The crystals used in this

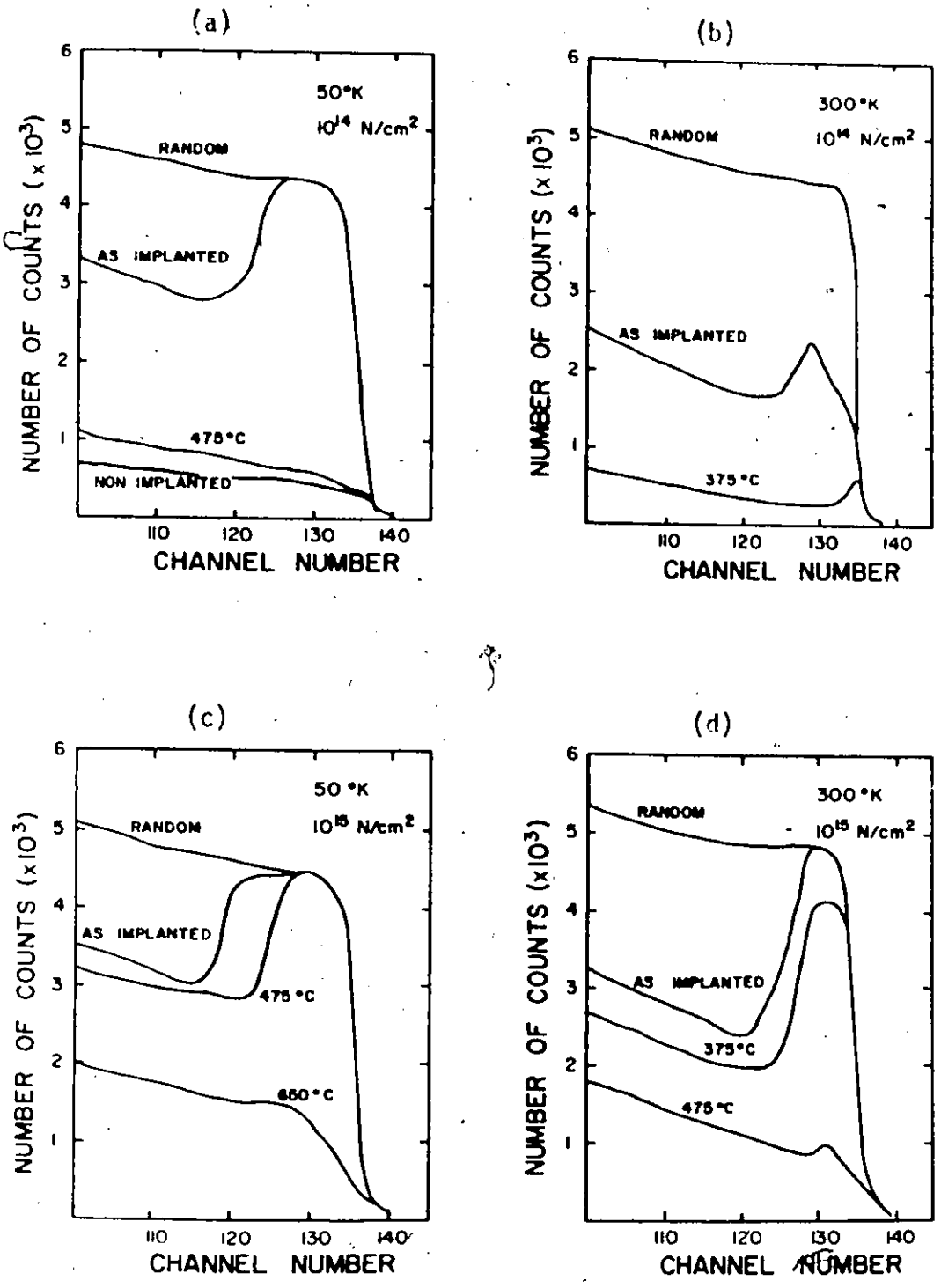

Figure 6.1 The results of a damage study of nitrogen implanted germanium. All anneals were performed in vacuum for 5 minutes.

damage investigation were obtained from RCA in a polished form. Etching these crystals produced a better χ_{min} (0.04) which implies that the value of 0.09 obtained before etching is due to a damaged surface layer rather than to poor crystal perfection. Other crystals obtained from Sylvania that were also etched showed a χ_{min} of 0.05. Although these crystals were used for some of the electrical and other damage measurements, they were not used for the measurements of figure 6.1.

For all except the most heavily damaged samples, good regrowth occurs following anneals to ~500°C, as shown in figure 6.1. This figure also shows that the annealing is initiated from the damage-crystalline interface and proceeds toward the surface. Parsons [83] has shown that 100 keV O^- ions implanted into germanium to a dose of $10^{15}/cm^2$ cause total damage which can be annealed (as measured by electron diffraction microscopy) at temperatures of 665°C. The results shown in figure 6.1 indicate that this is also the case for nitrogen implanted at room temperature. Mayer et al [75] found that 40 keV indium implanted into germanium to a dose of 6.2×10^{14} ions/cm^2 behaves in a similar manner following 10 minute anneals in an argon atmosphere.

The damage distribution versus depth for 80 keV nitrogen implanted into germanium has been calculated by Winterbon [20] and is shown in figure 6.2. The experimental damage distribution for a dose of 3×10^{14} N/cm^2 is also shown in this figure. This dose was calculated in Chapter II to be close to that required to produce saturation damage in germanium, assuming no annealing during the implantation. A dose of $\sim 8 \times 10^{14}$ N/cm^2 was actually required to achieve saturation damage. A RCA sample that had been lightly

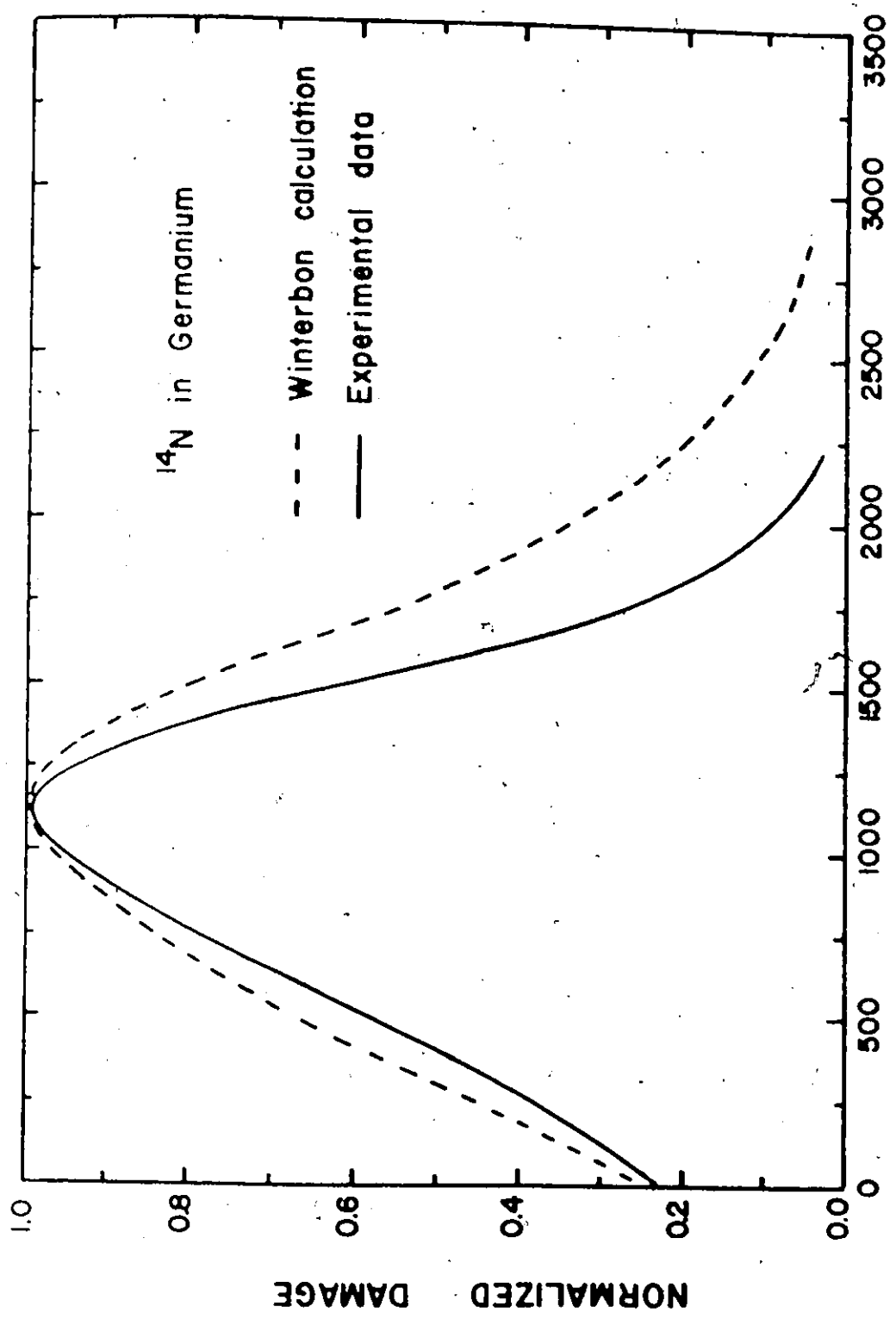

Figure 6.2 The theoretical and experimental damage profiles for 80 keV nitrogen in Germanium. The curves have been normalized to unity at the point of maximum damage. The implantation was performed at room temperature.

etched was used for this implantation. The stopping power of 2 MeV He^+ incident on germanium has been determined by Whaling[85] to be $(dE/dx)_{in}$ = 29 eV/A° and $(dE/dx)_{out}$ = 48 eV/A°. These values were used to obtain the experimental curve shown in figure 6.2. A linear de-channeling correction was used as in the silicon work.

Pavlov et al[77] have stated that donor activity has been observed for nitrogen implanted germanium following prolonged anneals at 500°C. They state that a dose of 1000 μCoulomb was necessary to obtain donor behaviour. It is unlikely that the germanium crystal would anneal properly at this temperature following such a heavy implant. In order to verify this, a germanium sample was implanted to a dose of 1000 μC and annealed for one hour at 500°C. The damage, as determined by back-scattering, is shown in figure 6.3 and shows that the germanium is still heavily damaged. This damage will seriously influence any electrical behaviour of the implanted nitrogen.

6.3 The Electrical Study

The information required to electrically characterize an ion implanted layer has been discussed in Chapter V. In particular, the number, mobility, depth distribution and activation energy of the dopant ions must be determined if the transport properties of the layer are to be understood. The measurement of the carrier concentration and sheet resistance of the implanted layer by the Hall effect techniques of Johannson et al[52] relies on the p-n junction formed by the implanted ions to electrically

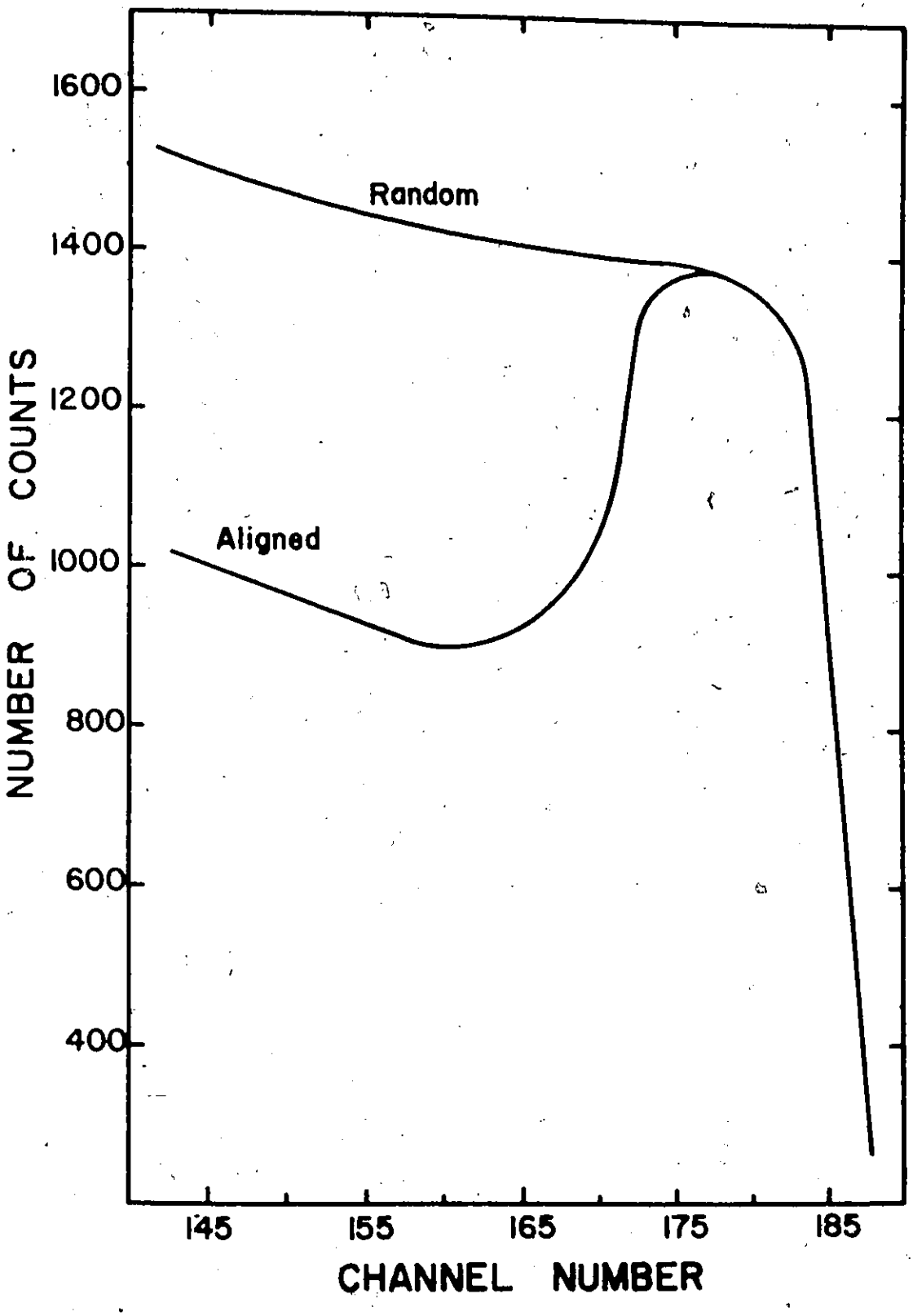

Figure 6.3 The damage spectrum for an 80 keV nitrogen implanted germanium sample following a 60 minute anneal at 500°C. The dose is 1000 μCoulomb.

isolate the layer from the substrate. This technique cannot be used unless a low leakage diode can be formed between the layer and the substrate. The first step then in the electrical characterization of a layer, is to determine whether type conversion has occurred and diodes can be formed.

The four implantation conditions that were used for the damage study were also characterized electrically. The implantations to doses of 10^{14} N/cm^2 were studied initially, as the damage study showed that these conditions annealed well. Samples were annealed for times of 2, 5, 10, 20, 40 or 60 minutes at temperatures from 200 - 700°C, in an attempt to see if nitrogen would become a donor in germanium. The samples (RCA - not etched) were studied by monitoring the I-V characteristics of mesa "diodes" etched in the implanted germanium. Electrical contact to both the implanted region and the substrate was with evaporated aluminum. In all cases, the I-V characteristics were completely linear and did not show rectification properties, indicating that nitrogen does not become a donor in germanium for these implantation and annealing conditions. A typical I-V curve for a 10^{14} room temperature implant mesa structure annealed for 10 minutes at 200°C is shown in figure 6.4(a).

Samples implanted to a dose of 10^{14} N/cm^2 were also annealed in a nitrogen ambient. This was done in case the implanted nitrogen was out-diffusing from the germanium during the vacuum anneals. Samples were annealed at 300, 400, 500 and 600°C for 10 minutes and no electrical activity was observed.

Since the germanium obtained from RCA was quite old, the electrical

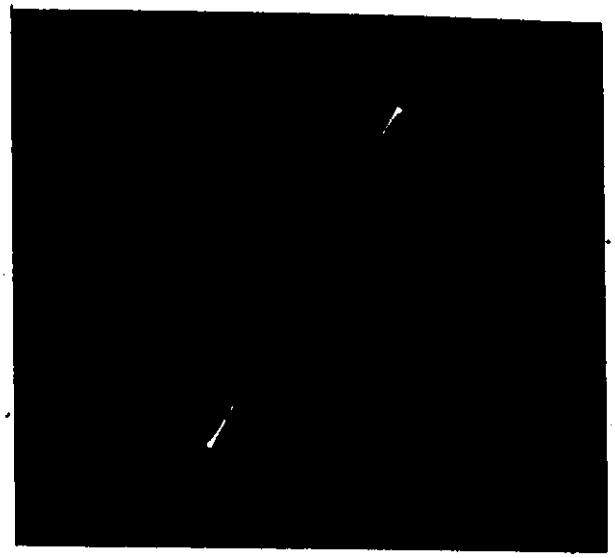

5 ma/div

0.5 V/div

Figure 6.4(a) The I-V characteristic for a RCA non-etched sample annealed at 200°C for 10 minutes. The dose is 10^{14} N/cm^2

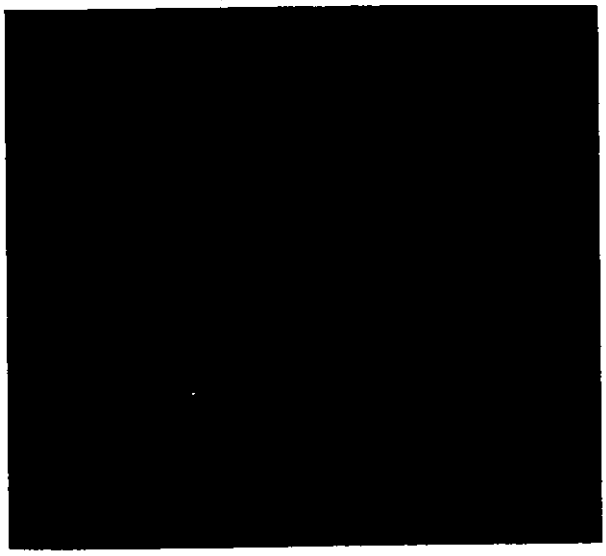

.1 ma/div

.2 V/div

Figure 6.4(b) The I-V characteristic of an etched Sylvania crystal following 300°C anneal. Dose is 10^{14} N/cm^2

properties of crystals obtained from Sylvania were also studied. The crystals were lightly etched, implanted to a dose of 10^{14} N/cm^2, and then annealed in vacuum for 10 minutes at 300, 400, 500 and 600°C. Although the I-V characteristics were not completely linear, electrical effects were not observed. The I-V relation for a Sylvania sample annealed at 300°C for 10 minutes is shown in figure 6.4(b).

The 10^{15} N/cm^2 implantations were also annealed and the same procedure used to determine if type conversion had occurred. The low temperature implantations were annealed between 500 - 675°C and the etched mesa structures were completely linear. The room temperature 10^{15} implantations however, were not linear, but exhibited rectification. This rectification was present for 500 and 600°C anneals up to 60 minutes in length, but disappears for a 10 minute anneal at 675°C, where the I-V relation becomes linear. This anneal temperature agrees with that found by Parsons for complete annealing of oxygen implanted germanium, and implies that any rectification obtained for anneal temperatures below 675°C is either a contact effect or due to residual damage.

In order to prove that the RCA germanium used in these experiments was not suspect, phosphorus diffused diodes were fabricated with germanium taken from the same lot as used for the implantation studies. The phosphorus source was "spin-on" phosphorus doped silicon dioxide,(86) having a source concentration of 5×10^{20} P/cm^3. The diffusion was performed in a nitrogen ambient at 725°C for one hour. Following the diffusion, the oxide was removed from the germanium surface with dilute HF acid, and mesa diodes etched in the germanium using the same procedure as for the implanted

samples. Aluminum was again used to contact both the diffused and the bulk surfaces. The resultant I-V curves for two representative diodes are shown in figure 6.5. The breakdown voltage of 54 volts agrees well with that expected for an abrupt junction in 1.4 - 1.8 ohm-cm p-type germanium.[54] Some of the diffused diodes broke down at lower voltages, but in all cases, good quality diodes were fabricated.

The I-V characteristics of a diffused diode was compared to the I-V characteristic obtained from a sample implanted at room temperature to a dose of 10^{15} N/cm^2 and annealed at 600°C. The results are shown in figure 6.6, where it can be seen that the reverse characteristic of the diffused diode agrees well with what would be expected from theory, while the reverse characteristic of the "contact" diode does not, and in fact is almost linear. The forward characteristics are also plotted and again the diffused diode obeys the expected shape while the "contact" diode does not.

6.4 The Lattice Location Study

The use of channeling to determine the lattice location of implanted ions was discussed in Chapter II, where it was mentioned that close-encounter reactions must be used if the mass of the dopant ion is less than the mass of the substrate. As this is the case for nitrogen in the substrates used in this investigation, the $^{14}N(d,\alpha)^{12}C$ reaction has been employed to study the lattice location of the implanted nitrogen. The technique is very similar to He^+ ion backscattering except the helium beam

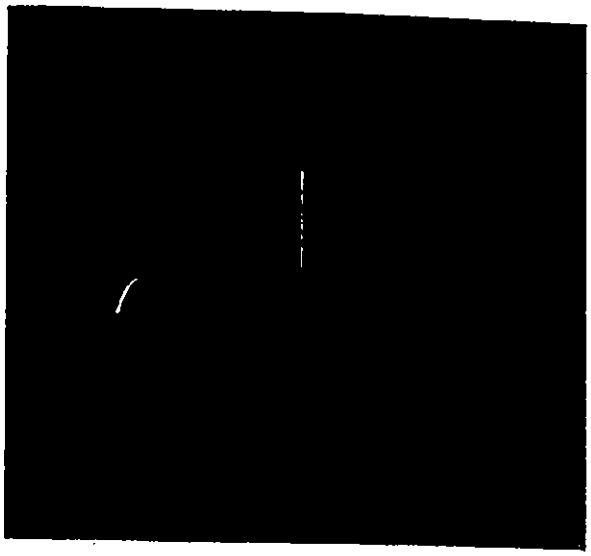

Current (10 ma/div.)

Voltage (10 volts/div.)

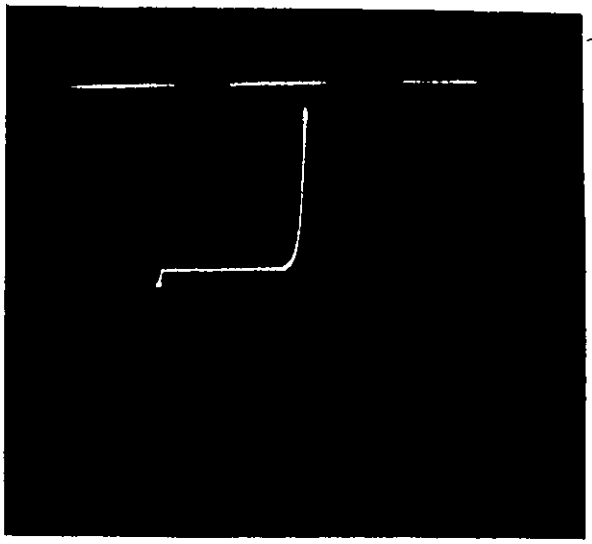

50 μa/div.

5 V/div. ← → 0.2 V/div.

Figure 6.5 The I-V characteristics of phosphorus diffused p-n junctions.

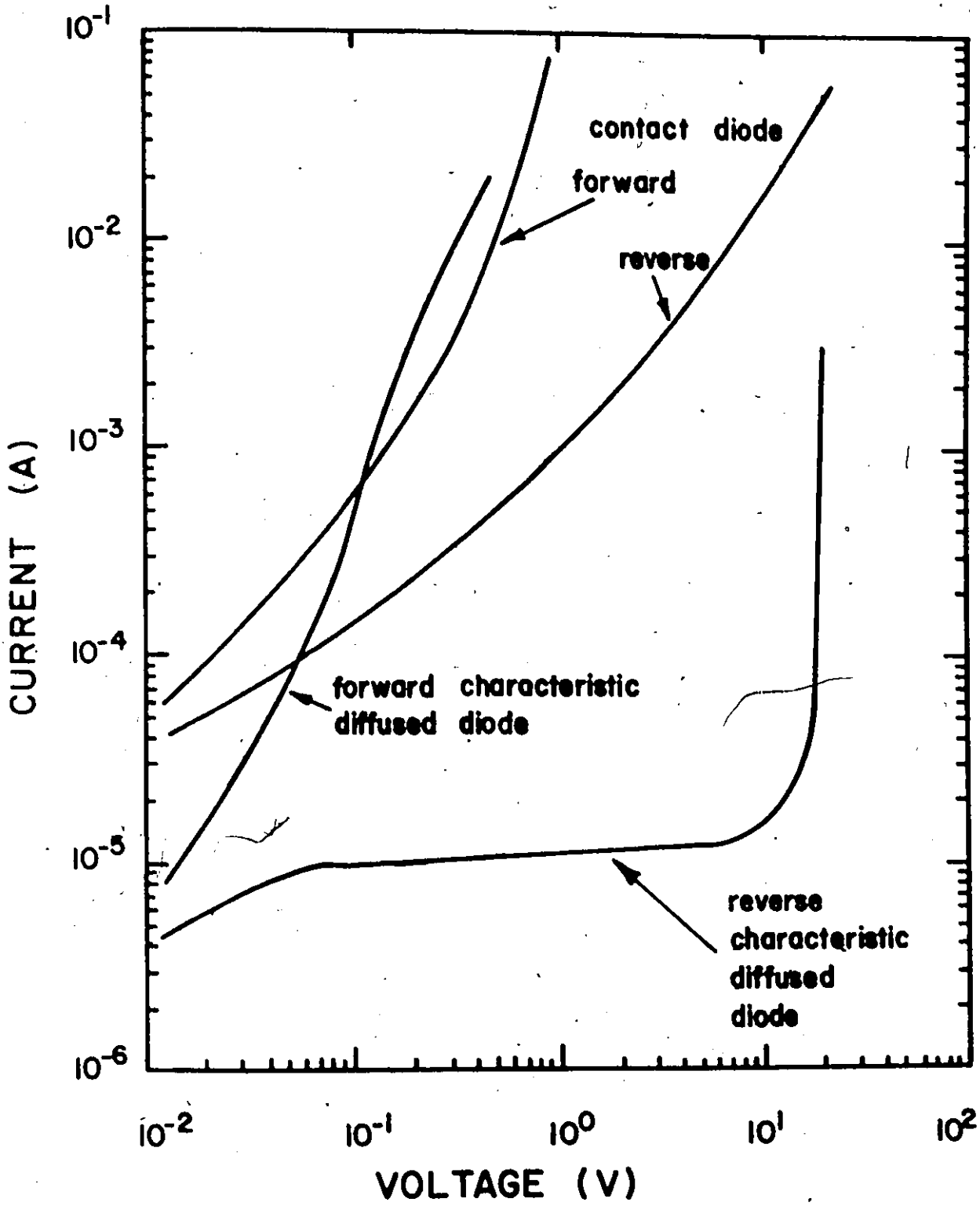

Figure 6.6 The I-V characteristics of a phosphorus diffused diode and a germanium sample implanted with 10^{15}N/cm^2 and annealed at 600°C.

is replaced with a deuterium beam and the alpha particles emitted from the reaction are detected rather than the backscattered helium ions. The backscattered deuterons have lower energies than the alpha particles and are blocked from the detector by means of a thin sheet of mylar placed in front of the detector. This is done to prevent pulse pileup and detector saturation. The experimental techniques have been discussed by Amsel et al[39,40] who has shown that some of the advantages of the micro-analysis of nitrogen by nuclear techniques include the following:

- the technique is non-destructive and fairly rapid
- the reaction yields a high energy peak unlikely to be hidden by interfering reactions
- by using a standard target, a precise quantitative measurement may be obtained
- analysis of the shape of the peak allows the determination of the concentration as a function of depth (the profile)
- the existence of energy ranges where the cross-section for the reaction varies slowly makes it possible to measure relatively thick layers.

In this reaction, the residual nucleus can exist in three states, each of which is characterized by a different, well defined Q-value. (The Q-value is the amount of energy released in the reaction). The corresponding alpha particles have characteristic energies which Amsel denotes as α_0, α_1 and α_2. The reactions and Q-values together with the energy of the α's before the mylar film are shown in Table 6.2.

In the present investigation, both the α_0 and α_1 peaks have been monitored and counted, although the intensity of α_0 is smaller than α_1. The sensitivity of this measurement has been found experimentally to be $\sim 2 \times 10^{14}$ N/cm^2. The minimum dose that can be detected is then $\sim 5 \times 10^{14}$ N/cm^2

Table 6.2

Reaction	State of Residual Nucleus	Q(in Mev)	α	Energy before Mylar (MeV)
$N^{14}(d,\alpha)C^{12}$	ground state	13.579	α_0	9.880
	1st excited	9.146	α_1	6.739
	2nd excited	5.923	α_2	4.482

and a dose of greater than 10^{15} N/cm^2 would have to be used in order to have meaningful data. As doses greater than 10^{15} N/cm^2 in silicon can result in poor annealing, especially if the implant is performed at low temperatures, the technique was used on nitrogen implanted germanium. A typical energy spectrum for a 1×10^{15} N/cm^2 implant analyzed with a 1.6 MeV deuterium beam is shown in figure 6.7. A silicon nitride standard is shown for comparison.

For the lattice location study, a germanium sample was implanted with 2×10^{15} N/cm^2 at room temperature and annealed at 550°C for 5 minutes in vacuum. The residual damage was analyzed with a 1 MeV He^+ beam and showed that the crystal structure had been restored, as χ_{min} was 0.10. The 1.6 MeV (d,α) analysis was then performed in both the aligned and random directions using a total integrated charge of 120 micro-coulombs. The results are shown in table 6.3, and indicate that the nitrogen is not substitutional.

Table 6.3

Results of (d,α) Analysis Following 550°C Anneal		
	Aligned	Random
α_1	94	101
α_o	51	51

The sample was then reannealed to 675°C for 5 minutes and the analysis repeated. The results are shown in table 6.4

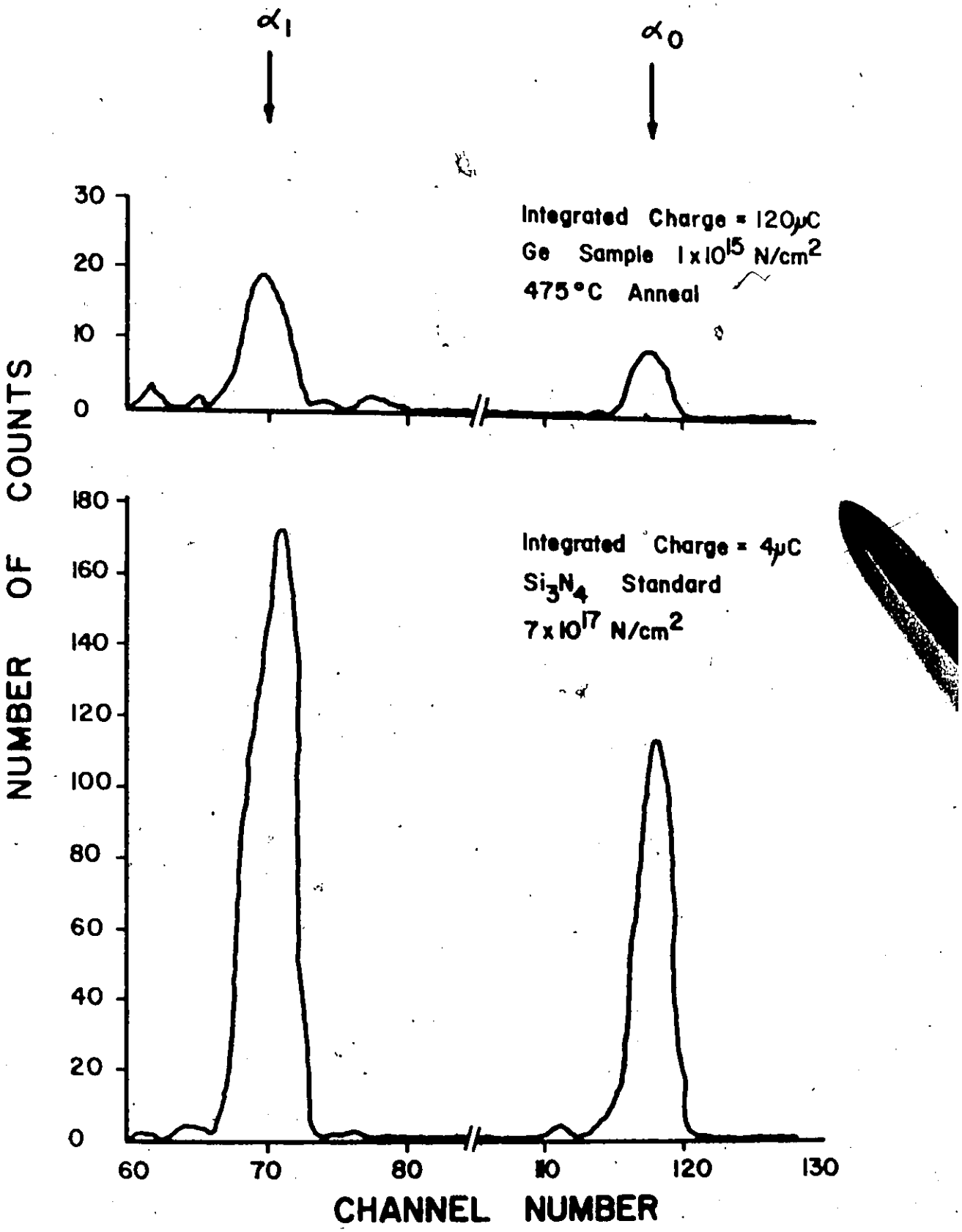

Figure 6.7 A typical energy spectrum, showing the α_0 and α_1 peaks for a $1 \times 10^{15} N/cm^2$ implant analyzed with a 1.6 MeV deuterium beam. A silicon nitride standard is shown for comparison.

Table 6.4

The results of (d,α) Analysis Following 675°C anneal		
	Aligned	Random
α_1	124	127
α_0	78	76

Again, the results indicate interstitial nitrogen. The sample was annealed again at 800°C for 5 minutes and the analysis repeated once again. The results, as shown in Table 6.5, indicate that the nitrogen is still interstitial, and that some of the nitrogen may have out-diffused.

Table 6.5

The results of (d,α) Analysis Following 800°C Anneal		
	Aligned	Random
α_1	70	68
α_0	47	44

Although the lattice location results presented are preliminary and have been made on only one sample, the indication that the nitrogen is sitting in interstitial positions following anneals of 550 - 800°C, supports the argument presented in the previous section that the rectification properties seen for these implantation conditions are not due to electrically active nitrogen.

6.5 Conclusions

The results presented in the previous sections indicate that implanted nitrogen does not become a donor in germanium. This result is not surprising, in view of the fact that it does not behave well in silicon, and that the covalent radius and bonding energy arguments presented in chapter II suggest that it is less likely to become a donor in germanium than in silicon.

Unlike the silicon results, the electrical data obtained on the nitrogen-germanium system have been confirmed with lattice location measurements. Although these measurements have an accuracy of (at best) 10%, the results imply that at least 90% of the implanted nitrogen is interstitial and does not out-diffuse from the germanium crystal until ~800°C. This also agrees with the suggestion in chapter II that nitrogen would be expected to sit in an interstitial position, as it does in metals.

The earlier results of Pavlov et al, who obtained donor behaviour for nitrogen implanted into germanium to a dose of 1000 μCoulombs and a subsequent "prolonged anneal" at 500°C have been shown to be in error. The damage level present in the germanium crystal following such an implant and a one hour anneal is too high to allow a discussion about the resultant electrical behaviour of the nitrogen ion. The role of nitrogen in germanium will be discussed in more detail in chapter VIII.

VII

The Damage, Electrical and Lattice Location Properties of Nitrogen Implanted Silicon Carbide

7.1 Introduction

This chapter presents the results of damage, lattice location and electrical measurements performed on nitrogen implanted silicon carbide. The results to be presented have been obtained using crystals supplied by three sources: the Norton Company, the Carborundum Company, and the Westinghouse Astronuclear Laboratory. The general unavailability of good crystals with well known properties has seriously hampered this study, and is the major reason why the role of nitrogen in silicon carbide has not been studied in more detail. When the dopant concentration, the amount and nature of unwanted impurities, and possibly the polytype vary from crystal to crystal, it is difficult to draw conclusions concerning the role of a dopant. Only the Westinghouse crystals were known to be similar in electrical and physical properties, and of the eight crystals obtained from this source, only half were large enough to allow them to be placed in the goniometer for damage and annealing experiments.

It is generally recognized that nitrogen is a natural dopant in silicon carbide.[49,87] Nitrogen doped samples are green in colour, and the nitrogen sits on a carbon lattice site.[49,88] Phosphorus is also known to be a donor in silicon carbide. Kroko[89] has stated that nitrogen

is a common impurity in silicon carbide, and that 10^{17} N/cm^3 is the minimum content of nitrogen ever observed in silicon carbide, although clearly any definitive statement is premature. The most common acceptors in silicon carbide are aluminum and boron. These p-type crystals are blue-black in colour while clear silicon carbide crystals are considered to be pure or compensated.

Silicon carbide can crystallize in two basic forms - cubic and hexagonal. The cubic form is usually referred to as beta (β) silicon carbide while the hexagonal form is known as alpha (α) silicon carbide. The hexagonal form has at least six variations of its basic structure, designated as α-I, II, III, IV, V and VI. These variations or polytypes may be regarded as being built up of identical layers of silicon atoms tetrahedrally surrounded by carbon atoms. The stacking of these layers is such that when only the relative position of second neighbours is considered, the atoms are either in a wurtzite or a zinc-blende structure. It is known that differences in the crystallographic structure of silicon carbide result in variations in band gap and the ionization energy of impurities.[49,90] Twinning and intergrowth of different structures are frequently occurring phenomena in silicon carbide crystals.[49,90]

The role of nitrogen as a dopant in p-type silicon carbide has been demonstrated both by diffusion and by ion implantation. Kroko[89] diffused nitrogen into single crystals of silicon carbide containing bulk aluminum concentrations of 10^{17} to 1.5×10^{19} Al/cm^3 at temperatures from 2000°C to 2550°C. Diffusion times up to 268 hours were used to produce diffusion depths of 0.3 to 5 microns. Nitrogen has been successfully implanted into

p-type silicon carbide to form a donor region by Dunlap and Marsh[91], Marsh and Dunlap[92], Hart et al[93], and Addamiano et al.[94] The electrical measurements of Marsh and Dunlap have been the most extensive, and they have found that an n-type layer has been formed following a room temperature implant and a subsequent 750°C, 15 minute anneal. The resistivity of the layer following the 750°C anneal was too high to allow Hall measurements, however Hall effect and sheet resistivity measurements performed as a function of annealing temperature in the range 1100-1700°C have confirmed the n-type region and shown that one-half the implanted nitrogen ions have become electrically active. The resultant carrier concentration is essentially constant for anneal temperatures of 1100°C to 1700°C, but the free carrier mobility increases with increasing anneal temperature, suggesting that the density of electron scattering centers is decreasing.

In their evaluation of p-n junctions formed by nitrogen implantation and subsequent anneal at 1200°C, Marsh and Dunlap found that a thick semi-insulating region existed between the n-type layer and the substrate, resulting in a p-i-n diode characteristic. The thickness of this intrinsic layer could be substantially reduced following anneals to ~1400°C, resulting in abrupt junction behaviour, as determined by the junction capacitance-voltage characteristics.

The profile of nitrogen implanted into silicon carbide at 60 keV has been measured by Addamiano et al[94] using a Cameca Ion Analyser. Both unannealed and annealed samples were studied. The peak of the nitrogen distribution prior to anneal was found to be ~1300 Å below the crystal surface,

which agrees quite well with the projected range of 1123 Å for 60 keV nitrogen in silicon carbide.[14] Following anneal, the nitrogen peak was slightly closer to the crystal surface.

The disorder produced in SiC by 30 keV nitrogen has been measured by Hart et al.[93] The number of lattice atoms displaced from their regular lattice sites was determined by the backscattered energy analysis of 280 keV He^{++} ions. They found that the regrowth of the disorder during anneal proceeds from both the underlying substrate and the target surface. An annealing stage was observed at 750°C which corresponds to the temperature at which n-type conversion was initially observed by Marsh and Dunlap.

The previous work on nitrogen implanted silicon carbide is summarized in Table 7-1. From the results shown in this table, it is evident that implanted nitrogen behaves as a donor in silicon carbide following a suitable anneal. The electrical results have been obtained using crystals obtained from a single supplier and having an aluminum concentration of $\sim 10^{18}$ Al/cm^3. Consequently, this work does not give insight into how the properties of the substrate may influence the behaviour of the implanted nitrogen. The initial damage measurements indicate that proper regrowth of the silicon carbide may not occur during anneal. This is similar to the results of nitrogen implanted silicon but may not necessarily be due to precipitation. In the studies of the growth mechanisms of silicon carbide [95], it has been found that the cubic (β) form of silicon carbide grows preferentially at temperatures lower than ~2000°C. It is possible that the heavily disordered region of the implanted crystal may regrow with this crystal structure rather than the hexagonal structure. High

TABLE 7-1

PREVIOUS WORK ON IMPLANTED SILICON CARBIDE

AUTHOR	Implanted Ion(s)	Dose	Energy (keV)	Implantation Temperature	Anneal Range (°C)	n-type conversion
Dunlap and Marsh (91)	N Sb	10^{15}	25 84 140	RT	to 1600°C	yes
Hart, Dunlap and Marsh (93)	N Sb Tl	10^{12} - 10^{15} 8×10^{14}	30 40 200	RT	to 1700°C	yes
Marsh and Dunlap (92)	N P Sb Bi	to 10^{15}	5 - 300	RT 500°C	to 1800°C	Yes
Addamiano et al (94)	N B Al	10^{14}-5×10^{15}	60	RT	to 1400°C	yes

anneal temperatures may be required to overcome this problem. Another possible cause of this poor regrowth is that different polytypes may regrow locally and may not be able to successfully join with each other at these temperatures. It is clear that a more detailed study of the damage annealing properties and a lattice location study may give a better understanding of the role of nitrogen in silicon carbide.

The first experiments with silicon carbide in the present study were aimed at gaining some knowledge of the damage and annealing properties of nitrogen implanted into this material. The concentration of the bulk silicon carbide crystals, as determined by neutron activation analysis or as supplied by the crystal supplier, was fairly high (5×10^{17} - 10^{20} Al/cm^3) and hence high doses would be required for any subsequent electrical study. To study the damage properties, the Norton and Westinghouse crystals were implanted and analysed by the backscattering technique as a function of anneal temperature. The results will be presented below.

The electrical measurements of nitrogen implanted silicon carbide presented more of a challenge. Initial studies using 80 and 40 keV nitrogen for various doses and Norton crystals gave a host of different results. It was realized that the 40 keV implantation resulted in a projected range that was too deep (cf. fig. 2.5) and a region near the surface was either not being doped, or was very lightly doped with nitrogen and was consequently influencing the results. Since the beam current available with the 150 keV accelerator is very low for energies less than 40 keV, and fairly high doses were required, a number of implantations at 45 and 20 keV were performed using the Chalk River isotope separator. These implantations

were performed into Norton, Westinghouse and Carborundum crystals, and the results obtained are presented below.

The lattice location of the implanted nitrogen following a high temperature anneal has been studied by the $^{15}N(p,\alpha)^{12}C$ reaction. The ^{15}N used for this investigation was implanted at room temperature using the Chalk River isotope separator. A description of the technique and some preliminary results will be presented in this chapter.

7.2 The Damage Study

The initial damage studies on nitrogen implanted silicon carbide consisted of comparing the damage and annealing properties of nitrogen introduced into p-type crystals obtained from Westinghouse and the Norton Company. The crystals from the Carborundum Company had been obtained for an earlier project and were very heavily doped with aluminum (concentration $\sim 5 \times 10^{20}$ Al/cm^3). As a consequence, they were not used for this damage study.

Prior to implantation, the backscattering technique was used to obtain a non-implanted spectrum of the crystals to ensure that they were of good quality. Values for χ_{min} (the ratio of the aligned to random backscattered yields) of 0.070 for the Westinghouse sample and 0.076 for the Norton sample implied that the samples had good crystal structure. The implantations were performed at room temperature into the smooth face of the crystal. This is believed to be the (0001) or silicon face, although it was not verified by X-ray techniques. A single implant at

80 keV to a total dose of 8×10^{14} N/cm^2 was used. The dose rate was approximately 50 nA/cm^2. Following implantation, the backscattering technique was used to determine the amount of damage and to follow the nature of the annealing for anneal temperatures as high as 1450°C. All anneals were performed in vacuum and were for 3 minutes duration. Marsh and Dunlap have performed an isothermal anneal at 1000°C and found that most of the annealing occurs in the first two minutes of the anneal. For this reason, an anneal time of 3 minutes was selected.

Figure 7.1 shows the results obtained for the Westinghouse crystal while the corresponding results for the Norton crystal are shown in figure 7.2. The damage of the Westinghouse crystal is seen to anneal much better than the Norton crystal. Table 7.2 compares the damage area and the χ_{min} values obtained for the two samples as a function of annealing temperature. It should be noted that the Norton crystal used for this experiment was much more heavily doped with aluminum than the Westinghouse sample, and this may be influencing the annealing behaviour.

The data of Hart et al[93] for 30 keV nitrogen implanted into crystals obtained from the Westinghouse Astronuclear Laboratory to a dose of 9×10^{14} N/cm^2 is compared to that obtained in the present study in figure 7.3. In both cases the relative disorder at room temperature prior to anneal has been normalized to unity. Although the crystals used by Hart et al came from the same source, it is not too likely that they came from the same growth batch. They specified that the χ_{min} prior to implantation was 0.05, slightly better than the 0.07 observed for the Westinghouse crystal used for the present study. The sample of Hart et al exhibits

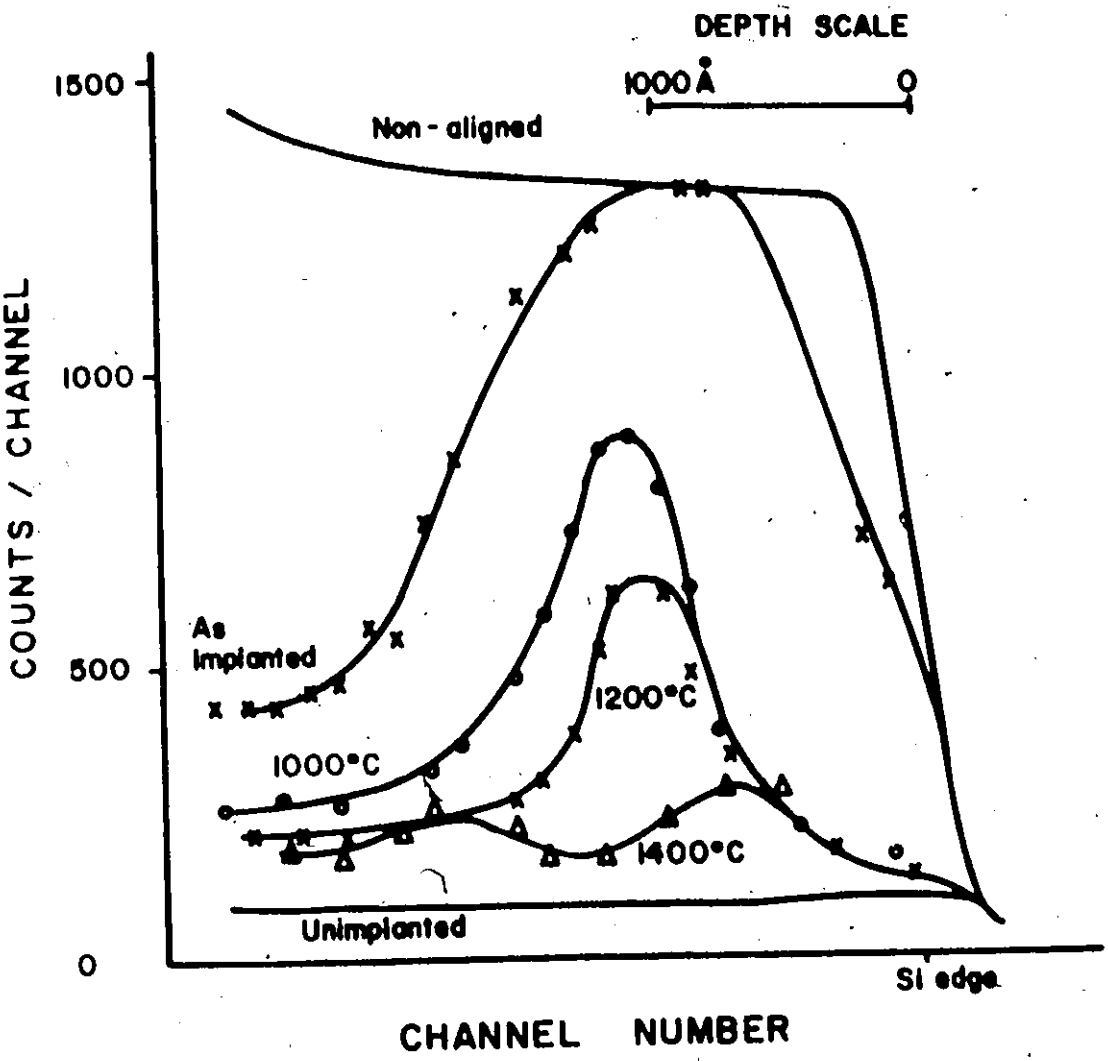

Figure 7.1 The damage spectra as a function of anneal temperature for the Westinghouse crystal. The dose was 8×10^{14} N/cm^2.

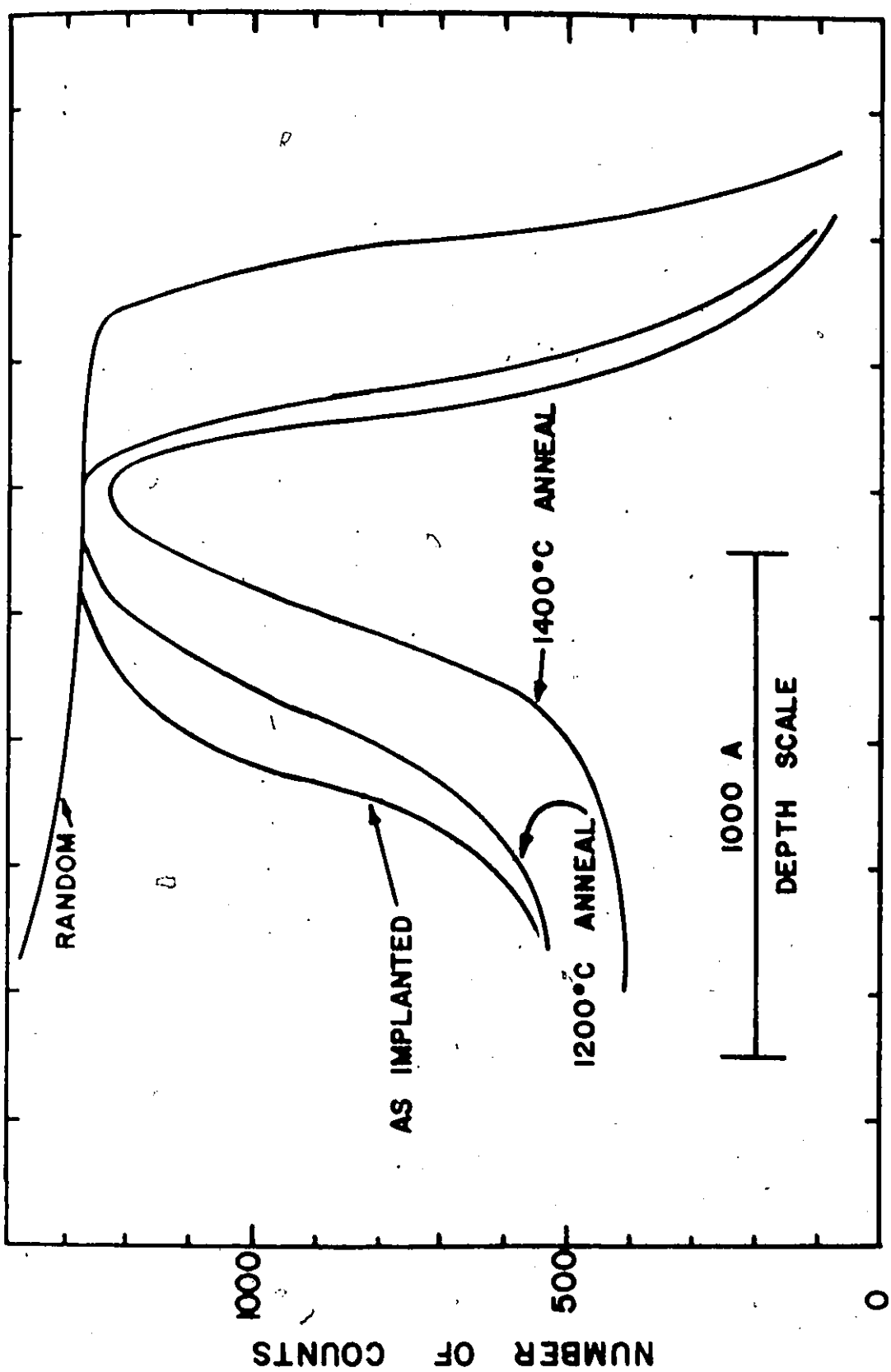

Figure 7.2 The damage spectra as a function of anneal Temperature for the Norton crystal. The dose was 8×10^{14} N/cm^2

TABLE 7.2

A COMPARISON OF THE ANNEALING BEHAVIOUR OF WESTINGHOUSE AND NORTON SILICON CARBIDE

	Before Implant	As Implanted	700°C	800°C	900°C	1000°C	1100°C	1200°C	1400°C
Norton	-	16,549	14,591	13,208	10,866	-	11,261	11,298	9,744
Damage Area (arb. units)									
x_{min}	0.076	0.38	0.33	0.34	0.43	-	0.41	0.38	0.34
Westinghouse	-	15,116	9,353	7,520	7,084	5,413	4,870	3,796	3,428
Damage Area (arb. units)									
x_{min}	0.070	0.31	0.24	0.25	0.25	0.21	0.23	0.14	0.15

Implantation: 8×10^{14} N/cm^2, room temperature, 80 keV

Damage Area : measured over 25 channels below edge; linear dechanneling correction made

x_{min}: measured as the ratio of the aligned level to random level, 5 channel average taken behind the damage peak

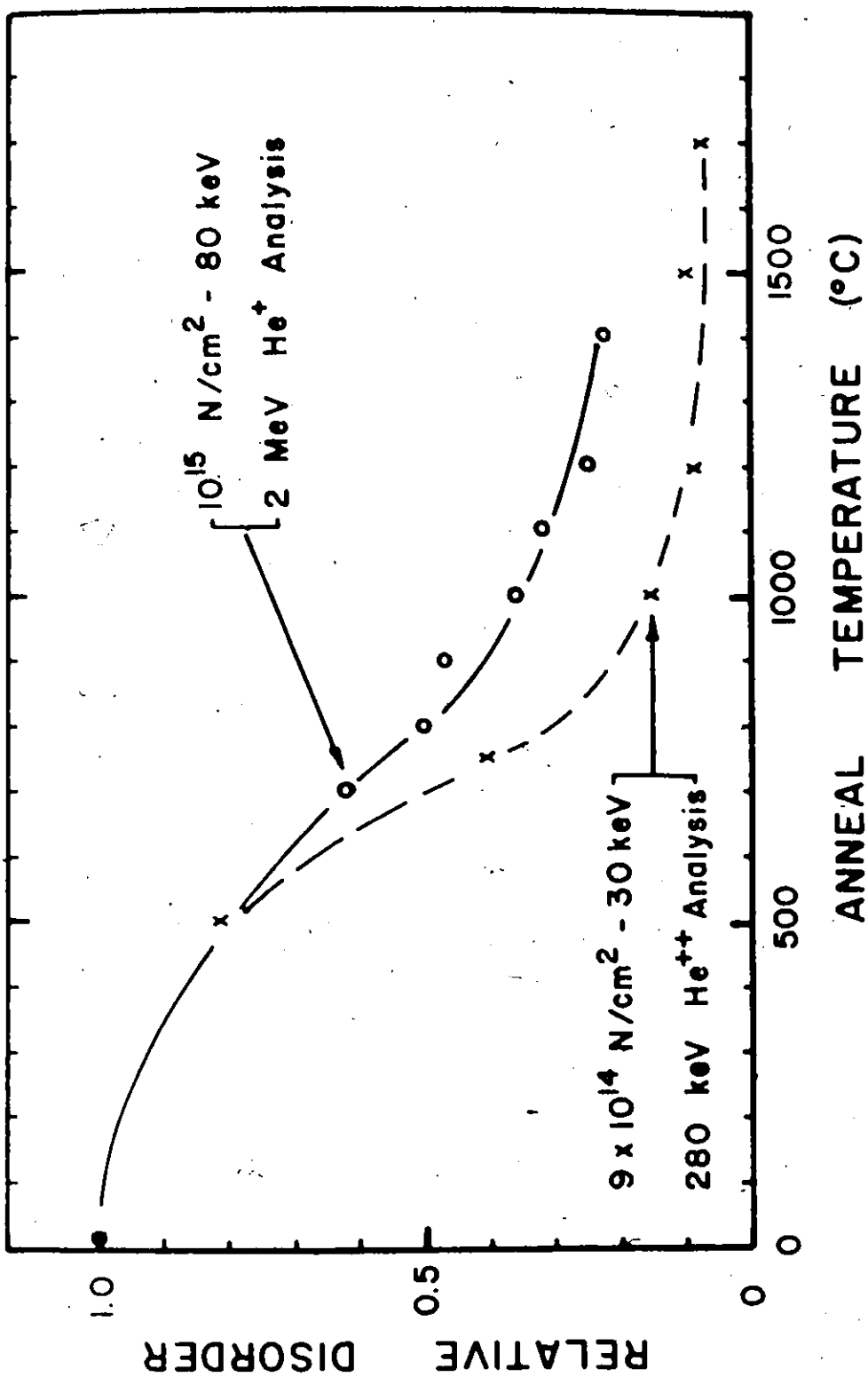

Figure 7.3 The relative disorder versus anneal temperature for this work (o) and that of Hart et al[93] (x).

better annealing properties than the crystal used in this investigation. Hart et al used a 280 keV He^{++} beam to determine the damage and annealing behaviour while the present study used a 2 MeV He^{+} beam. Better depth resolution would be expected for the higher energy beam. In the present study, the area of the damage peak (after subtracting a linear dechanneling correction) was used to determine the amount of disorder whereas Hart et al used the height of the aligned spectrum behind the damage peak as a measure of the lattice disorder. Because of the better resolution and the more accurate method of analysis, the results of this work should be more authoritative.

It is interesting to note that the Norton crystal does not completely anneal even for anneals to 1400°C. This large residual damage peak could explain the poor electrical results obtained with these crystals, as discussed in the next section. The Westinghouse crystal, although still not perfectly annealed following a 1400°C anneal, has annealed sufficiently to allow lattice location measurements, as discussed later. Figures 7.1 and 7.2 show that the annealing is taking place from both the substrate and the target surface, as observed by Hart et al. Some of the Norton samples had a high mass impurity which was calculated from the backscattered energy to be iron. It is known that iron is a common impurity in silicon carbide,[90] and can be present to levels as high as 10 ppm. The Westinghouse crystals did not show this impurity. The difference in the annealing behaviour might be linked to the purity of the starting crystal.

It is well known that silicon carbide is a polar crystal, with one

face being the (0001) or silicon face while the other is the (000$\bar{1}$) or carbon face. It is interesting to see if the damage and annealing properties of the two faces are identical. A nitrogen doped Norton sample was analyzed by means of backscattering and then had both faces implanted at room temperature with nitrogen to a dose of 2×10^{14} N/cm^2. The amount of damage on each face was measured following implantation and following a 650°C vacuum anneal. The results are presented in Table 7.3 and show that the damage and annealing characteristics are totally different for the two faces. This experiment could not be duplicated with a Westinghouse crystal because of a shortage of samples.

Unfortunately, the results of the present study as discussed above have not been repeated due to a lack of crystals. For this reason, no estimate of the reproducibility from crystal to crystal can be made. It is clear that the level of doping and the amount and nature of trace impurities may influence the annealing of the implanted nitrogen, and will be important if good quality devices are to be fabricated.

7.3 The Electrical Study

The initial attempts to form p-n junctions in silicon-carbide by nitrogen implantation failed. The resultant I-V characteristics showed that the junctions broke down at low voltages and turned on poorly. These diodes were formed in Norton material of doping concentrations greater than 10^{18} Al/cm^3. Some of the samples were known to have concentrations

Table 7.3

A COMPARISON OF THE A AND B FACES FOR

NORTON SILICON CARBIDE

	Before Implant	Before Anneal	650°C
A Face	-	1177	503
Damage Area (arb units)			
x_{min}	0.06	0.075	.057
B Face	-	2597	1800
Damage Area (arb units)			
x_{min}	0.079	0.124	0.123

Implantation: 2×10^{14} N/cm^2, room temperature, 80 keV

Damage Area : linear dechanneling correction made

close to 10^{20}Al/cm^3. It was believed that the 40 keV implantation was too high in energy, and that the surface region was not being doped n-type. Consequently, lower energies were used (45 and 20 keV). A Westinghouse crystal, a Carborundum sample, and a clear Norton crystal were implanted at these lower energies. The clear silicon carbide samples are known to be compensated. This clear crystal was selected as it was large enough to allow a van de Pauw pattern to be formed on it. All the crystals were coated with aluminum and had holes (or, for the clear sample, a Hall pattern) opened in the aluminum using photolithographic techniques. The implants were performed at room temperature and consisted of 1.06×10^{15} N/cm^2 at both 45 and 20 keV for the Westinghouse and Norton samples and 5×10^{15} N/cm^2 and 2.5×10^{15} N/cm^2 at 45 keV and 20 keV respectively, for the Carborundum sample. Following implantation, the samples had the aluminum mask removed and were annealed.

The Westinghouse crystal was annealed at 1450°C for 3 minutes in vacuum. This temperature was selected on the basis of the earlier damage studies. The I-V relation for the resultant diode is shown in figure 7.4. A pressure indium contact was made to the bulk substrate and a tungsten probe was used to contact the implanted region. The characteristic is very similar to that observed by Dunlap and Marsh[91] except the reverse breakdown voltage is ~28 volts, while their mesa etched diode broke down more sharply at ~46V. There is no reason to believe that the acceptor concentration in their samples was identical to that of the crystal used in this investigation, and consequently, the

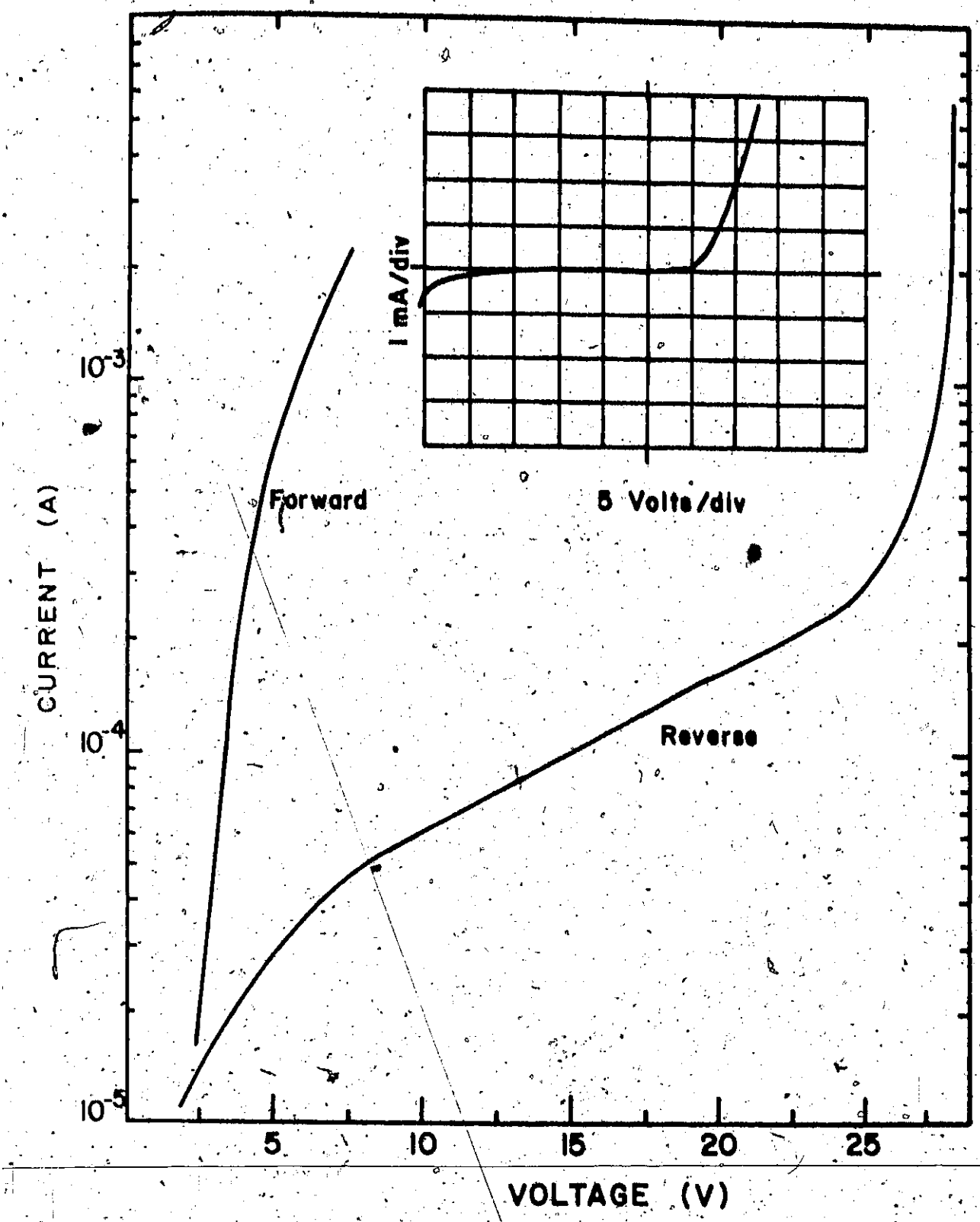

Figure 7.4 - The I-V relation for a Westinghouse crystal implanted at room temperature to 2×10^{15} N/cm^2 at 45 and 20 keV. The sample was annealed at 1450°C for 3 minutes following the implantation.

breakdown voltages should not necessarily agree.

Following implantation, the Van der Pauw pattern implanted through the aluminum mask into the Norton crystal was dark brown in colour and clearly visible on the clear Norton sample. Difficulties were not anticipated in making Hall measurements as a function of anneal temperature, as the n-type region should remain green following anneal, and hence be visible. However, following a 3 minute 1000°C anneal, the pattern had completed disappeared, and consequently Hall measurements were not performed. Subsequent damage studies, that were reported in the previous section, have shown that the Norton crystals do not recrystallize well even after anneals of 3 minutes at 1450°C. Consequently, Hall measurements should be performed with the Westinghouse crystals. None of these crystals however is large enough to allow a 2 mm Van der Pauw pattern to be defined.

The Carborundum samples had a bulk aluminum concentration of $\sim 5 \times 10^{20} Al/cm^3$ and were obtained for an earlier project where the objective was to produce a SiC tunnel diode by an alloying technique. Because of the high substrate doping, a total dose of 7.5×10^{15} N/cm^2 was used. The sample failed to exhibit rectification properties following an anneal at 1000°C for 3 minutes. As no backscattering damage data was obtained for these crystals, it is not known how the crystal regrows. Rectification was not observed following another 3 minute anneal at 1485°C.

The results of these electrical measurements have shown that implanted nitrogen can act as a donor in the Westinghouse silicon carbide following a suitable anneal. The annealing and electrical behaviour of

these diodes closely resembles those formed in similar material by Marsh et al. For this reason, and because of a shortage of crystals, a more complete study of the electrical properties of the diode, (for example C-V measurements) has been omitted.

7.4 The Lattice Location Study

The location of the implanted nitrogen ions in the silicon carbide lattice following a high temperature anneal has been determined by the $^{15}N(p,\alpha)^{12}C$ reaction. The techniques used for this study were similar to those described in the previous chapter for the $^{14}N(d,\alpha)^{12}C$ reaction, where the alpha particles induced by the reaction are monitored as a function of sample orientation. The sample is first aligned with the He^{+} beam and then the 800 keV proton beam is turned on an the reaction induced alpha particles are counted. The sample is then placed in a random direction, and the induced alpha particles are again counted. The same total integrated beam current is used for both orientations of the sample. The backscattered protons are shielded from the detector by thin sheets of aluminum and mylar placed in front of the detector. A discussion of the $^{15}N(p,\alpha)^{12}C$ reaction has been presented by Hagedorn and Marion[96]. Clearly resolved alpha peaks of 2.75 MeV energy (after the absorber) were obtained, free from background. The sensitivity of the technique has been estimated at 2×10^{14} $^{15}N/cm^2$ and is limited by background noise.

The results of the damage study presented earlier showed that both the Westinghouse and the Norton crystals had damaged regions at the

mean damage depth following anneals to 1300°C. Following 1400°C anneals, the Westinghouse crystals had annealed quite well, with only a small peak remaining at the mean damage depth, while the Norton crystal was still heavily damaged, as shown in figure 7.2. Since the lattice structure of the implanted crystal must be restored before a lattice location study has any meaning, a Westinghouse crystal was selected for this study. The implantation was performed using the Chalk River isotope separator. A dose of 5.1×10^{14} $^{15}N/cm^2$ at 45 keV and 5.3×10^{14} $^{15}N/cm^2$ at 20 keV was implanted into the silicon face of the crystal at room temperature. A silicon sample was also implanted to a dose of 5×10^{15} $^{15}N/cm^2$ as a standard. Prior to analysis, the Westinghouse sample was annealed at 1450°C for 3 minutes.

The results of this experiment are presented in figure 7.5. The number of counts in the aligned and the random orientation for both the silicon standard and the silicon carbide sample are shown. The area under the aligned curve is 62% of the area under the non-aligned or random curve.

The substitutional percentage of the implanted nitrogen can be calculated from

$$S = \frac{1 - N_A/N_R}{1 - \chi^*_{min}} \times 100 \qquad (7.1)$$

where N_A and N_R are the areas under the α-peaks in the aligned and random directions and χ^*_{min} is the average value of the ratio of the aligned to random backscattered yields in the implanted region. In order to get reasonable statistics, proton doses of the order of 1000μCoulombs

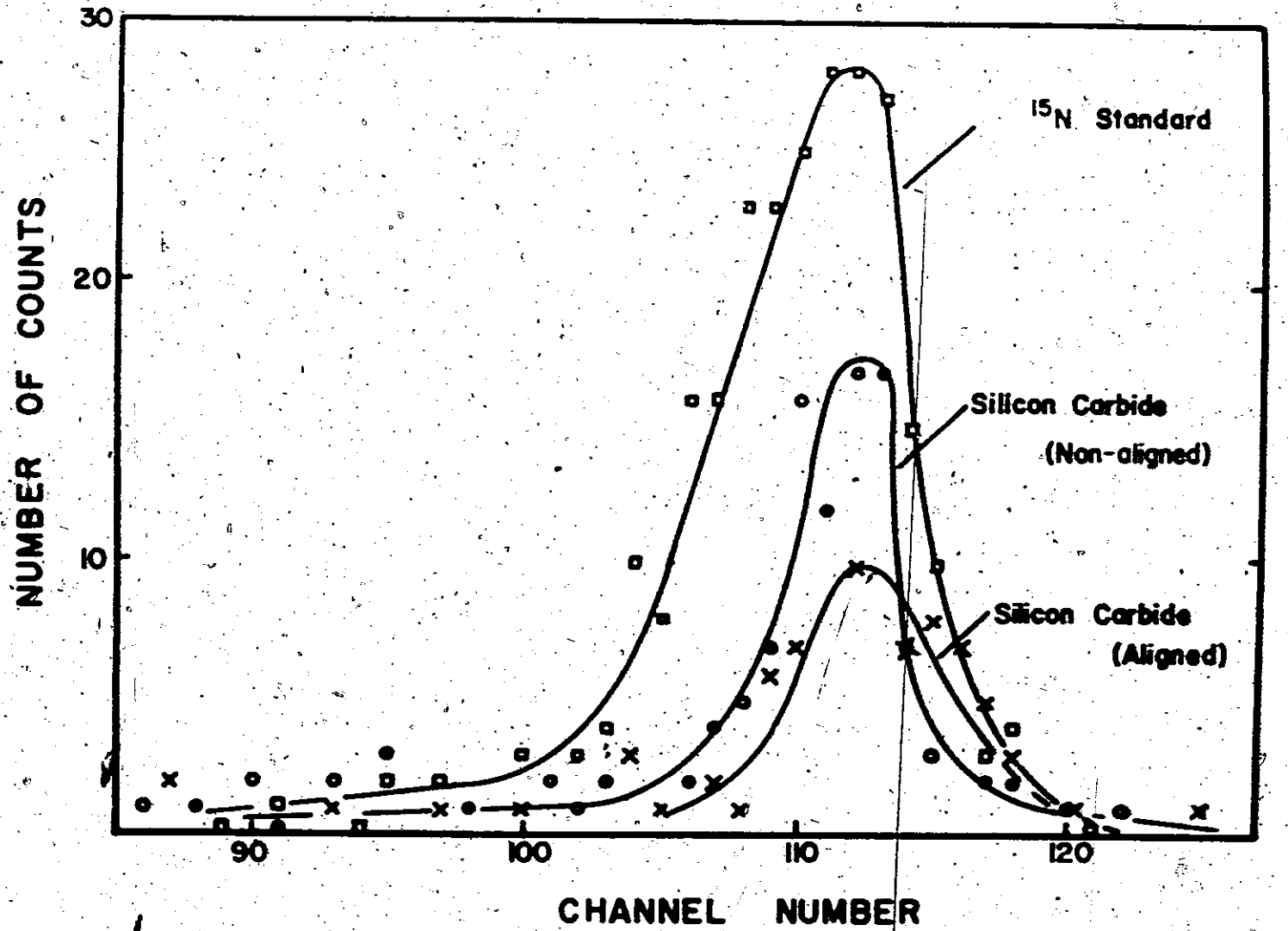

Figure 7.5 The spectra from the $^{15}N(p,\alpha)^{12}C$ reaction on implanted and annealed SiC. A spectrum from a ^{15}N standard is shown for comparison.

are necessary. The data shown in figure 7.5 was obtained with a total proton dose of 320μC. Attempts to improve the statistics were unsuccessful due to excessive damage from the proton beam. Even after the 320μC dose, subsequent backscattering analysis using a 2 MeV He^+ beam indicated that χ_{min} had increased to 36% from the 15% value at the beginning of the analysis.

Substituting the area ratio of 62% and a χ^*_{min} value of 25%, which is a reasonable average χ_{min} value during the analysis, a substitutional percentage of 51% is obtained. This result implies that 51% of the implanted ^{15}N atoms are shadowed by atomic rows when the crystal is viewed down the c-axis, and therefore are probably on substitutional sites. This is in good agreement with the substitutional component of 50% deduced by Marsh and Dunlap[92] from electrical measurements.

7.5 Conclusion

The results presented in this chapter have shown that nitrogen can be successfully introduced as a donor into p-type silicon carbide using the techniques of ion implantation. The limiting factor on its usefulness and role as a donor is the quality of the starting crystal. Although the Norton and Westinghouse crystals had pre-implanted χ_{min} values that were similar (0.070 for the Westinghouse and 0.076 for the Norton) which suggests that the crystalline perfection of the crystals was similar, the Norton samples had high mass impurities (notably iron) which were

observed during the backscattering analysis. The poor recrystallization of the damaged layer for the Norton crystals may be due to these impurities.

The damage and lattice location results have confirmed the results of the earlier electrical results of Hart et al[93] and Marsh et al[92]. The damage peak anneals at ~1450°C and approximately 50% of the implanted nitrogen is substitutional. The thick semi-insulating region observed by Marsh et al by electrical studies has been shown to be a damaged region. The annealing temperature at which they observed abrupt junction behaviour agrees well with the anneal temperature at which the damage peak is observed to anneal. The lattice location experiments in the present study confirm the 50% electrical conversion efficiency observed by Marsh et al.

It would appear from the results presented above, that ion implantation is a viable technique for doping silicon carbide and forming high temperature devices, but that the state of silicon carbide crystal growth is such as to hinder advances in this direction. Until uniform, fairly large crystals with controllable impurity levels can be grown, silicon carbide device technology will not advance. The role of nitrogen and other dopants in silicon carbide will be discussed in the final chapter.

VIII

Conclusions

8.1 Introduction

This chapter discusses the role of nitrogen in the three semiconductor materials studied in this investigation. An attempt is made to expand on the conclusions presented earlier, especially those that are common to all three materials. Suggestions or recommendations for further work or additional interesting experiments are presented.

8.2 The Nitrogen-Silicon System

The results of the damage and electrical properties of nitrogen in silicon obtained in this investigation confirm the theoretical predictions presented in Chapter II. In that chapter, it was suggested that the small size of atomic nitrogen (covalent radius of 0.70 Å compared to 1.17 Å for silicon) would strain the silicon lattice and the nitrogen would probably occupy an interstitial position. It was further shown that this size difference was greater than 15% and hence a substitutional solid solution would not be predicted by the Hume-Rothery rule. The results of the damage study show that although the lattice anneals well for doses of 10^{14} N/cm^2 implanted at room temperature, for doses of 10^{15} N/cm^2, the damage does not totally anneal and in fact regrows at anneal temperatures

of ~900°C (cf. fig. 4.8). The electrical results, which are more sensitive than the backscattering technique, shows that the implanted region behaves as if it were an insulator for doses greater than $\sim 6 \times 10^{14}$ N/cm^2 regardless of the anneal temperature. The regrowth of the damage for the 10^{15} N/cm^2 implants at high anneal temperatures is probably the result of precipitation. Schwuttke[4] has observed the formation of Si_3N_4 for high dose nitrogen implantations.

A definitive explanation for the observed donor behaviour presented in Chapter V is difficult. There are arguments to support either a defect conduction mechanism or substitutional donor behaviour of the implanted nitrogen. The fact that the nitrogen does not fit into the silicon lattice very well and hence could easily trap or stabilize defects supports the idea of a defect conduction mechanism. The inability to fit the normalized carrier concentration versus reciprocal temperature curves of the theoretical expression for a single donor level, indicates the presence of some defect centers.

The fact that there is a unique ionization energy which is independent of anneal time and implantation temperature (and consequently, the initial amount of damage) suggests a substitutional position for the nitrogen. The shallowness of the level (0.017 ± 0,002 eV) below the conduction band also suggests a substitutional site, as all known defect centres in silicon give rise to deeper states in the band-gap.[97] The diode characteristics presented in Chapter V are well behaved, with low saturation currents and good capacitance voltage characteristics. These would be unlikely to occur of active deep centers were responsible for the observed

donor behaviour, as centers located in the space charge region of a diode would influence the observed saturation current and not necessarily sweep out with reverse bias in the expected manner. The breakdown voltages for the nitrogen implanted diodes agree well with that expected for avalance breakdown in the bulk substrate material. It is unlikely that an active defect would not influence the observed breakdown voltage.

There is another reason why nitrogen may assume a substitutional position in the silicon lattice for the doses studied in the present investigation. It is known that the solubility of nitrogen in silicon is very low ($4.5 \pm 1.0 \times 10^{15}/cm^3$).[74] For very low nitrogen doses, no electrical effects are observed (cf. fig.5.6). However, as the dose is increased to $\sim 10^{14}/cm^2$, electrical effects are observed. For a dose of 1.4×10^{14} N/cm^2, the peak nitrogen concentration is $\sim 6 \times 10^{19}$ (cf. fig. 2.3). This is a factor of $\sim 10^4$ over the reported solubility limit. For these concentrations, the nitrogen may be forced into a substitutional position. This is plausible when it is realized that nitrogen introduced to a dose of $\sim 6 \times 10^{14}$ N/cm^2 causes poor crystallization to occur for all anneal temperatures. The observed saturation donor level may be the maximum possible before the lattice strain results in poor crystallization. This severe lattice strain may cause other conduction mechanisms which would explain the inability to fit the normalized carrier concentration versus reciprocal temperature curves to a single donor level.

The question of why the observed donor activity disappears for high anneal temperatures is a difficult one to answer. If defects are responsible for the donor centers, they may break up and result in non-active

centers or migrate to sinks. If this is the case, the break up is not occurring at a specific temperature, as the annealing temperature at which the electrical activity is lost depends on the dose - the higher the dose, the higher the type conversion temperature. It is more likely that the nitrogen is in a forced substitutional position. This would explain why the loss of donor activity is dependent on the dose (or total nitrogen concentration) while independent of the donor concentration.

Unfortunately, the lattice location techniques used in the present study with germanium and silicon carbide do not have sufficient sensitivity to be used with silicon. This is due to the fact that the silicon lattice does not anneal properly for nitrogen doses greater than $\sim 6 \times 10^{14}$ N/cm^2, as determined by the electrical measurements. Hence, if a meaningful indication of the position of nitrogen in silicon is to be obtained, the dose must be kept below this. As the sensitivity of the $^{15}N(p,\alpha)^{12}C$ reaction is $\sim 2 \times 10^{14}$ $^{15}N/cm^2$, the experiment would be difficult. Of course, even if the experiment were possible, the low (<1%) substitutional component could not be determined.

8.3 The Nitrogen-Germanium System

The results on the nitrogen-germanium system presented in this thesis show that nitrogen does not become a donor in germanium. The lattice location measurements have indicated that the nitrogen is sitting in an interstitial position in the germanium lattice within measurable accuracy (~10%) as suggested by the theoretical considerations in Chapter II. These measurements have also shown that the nitrogen is not outdiffusing

for anneal temperatures less than 800°C. Previously reported donor behaviour observed in germanium implanted with nitrogen to a dose of 1000μCoulomb and annealed at 500°C, have been shown to be due to damage.

8.4 The Nitrogen-Silicon Carbide System

The previous chapter has presented the results of a study of nitrogen in silicon carbide. The role of nitrogen as a donor, which was suggested from the atomic size and energy considerations presented in Chapter II, has been confirmed. Lattice location studies have shown that ∿50% (±5%) of the implanted nitrogen is sitting on substitutional lattice sites following an anneal for 3 minutes at 1450°C. This result, which was obtained on a crystal that was fairly lightly doped (∿5×10^{17} Al/cm^3), was in excellent agreement with that deduced earlier[92] from electrical measurements.

Material that had a higher acceptor concentration and that had a higher concentration of impurity elements was found not to recrystallize as well as the more pure material, that also had a lower acceptor level. This suggests that impurity elements or higher acceptor doping levels may seriously influence silicon carbide device formation by implantation. These results indicate that this poor regrowth is related to the material and not a property of the nitrogen or related damage. As mentioned in Chapter VII, the various polytypes of silicon carbide may form during anneal and be unable to successfully join together, resulting in poor damage annealing.

It would be interesting to examine the amount and subsequent annealing behaviour of the nitrogen induced damage when the substrates is held at an elevated temperature during the implantation. Such a hot implant may lower the amount of implantation damage and greatly reduce the anneal temperatures required for donor behaviour.

It should be pointed out that recent attempts to implant aluminum into nitrogen doped n-type silicon carbide with resultant acceptor behaviour have failed except for a sample that had a relatively low nitrogen concentration.[92] If the covalent radii of aluminum and nitrogen (1.26 Å and 0.70 Å; sum = 1.96 Å), are compared to those for silicon and carbon (1.17 Å and 0.77 Å; sum = 1.94 Å), it is seen that an aluminum and nitrogen pair could replace a silicon carbon pair and fit into the lattice with little resultant strain. It may be that the resultant compensation effects may influence device fabrication using nitrogen and aluminum as the donor and acceptor respectively. The results of implanting nitrogen into boron doped silicon carbide would be interesting.

8.5 Conclusions

This thesis has investigated the radiation damage and electrical behaviour of nitrogen introduced into silicon, germanium and silicon carbide by the techniques of ion implantation. It has been found that nitrogen does not behave as a donor in germanium. The formation of precipitates at high doses, and the small donor behaviour of nitrogen in silicon, which is probably due to substitutional nitrogen, makes nitrogen

unsuitable as a dopant in silicon. Nitrogen does become a donor in silicon carbide, providing the radiation damage can be annealed. The doping level and/or impurity level of the initial silicon carbide crystal significantly influences the annealing behaviour.

The techniques of ion implantation, when combined with a consideration of the known size and bonding energy of the implanted atom, have been shown to be a powerful analytical tool for the investigation of implanted systems. A recent conference on silicon carbide has presented many ideas and suggestions for new dopants, etching methods and annealing and crystal growth techniques. For example, Scandium has been found to produce yellow light-emitting-diodes when implanted into silicon carbide[98] and Indium has been found to go 100% substitutional when implanted into silicon carbide at 350°C and then annealed.[99] The combined use of the lattice location, damage studies and electrical measurements, as presented in this thesis, should be continued with other dopants in silicon carbide.

APPENDIX A

HALL EFFECT AND CONDUCTIVITY MEASUREMENTS ON ION IMPLANTED LAYERS

Experimental techniques for the determination of the carrier concentration and carrier mobility in ion-implanted layers have been considered by several authors.[100,101] One of the best descriptions of these techniques has been presented by Johansson et al.[52]

The room temperature Hall effect measurements used in this investigation were performed on Van der Pauw-type[102] patterns, a plan view of which is shown in figure A-1. In the Hall effect measurement, the current must be confined to the implanted layer. This is usually accomplished by the formation of a low leakage junction or by the use of an extremely high resistivity substrate. To obtain meaningful data, all leakage currents (including that of the diode and any surface currents) should be less than 5% of the measurement current.

The sheet Hall coefficient R_s for the pattern shown in figure A-1 is determined by measuring the voltage change ΔV_{13} normal to the current path I_{24} when a magnetic field is applied perpendicular to the sample:

$$R_s = 10^8(\Delta V_{13}/BI_{24}) \qquad \text{(A-1)}$$

where B = magnetic field in gauss.

I_{24} = current (in Amps.) between terminals 2,4

ΔV_{13} = Change in voltage between terminals, 1,3 when field is applied (volts)

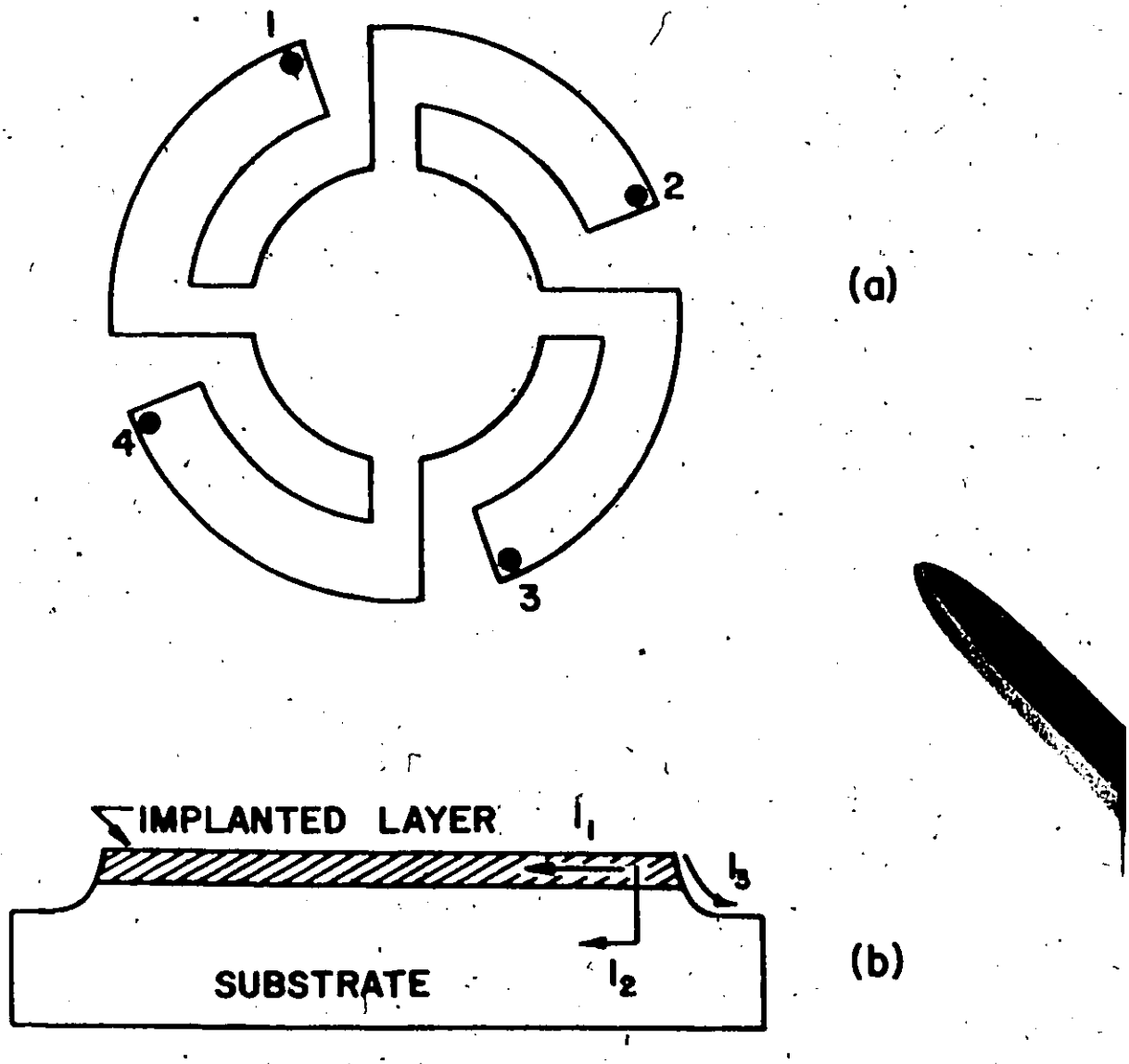

Figure A-1 (a) A plan view of the Van der Pauw pattern used for the Hall effect and sheet resistivity measurements.

(b) A cross-sectional view of the Van der Pauw pattern. To obtain meaningful data, the sum of the junction leakage current I_2 and any surface currents I_3 must be less than 5% of the measurement current I_1.

The sheet resistivity ρ_s is obtained from the equation

$$\rho_s = \left(\frac{\pi}{\ln 2}\right)\left(\frac{V_{34}}{I_{12}}\right) \qquad \text{(A-2)}$$

where ρ_s = sheet resistivity (ohms/square)

V_{34} = change in voltage between terminals 3,4, when current I_{12} is passed between terminals 1,2 (volts)

I_{12} = current between terminals 1,2 (Amps.)

For a sample with a uniform concentration of carriers (n) to a depth t, the sheet concentration

$$N_s = nt \qquad \text{(A-3)}$$

$$= \frac{r}{R_{sq}} \qquad \text{(A-4)}$$

where t = layer thickness

n = concentration of carriers/cm^3

r = ratio of Hall mobility to conductivity mobility

q = 1.6×10^{-19} coulombs

The Hall mobility is given by

$$\mu_H = \frac{R_s}{\rho_s} \qquad \text{(A-5)}$$

The value of the mobility ratio (r) is dependent on the impurity concentration and the scattering mechanisms in the sample. For lightly doped silicon, r has been found to be ~1.2 - 1.3 for electrons and ~0.7 - 0.8 for holes.[103] For heavily doped material, r ≈ 1.0. In the present investigation, it has been assumed that r = 1.0, although this

assumption might lead to errors of 20 - 30%, as discussed by Johansson.[52]

The values obtained for N_s, ρ_s and μ_H using the above expressions are averages which depend on the distribution on depth of the carriers and their mobility. The profiles of the carrier concentration and mobility may be determined by making Hall effect and conductivity measurements as successive layers are removed from the sample.

The number of carriers n_i and their mobility μ_i in the i^{th} layer can be determined from[52]

$$(R_s)_i/(\rho_s)_i^2 - (R_s)_{i+1}/(\rho_s)_{i+1}^2 = q\, n_i \mu_i^2\, t_i \qquad (A\text{-}6)$$

and

$$1/(\rho_s)_i - 1/(\rho_s)_{i+1} = q\, n_i \mu_i\, t_i \qquad (A\text{-}7)$$

giving $$\mu_i = \Delta\left(\frac{R_s}{\rho^2}\right)_i / \Delta\left(\frac{1}{\rho_s}\right)_i \qquad (A\text{-}8)$$

and $$n_i = \Delta\left(\frac{1}{\rho_s}\right)_i / q\, t_i \mu_i \qquad (A\text{-}9)$$

where $(R_s)_i$ = sheet Hall coefficient after removal of i^{th} layer

$(\rho_s)_i$ = sheet resistivity after removal of i^{th} layer

t_i = thickness of i^{th} layer

APPENDIX B

THE MOS CAPACITOR TECHNIQUE AS APPLIED TO THE DETERMINATION OF FREE CARRIER CONCENTRATION

This appendix describes the use of the MOS capacitor techniques for determing the concentration of free carriers in the surface region of a semiconductor. Since this subject has been considered extensively elsewhere,[54,55] only the relations needed in the present study will be considered.

The MOS capacitor (or C-V) technique consists of measuring the total capacitance of the metal-oxide-semiconductor system, which is a series combination of the oxide capacitance $C_{ox} = \epsilon_{ox} A/d_{ox}$, and the silicon depletion layer capacitance C_{dep}. In the present investigation, there is also a p-n junction capacitance C_j. The relative values of these capacitors are shown in figure B.1, from which it can be seen that the effective capacitance of the junction has little effect on the observed capacitance due to the large area of the junction capacitance as compared to the other capacitances.

The depletion layer capacitance is a function of voltage. For a positive voltage applied to the metal contact, there is an accumulation of electrons in the n-type semiconductor layer near the oxide-semiconductor interface, and therefore a high differential capacitance. The total capacitance is close to that of the oxide, C_{ox}. As the voltage is swept from positive to negative, a depletion region that acts as a dielectric in

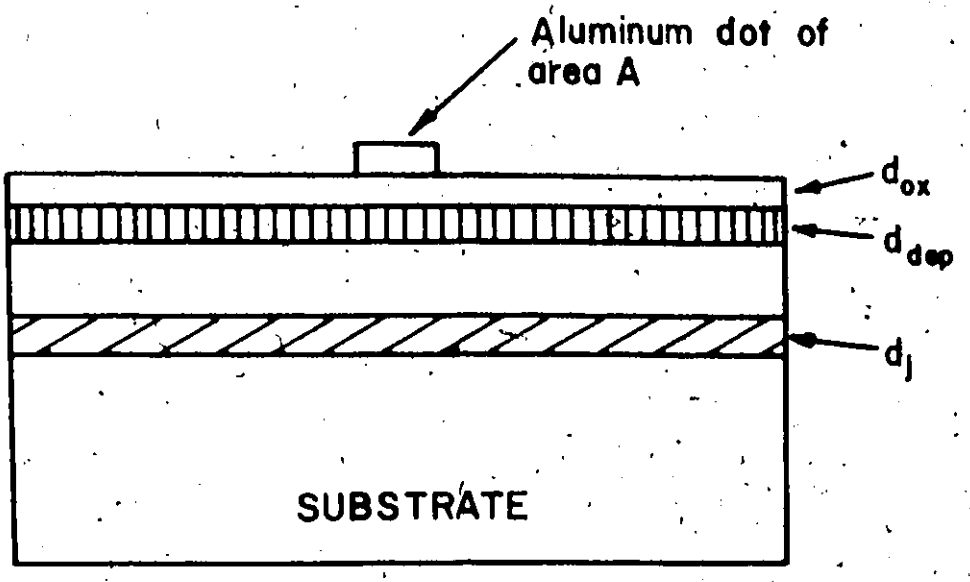

$$C_{ox} = \frac{\epsilon_{ox} A}{d_{ox}} \qquad C_{dep} = \frac{\epsilon_{si} A}{d_{dep}} \qquad C_j = \frac{\epsilon_{si} A_j}{d_j}$$

The total capacitance C_T is given by

$$C_T = \frac{C_{ox} C_{dep} C_j}{C_{ox} C_{dep} + C_{ox} C_j + C_{dep} C_j}$$

But the area of the junction capacitance (A_j) is much greater than that of the Metal-Oxide-Semiconductor area (A)

$$C_j >> C_{ox}, C_{dep}$$

and

$$C_T \simeq \frac{C_{ox} C_{dep}}{C_{ox} + C_{dep}}$$

Figure B.1 A schematic representation of the metal-oxide-semiconductor capacitor system.

series with the insulator is formed near the semiconductor surface and the total capacitance decreases. The capacitance goes through a minimum and then, if the hole concentration can follow the applied a.c. signal, will increase again. The increase in capacitance is only possible at low frequencies where the recombination-generation rates of minority carriers can keep up with the small signal variations and lead to charge exchange with the inversion layer in step with the measurement signal. As an a.c. signal of 10 kHz was used in this investigation, this increase in capacitance in the depletion region was not observed.

As the d.c. bias is reduced further, the hole concentration near the surface will equal the concentration of the substrate impurity atoms N_D^*, and strong inversion will occur. When this happens, the surface depletion region reaches a maximum. The relation between the maximum depletion layer width versus impurity concentration has been presented by Sze:(54)

$$W_m = \left(\frac{2\varepsilon_s \psi_s(inv)}{qN}\right)^{1/2}$$

where ε_s = dielectric constant of silicon

q = 1.6×10^{-19} coulomb

N = Majority carrier concentration at the surface

ψ_s = surface potential at high inversion

$\simeq 2\phi_F$ where ϕ_F is the intrinsic Fermi level

The corresponding minimum capacitance for high frequency a.c. signal conditions is

$$C_{min} = \frac{\varepsilon_{ox}}{d + \left(\frac{\varepsilon_{ox}}{\varepsilon_s}\right) W_m} \qquad \text{(B-2)}$$

where d = thickness of the oxide

ε_{ox} = dielectric constant of the oxide

The ideal MOS curves have been computed for various oxide thicknesses and semiconductor doping densities. The normalized minimum capacitance (C_{min}/C_{ox}) versus oxide thickness with silicon doping concentration as a parameter have been presented by Sze.[54]

To illustrate the technique, consider the capacitance-voltage curve shown in figure 3.7, where C_{ox} = 22.4 pF and C_{min} = 17.6 pf. The value of the oxide thickness is calculated from the measured value of the oxide capacitance, viz.-

$$C_{ox} = \frac{\varepsilon_{ox} A}{d_{ox}} \qquad \text{(B-3)}$$

or

$$d_{ox} = \frac{\varepsilon_{ox} A}{C_{ox}} \qquad \text{(B-4)}$$

The area of the metal dot was calculated from the diameter (0.02")

$$A = \frac{\pi d^2}{4} \qquad \text{(B-5)}$$

$$= 2.04 \times 10^{-3} \text{ cm}^2$$

Then

$$d_{ox} = \frac{(3.6)(8.86 \times 10^{-14})(2.04 \times 10^{-3})}{22.4 \times 10^{-12}} \qquad \text{(B-6)}$$

$$= 2890 \text{ Å}$$

The normalized minimum capacitance C_{min}/C_{ox} is 17.6/22.4 = 0.787. Using the graph presented in figure B.2, the value of 1.7×10^{16} N/cm^3 is obtained.

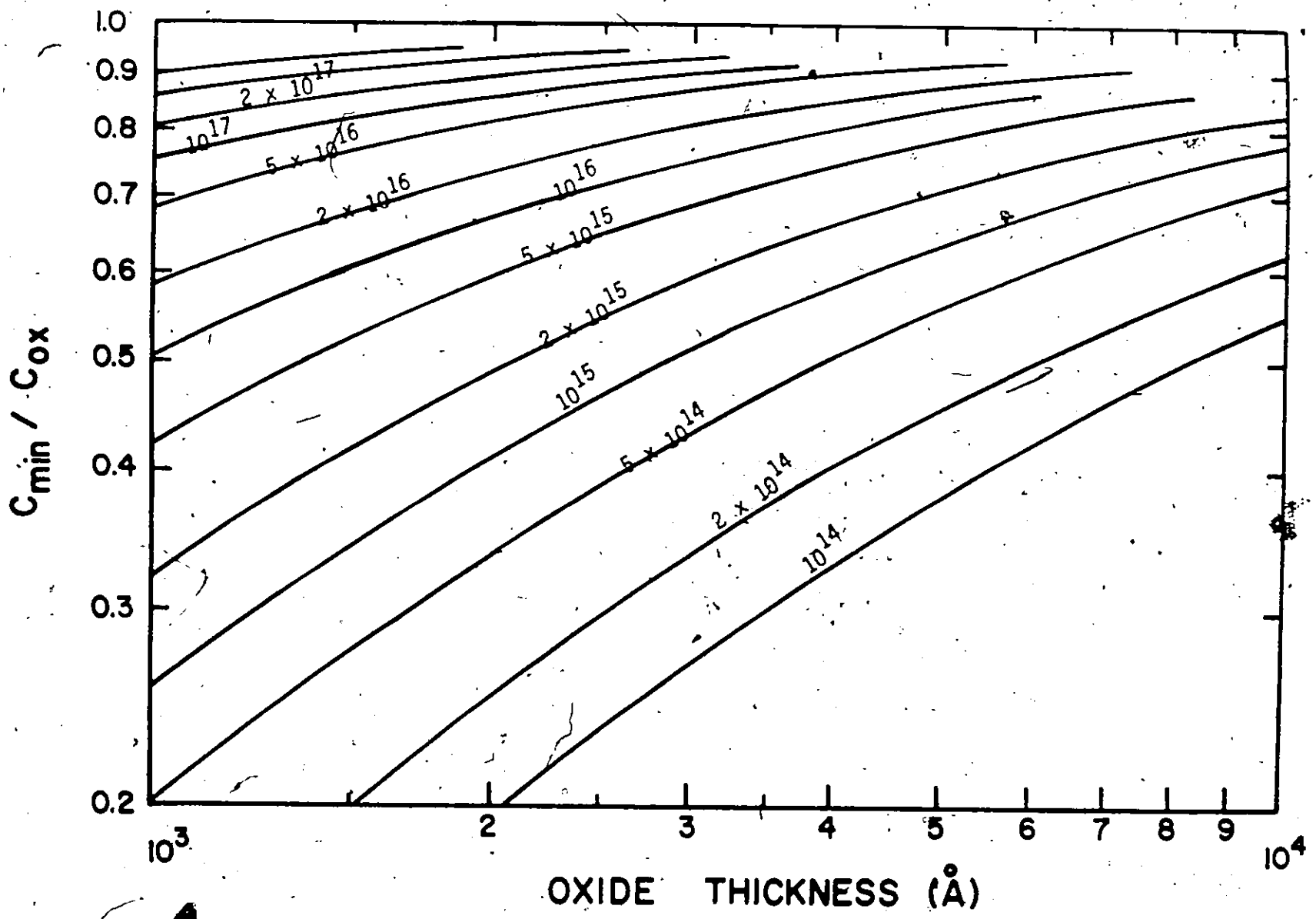

Figure B.2 The normalized minimum capacitance (C_{min}/C_{ox}) versus oxide thickness with doping concentration as a parameter. (High frequency conditions)

REFERENCES

1. P.V. Pavlov, E.I. Zorin, D.I. Tetel'baum and Yu.S. Popov, Soviet Physics - Doklady, 10, 786 (1966)
2. P.E. Roughan et. al., 133rd Meeting Electrochem. Soc. Abstracts, Boston, Mass., U.S.A., 5-9 May, 1968 (New York Electrochem. Soc. 1968) p.19
3. E.I. Zorin, P.V. Pavlov and D.I. Tetel'baum, Soviet Physics - Semiconductors, 2, 111 (1968)
4. G.H. Schwuttke, K. Brack, E.E. Gardner and H.M. DeAngelis, in "Radiation Effects in Semiconductors", Ed. F.L. Vook (New York, 1968) p.406
5. D.E. Davies, Appl. Phys. Lett., 14, 227 (1969)
6. H.L. Dunlap and O.J. Marsh, Appl. Phys. Lett., 15, 311 (1969)
7. N. Bohr, Kgl. Danske Videnskab. Selskab, Mat. Fys. Medd. 18, No.8 (1948)
8. K.O. Nielsen, in "Electromagnetically Enriched Isotopes and Mass Spectroscopy", Ed. M.L. Smith, Academic Press, New York (1956) p.68
9. J. Lindhard, M. Scharff, and H.E. Schiott, Kgl. Danske Videnskab. Selskab, Mat. Fys. Medd. 33, No. 14 (1963)
10. J. Lindhard and M. Scharff, Phys. Rev. 124, 128 (1961)
11. O.B. Firsov, Soviet Phy. - JETP 9, 1076 (1959)
12. A.H. El-Hoshy and J.F. Gibbons, Phys. Rev. 173, 454 (1968)
13. H.E. Schiott, Can. J. Phys. 46, 449 (1968)
14. W.S. Johnson and J.F. Gibbons, "Projected Range Statistics in Semiconductors", dist. by Stanford University Bookstore (1969)

15. J. Lindhard, V. Nielsen, M. Scharff and P.V. Thomsen, Kgl. Danske Videnskab. Selskab, Mat. Fys. Medd. 33, No.10 (1963)

16. K.B. Winterbon, private communication (1972)

17. G.H. Kinchin and R.S. Pease, Rept. Prog. Phys. 18, (1955)

18. P. Sigmund and J.B. Sanders, in "Proc. Intern. Conf. Appl. Ion Beams Semiconductor Tech.", Ed. P. Glotin, Editions Ophrys, Grenoble (1957) p.215

19. D.K. Brice, Rad. Effects 6, 77 (1970)

20. K.B. Winterbon, private communication (1973)

21. A. Sosin and W. Bauer, in "Studies in Radiation Effects", Ed. G.J. Dienes, Vol.3, Gordon Breach, New York (1969)

22. S.T. Picraux and F.L. Vook, Rad. Effects 11, 179 (1971)

23. G.R. Piercy, F. Brown, J.A. Davies and M. McCargo, Phys. Rev. Letters 10, 399 (1963)

24. H. Lutz and R. Sizmann, Phys. Letters 5, 113 (1963)

25. R.S. Nelson and M.W. Thompson, Phil. Mag. 8, 1677 (1963)

26. B. Domeij, F. Brown, J.A. Davies, G.R. Piercy and E.V. Kornelsen, Phys. Rev. Letters 12, 363 (1964)

27. J.A. Davies, G.C. Ball, F. Brown and B. Domeij, Can. J. Phys. 42, 1070 (1964)

28. M.T. Robinson and O.S. Oen, Phys. Rev. 132, 2385 (1963)

29. C. Lehmann and G. Leibfried, J. Appl. Phys. 34, 2821 (1963)

30. J. Lindhard, Phys. Letters 12, 126 (1964)

31. J. Lindhard, Kgl. Danske Videnskab. Selskab, Mat. Fys. Medd. 34, No.14 (1965)

32. W.M. Gibson, F.W. Martin, R. Stensgaard, F. Palmgren-Jensen, N.I. Meyer, G. Galster, A. Johansen, and J.S. Olsen, Can. J. Phys. 46, 675 (1968)

33. K. Bulthuis and R. Tree, Phys. Letters 28A, 558 (1969)

34. J.E. Westmoreland and J.W. Mayer, Rad. Effects 6, 161 (1970)

35. W.H. Weisenberger, S.T. Picraux and F.L. Vook, Rad. Effects 9, 121 (1971)

36. F.H. Eisen, in "Channeling in Solids", Ed. D.V. Morgan, John Wiely and Sons, England, (1973), Chapter 14

37. L.C. Feldman and J.W. Rodgers, J. Appl. Phys. 41, 3776 (1970)

38. F.H. Eisen, G.J. Clark, J. Bottiger and J.M. Poate, Rad. Effects 13, 93 (1972)

39. G. Amsel, J.P. Nadai, E. D'Artemare, D. David, E. Girard and J. Moulin, Nucl. Instr. and Meth. 92, 481 (1971)

40. G. Amsel and D. David, Rev. Phys. Appl. 4, 383 (1969)

41. L.N. Large and R.W. Bicknell, J. Mater. Sci. 2, 589 (1967)

42. J.R. Parsons, Phil. Mag. 12, 1159 (1965)

43. N.N. Sirota, in "Chemical Bonds in Semiconductors and Solids", Ed. N.N. Sirota, Consultants Bureau, New York (1967) p.7

44. L. Pauling, "The Nature of the Chemical Bond", Cornell University Press, Ithaca, New York (1942) p.179

45. D.S. Tulloch, "Physical Fundamentals of Materials Science", Butterworth and Co., England (1971) p.168

46. D.S. Tulloch, ibid., p.169

47. R.R. Hultgren, in "An Atomistic Approach to the Nature and Properties of Materials", Ed. J.A. Pask, John Wiley and Sons, New York (1967) p.61

48. W. Kaiser, H.L. Frisch and H. Reiss, Phys. Rev. 112, 1546 (1958)

49. H.J. vanDaal, Phillips Res. Rept. Suppl., No.4 (1965)

50. W.R. Hardy, R. Yager and J. Shewchun, Nucl. Instr. and Meth. 77, 331 (1970)

51. P.P. Pronko, W.R. Hardy and J. Shewchun, Rad. Effects 10, 79 (1971)

52. N.G.E. Johansson, J.W. Mayer and O.J. Marsh, Solid State Electronics 13, 317 (1970)

53. J. Shewchun, K.M. Ghanekar, R. Yager, H.D. Barber and D.A. Thompson, Rev. Sci. Instr. 42, 1797 (1971)

54. S.M. Sze, "Physics of Semiconductor Devices", John Wiley and Sons, New York (1969) p.437

55. K.H. Zaininger and F.P. Heiman, Solid State Tech. (May 1970) p.49 and (June 1970) p.46

56. P.F. Schmidt and W. Michel, J. Electrochem. Soc. 104, 230 (1957)

57. B.L. Crowder and J.M. Fairfield, J. Electrochem. Soc. 117, 363 (1970)

58. J.C. North and W.M. Gibson, Rad. Effects 6, 199 (1970)

59. F.H. Eisen and B. Welch, Rad. Effects 7, 143 (1971)

60. S.T. Picraux, W.H. Weisenberger and F.L. Vook, Rad. Effects 7, 101 (1971)

61. F.F. Morehead and B.L. Crowder, Rad. Effects 6, 27 (1970)

62. F.L. Vook and H.J. Stein, Rad. Effects 6, 11 (1970)

63. G.D. Watkins, in "Radiation Effects in Semiconductors", Ed. F.L. Vook, Academic Press, New York (1970) p.67

64. W.J. Kleinfelder, Thesis, Stanford University, Stanford, Calif. SEL Tech. Report No. K701-1

65. S. Roosild, R. Dolan and B. Buchanan, J. Electrochem. Soc. 115, 307 (1968)

66. F. Cianfrone and U. Fasoli, Nuevo Cimento LVIIB, 534 (1968)

67. H. Niu, T. Matsuda, K. Yamauchi and M. Takai, Appl. Phy. Lett. 21, 423 (1972)

68. R.R. Ferber, IEEE Trans. N. S. __, 15 (1963)

69. F.J. Morin and J.P. Maita, Phys. Rev. 96, 28 (1954)

70. R. Kelly, private communication (1973)

71. E.I. Zorin, P.V. Pavlov, D.I. Tetl'baum and A.F. Khokhlov, Soviet Physics-Semiconductors 4, 2026 (1971)

72. A. Mayer, Solid State Tech. (April 1972) p.38

73. W. Kaiser and C.D. Thurmond, J. Appl. Phys. 30, 427 (1959)

74. Y. Yatsurugi, N. Akiyama, Y. Endo and T. Nozaki, J. Electrochem. Soc. 120, 975 (1973)

75. J.W. Mayer, L. Eriksson, S.T. Picraux and J.A. Davies, Can. J. Phys. 46, 663 (1968)

76. W.D. Cussins, Proc. Phy. Soc. 68, 213B (1955)

77. P.V. Pavlov, E.I. Zorin, D.I. Tetel'baum and Yu. S. Popov, Soviety Physics - Doklady 10, 786 (1966)

78. G.D. Alton and L.O. Love, Can. J. Phys. 46, 695 (1968)

79. L. Eriksson, J.A. Davies, J. Denhartog, J.W. Mayer, O.J. Marsh and R. Mankarious, Appl. Phy. Lett. 10, 323 (1967)

80. J.A. Davies, J. Denhartog, L. Eriksson and J.W. Mayer, Can J. Phys. 45, 4053 (1967)

81. K. Bjorkquist, D. Sigurd, G. Fladda and G. Bjarnholt, Rad. Effects 6, 141 (1970)

82. K. Bjorkquist, B. Domeij, L. Eriksson, G. Fladda, A. Fontell, and J.W. Mayer, Appl. Phys. Lett. 13, 379 (1968)

83. J.R. Parson, Phil. Mag. 12, 1159 (1965)

84. J.W. Mayer, L. Eriksson and J.A. Davies, "Ion Implantation in Semiconductors", Academic Press, N.Y. (1970) p.254

85. W. Whaling, Hond. der. Phys. 34, 193 (1958)

86. Available from the Emulsitone Company, 41 East Willow St., Millburn, New Jersey, U.S.A., 07041

87. J.A. Lely, Ber. dtsch. keram. Ges 32, 229 (1955)

88. J.A. Lely and F.A. Kroger, Proc. int. conf. Semiconductors and Phosphors, Vieweg, Braunschweig (1958) p.525-533

89. L.J. Kroko and A.G. Milnes, Solid State Electronics 9, 1125 (1966)

90. G.J. Caras, "Silicon Carbide for Semiconductors", Tech. Report AD464777, Prepared for Redstone Scientific Information Center, Redstone Arsenal, Alabama (1965)

91. H.L. Dunlap and O.J. Marsh, Appl. Phys. Letters 15, 311 (1969)

92. O.J. Marsh and H.L. Dunlap, Rad. Effects 6, 301 (1970)

93. R.R. Hart, H.L. Dunlap and O.J. Marsh, Rad. Effects 9, 261 (1971)

94. A. Addamiano, G.W. Anderson, J. Comas, H.L. Hughes and W. Lucke, J. Electrochem. So. 10, 1355 (1972)

95. D.R. Hamilton, in "Silicon Carbide", Ed J.R. O'Connor and J. Smiltens, Pergamon Press, London (1960) p.43-52

96. F.B. Hagedorn and J.B. Marion, Phys. Rev. 108, 1015 (1957)

97. J.W. Corbett, "Electron Radiation Damage in Semiconductors and Metals", Academic Press, N.Y. (1966) Chap. 3.

98. E. Ye Violin and Yu. M. Tairov, Inter. Conf. on Silicon Carbide-1973, Miami Beach, Fla, U.S.A. (Abstract 62)

99. O.J. Marsh, Inter. Conf. on Silicon Carbide-1973, Miami Beach, Fla. U.S.A. (Abstract 52)

100. J.W. Mayer, O.J. Marsh, G.A. Shifrin and R. Baron, Can. J. Phys. 45, 4073 (1967)

101. A.H. Clark and K.E. Manchester, Trans, Metal. Soc. AIME 242, 1173 (1968)

102. L.J. Van Der Pauw, Philips Res. Rept. 13, 1 (1958)

103. K.B. Wolfstirn, J. Phys. Chem. Solids 16, 279 (1960)